Optimization and quantification of Urease in a magnetoresistive biochip platform with integrated Microfluidics

Débora Cristina Batista de Albuquerque

Thesis to obtain the Master of Science Degree in

Biological Engineering

Supervisor: Prof. Susana Isabel Pinheiro Cardoso

Examination Committee

Chairperson: Prof. Gabriel António Amaro Monteiro

Supervisor: Prof. Susana Isabel Pinheiro Cardoso

Member of the Committee: Dr. Verónica Cristina Baião Martins Romão

November, 2017

ACKNOWLEDGMENTS

First of all, I would like to thank Professor Susana Freitas for giving me this amazing opportunity. The work I developed under your oversight in the past year not only allowed me to obtain my Master's degree (hopefully) but also gave me a once in a lifetime opportunity to work in the area that I always dreamed of. I am also grateful for you always believing in my capabilities even when I didn't. You were and are an inspiration.

I also want to thank Professor Gabriel Monteiro for helping me with the biologic aspects of this thesis and showing great availability. Sofia and Cláudia, thank you so much for teaching me how to work with everything and having the patience to serve as my borrowed teachers! You two are wonderfully people and I can only hope that everything goes well in your future. Thank you also to Professor Rafaela Cardoso for the work, ideas and time provided.

Thank you Elisabete for taking the time to elucidate the mind of a stranger and for being extremely nice and helpful when you didn't need to.

I would like to thank my amazing family, especially my dad, for helping me whatever I needed and believing in the best I could offer, my mom, for always supporting me and making me laugh, my sister, for just existing and being the unapologetic self she is, my cousin Catarina for putting up with me for all these years and basically being my best friend, and my grandmother Teresa, for being such a giving and caring person and always encouraging me and giving me the best conditions one could desire. This is your conquest too. Your unconditional love, patience, and support during all these years was everything, and without it none of this would have never happened.

One of the major acknowledgments goes to Tomás Dias. Without him this thesis would probably be a lot worse. He was the man behind so much of the ideas, including the microfluidic device. You were my mentor and my friend. Such a bright individual full of plans and super funny! Our biolab sessions were the best. I was always learning with you. I miss you, but I know you are off to big and greater things. Hope you achieve everything you deserve. I also need to thank to Joanna Brzezinska for being my amazing coworker and friend. Probably the most nice and crazy friend of all! You were also part of the development of some of the work presented here and you deserve the credit. I hope you can realize your dream to come work here in Portugal and that you keep being the awesome and hardworking person you always were. Tomás and Joanna, rich (something not so PG-13) forever!

I also need to acknowledge my summer intern colleague, Ricardo, for the magnetic separator layout creation!

I need to thank all my friends and colleagues at INESC for the wonderful times and learning experience: Pedro Alves, the first person I met at INESC and the most energetic and idealistic one of all, for always being willing to help and have deep conversions with; Jorge, for basically putting up with me as my table sharing comrade and not throwing me through the window, and for making me laugh(when I should probably be working); João Serra, best friend for life, for all that we talked and shared and everything really (You are an amazing person!); Rita Soares, for always giving me a hand (though sometimes that hand was beating me!) and for being a truly nice person with such a quirky personality. Hope you have a wonderful future and a great family.; Tomás Ribeiro, for being my same course partner and for accompanying me in the sea of Physics students; Tiago, for being an all-around cheerful guy always smiling and listening; Rui Garcia, for being the (not so) grown up in the group, guiding us and always with a suggestion for our problems and Paulo, for your crazy semi autistic and super nice, intelligent self. Our lunches were always the most entertaining! And our conversations always interesting/disgusting!

Thank you to the biostuff crew: Rita Soares, Tomás Ribeiro and Pedro Fonseca for the fantastic niche group we formed! Thank you as well to Catarina Caneiras for the great chats about Koreans and life in general, as well as your help. You will be a great researcher!

I would also like to thank Vânia for helping me through some of the work and for always being available to land a hand.

Next, I must thank to my friends made during the ISt Journey! Thank you Rita, Maryna, Sara Crucho, Beatriz, Maria João, Pedro Oliveira, Catarina Carinhas, Catarina Oliveira and Inês Apolónia for all the great times and adventures! For all the work projects and sleepless nights we spent together, for all the pain and happiness we shared, for all the card games we played when we should be in classes or studying (Rita cofcof), for this amazing friendship that we share. I hope you all have a fantastic future, wherever it may lead you. Thank you for the precious memories.

Lastly, but not least, I need to thank to my best friend Sofia Jones. You were always there for me, all these years. We started and finished this journey together. You always supported me and my crazy ideas and you made sure I enjoyed my time. Also, thank you to Joana Neves, Laura Nascimento and Mariana. Thank you for the great moments and talks over coffer! You are all amazing individuals and friends!

All of you, my sincere and immensurable, Thank you.

And honestly, I should’ve probably studied more.

.

Débora Albuquerque

ABSTRACT

In recent years there has been an exploration of sustainable and environmental-friendly technologies for ground improvement to be used in civil engineering infrastructure developments. One of the most studied and promising biological ground improvement method is biocementation through microbially induced calcite precipitation (MICP). The biological induced precipitation of $CaCO_3$ involves the use of bacteria capable of producing a high amount of precipitates within a short period of time in the presence of urea due to their high urease activity. The analysis of this enzyme allows then a possible method for quantifying the amount of biocement produced. The present thesis is dedicated to the quantification of urease present in a given soil sample in a way that can be used *in situ*. This is accomplished by employing a lab-on-a-chip (LOC) device utilizing magnetoresistive biochips as biosensors in tandem with a read-out electronic set-up, magnetic labels and an integrated microfluidics system. In this thesis it was also studied a method of urease sample preparation involving the use of a microfluidic mixer and magnetic separator. A calibration curve between 0.5 and 70 mg/ml was obtained using the biochip platform for a pure urease extract from *Canavalia ensiformis*. Urease from *Bacillus pasteurii* was grown and its urease activity was measured. The urease from *B. pasteurii* was not quantified using the platform since no magnetic signal could be detected, further optimization in the sample preparation being needed. The preparation of a urease sample was successfully carried out using only microfluids, though with lower sensitivity.

KEYWORDS

Microbially induced calcite precipitation; Urease; Lab-on-a-chip; Magnetoresistive biochips; Microfluidics

RESUMO

Nos últimos anos tem ocorrido uma maior exploração de tecnologias sustentáveis a serem usadas para a estabilização do solo em desenvolvimentos de infraestruturas na área de engenharia civil. Um dos métodos de melhoramento do solo biológico mais estudado e promissor é a biocimentação através da precipitação de calcite induzida por microrganismos (MICP). Este tipo de precipitação do $CaCO_3$ envolve o uso de bactérias capazes de produzir uma grande quantidade de precipitados num curto intervalo de tempo na presença de ureia devido a uma elevada atividade enzimática por parte da urease. A análise desta enzima torna-se então um possível método para quantificar o biocimento produzido. A atual tese é dedicada a quantificar a urease presente numa determinada amostra de solo de maneira que possa ser utilizada *in situ*. Isto é conseguido empregando um dispositivo lab-on-a-chip (LOC) que engloba biochips magnetoresistivos como biossensores em conjunto com um sistema eletrónico de aquisição, marcadores magnéticos e um sistema de microfluídica integrado. Nesta tese também foi estudado um método de preparação de amostras de urease envolvendo o uso de um misturador e separador magnético microfluídicos. Uma curva de calibração entre 0,5 e 70 mg / ml foi obtida usando a plataforma de biochips para um extrato de urease pura de *Canavalia ensiformis*. A urease de *Bacillus pasteurii* foi cultivada e a actividade da urease produzida foi medida. A urease de *B. pasteurii* não foi quantificada usando a plataforma, não se tendo conseguido detetar um sinal magnético, sendo como tal necessária uma maior otimização na preparação da amostra. A preparação de uma amostra de urease foi realizada com sucesso utilizando apenas microfluídica, embora com menor sensibilidade.

PALAVRAS-CHAVE

Precipitação de calcite induzida por microrganismos; Urease; Lab-on-a-chip; Biochips magnetoresisitivos; Microfluídica

Table of Contents

LIST OF TABLES

LIST OF FIGURES

LIST OF ABBREVIATIONS

Ab Antibody

ACoM Autonomous Communication Module

AMR Anisotropic Magnetoresistance

AP Alkaline Phosphatase

APS Ammonium Persulfate

ATP Adenosine Triphosphate

BCA Bicinchoninic Acid

BLAST Basic Local Alignment Search Tool

B. pasteurii *Bacillus pasteurii*

BSA Bovine Serum Albumine

C. ensiformis *Canavalia ensiformis*

COC Cyclic Olefin Copolymers

COP Cyclic Olefin Polymers

CVS Comma Separated Value

DI Deionized Water

DSP 16-bit Digital Signal Processor

ECM Extracellular Matrix

ELISA Enzyme-linked Immunosorbent Assay

EPS Extracellular Polymeric Substances

GMR Giant Magnetoresistance

HDMS Hexamethyldisilane

HRP Horseradish Peroxidase

IPA Isopropanol

K_{sp} Calcite solubility product

LOC Lab-on-a-chip

MICP Microbially Induced Calcite Precipitation

MP Magnetic Particles

MR Magnetoresistance

MTJ Magnetic Tunnel Junction

MWCO Molecular Weight Cut-Off

NIH National Institute of Health

OD Optical density

PC Polycarbonate

PCB Printed Circuit Board

PCR Polymerase Chain Reaction

PDMS Polydimethylsiloxane

Pe Péclet number

PEB Post Exposure Bake

PECVD Plasma-enhanced Chemical Vapor Deposition

PGMEA Propylene Glycol Methyl Ether Acetate

PMMA Poly(methyl methacrylate)

POC Point-of-care

PR Photoresist

PVDF Polyvinylidene Difluoride

Re Reynolds number

RIE Reactive Ion Etch

S Saturation level

SAM Self-assembled Monolayer

SEM Scanning Electron Microscopy

SPM Sensing and Processing Module

Sulfo-LC-SPDP Sulfosuccinimidyl 6-(3'-[2-pyridyldithio]-propioamide)hexanoate

SVG Silicon Valley Group

TEMED Tetramethylethylenediamine

VSM Vibrating Sample Magnetometer

XML Extensible Markup Language

µPAD Microfluidic Paper-based Analytical Device

1. INTRODUCTION

1.1. GENERAL INTRODUCTION

Population and civil infrastructure continue to expand at unprecedented rates, with infrastructure being insufficient in countries such as China, where 10 million people immigrate to major cities each year. As such, rehabilitation and expansion of civil infrastructure is required to meet ever-growing societal needs, being directly limited by the availability of competent soils upon which they can be constructed. Alongside these needs, there exists the issue correlating to the environment sustainability, which is endangered by the manufacturing of cement, a material used commonly in construction processes, including in ground improvement [1]. As a result, there is a clear societal need for the technologies developed to improve soil and be environmentally-friendly. That's where the harnessing of biological processes in soils promises to be the next transformative practice in geotechnical engineering. Some of these biological processes include biomineralization, biofilm formation, and the production of other extracellular polymeric substances (EPS), biogas generation, and other processes less developed like algal and fungal growth for near surface soil stabilization and bacteria and worms for methane oxidation [2].

The use of microbes to control and manage the chemical processes is attractive given their ubiquitous presence in the near and sub-surface and the millennia over which they have been active [1]. They also exist in high concentrations, almost regardless of saturation, mineralogy, pH, and other environmental factors. Near the ground surface, more than 10^{12} microbes exist per kilogram of soil [3]. Biomineralization, more specifically, microbially induced calcite precipitation (MICP), has been the primary focus of research in biogeotechnical engineering to date. Microbially induced calcite precipitation is the creation of calcium carbonate (calcite) as a consequence of microbial metabolic activity [4]. Calcite precipitation may be achieved by many different processes, of which enzymatic hydrolysis of urea by urease being the most energy efficient of these [1]. This process also has the added advantage correlating to the wide range of microorganisms and plants displaying urease activity [5].

One of the challenges involving the biological approach to biocementation is centered around the performance monitoring. Monitoring during treatment is necessary to verify that the required distribution and magnitude of improvement are realized, and, after treatment, to verify that the improvement level remains adequate throughout the service life [2]. Three different set of components can be analyzed: biological, chemical and geotechnical. The state of the biological and chemical components is intimately linked. The biological component can primarily be captured by monitoring the microbial concentration,

activity state, activity potential, biomass, and nutrient concentrations. The chemical component can primarily be captured by monitoring the pH, chemical concentrations, and conductivity [1]. The experimental methods used to assess these components are generally well established in the respective fields (Madigan and Martinko, [6]) but do require discrete (often pore fluid) samples to be obtained and subsequent tests performed on them, usually in a laboratory. The urease activity, for example, is usually determined by measuring the amount of ammonia released from urea according to phenol-hypochlorite assay method [7]. Consequently, real-time information is not attainable, labor is intensive, and potentially destructive invasive sampling is required. This leads to a need for a method of monitoring that is non-invasive, fast, reliable, and most importantly, able to give *in situ* information about the state of the system.

A Lab-on-a-chip (LOC) consists of a device that integrates one or several laboratory functions on a single integrated circuit of only millimeters to a few square centimeters to achieve automation and high-throughput screening [8]. By applying the LOC approach to monitor a specific biological component of the geosystem, one could overcome some of the issues related with the current methods of analysis, mainly the *in situ* monitoring, possible due to the portability of the device.

In this thesis a Lab-on-a-chip device is used for the quantification of urease. The LOC apparatus consists of five main components: biochips with magnetoresistive sensors, magnetic labels, surface chemistry, electronic set-up, and a reusable microfluidics system. The optimization of the surface chemistry and application of microfluidics in sample preparation were also carried out.

1.2. AIM OF STUDIES

The purpose of this dissertation is to optimize a Lab-on-a-chip device for the quantification of urease in a sample of soil so as to allow for *in situ* monitorization of the biocementation. The LOC apparatus and the biochips used for the detection of urease were both developed by INESC-MN/ INESC-ID. The work in the present thesis is a continuation of the work done in the thesis of Sara Cardoso [9] and João Valentim [10].

The main objective of this thesis was to obtain a calibration curve for jack bean urease allowing for the quantification of urease on field. Considering that the urease present in soil is from *Bacillus pasteurii*, a correlation between the calibration curve of the jack bean urease and the resistance values obtained for the *B. pasteurii* urease should be checked to see if the previous calibration curve can be applied in the field for the latter enzyme. Finally, the last objective is to optimize the sample preparation using microfluidics in order to diminish the need for other laboratory material and also to increase portability.

1.3. SYNOPSIS

The thesis is structured in 5 chapters. Chapter 1 consists of an introductory overview of the biogeotechinal field with a resume of the current methods using biological processes for soil improvement. It's also

explained why MICP is the preferably method for biocementation and what are the current challenges associated with it and how the work in this thesis is aimed at solving some of them. The aim of studies is described in this chapter.

The state of the art on biological processes for soil improvement, biosensors and microfluidics and can be found in chapter 2. It's in this chapter that the theoretical background is discussed.

Chapter 3 describes the different methodologies and materials used in this work. In Chapter 4 the results and respective discussion are presented.

Finally, in chapter 5, the thesis general conclusions are articulated. The Future work needed for the continuous optimization of the LOC is also described.

2. FIELD OVERVIEW

Due to social factors and to contribute to the sustainability of the environment, exploration and development of new alternative soil improvement methods and associated reliable monitoring techniques are needed. As a response to this need, biological processes to mediate the improvement of soil properties have recently emerged. These opportunities have been enabled through interdisciplinary research involving the fields of microbiology, geochemistry, and civil engineering.

This chapter sets forth to present an overview of bio-mediated soil improvement. First, the different biological methods for soil improvement are described, followed by an overview of the primary components of bio-mediated soil improvement systems. Focus is placed on bio-mediated calcite precipitation of sands since research for this process is currently more advanced than the alternatives. After describing the biochemical process, alternative biological processes for inducing calcite precipitation are identified. Biochemical and non-destructive geophysical process monitoring techniques are then described and their utility explored. In this chapter the state of the art of biosensors and microfluidics is also discussed, with special focusing on spin valve sensors and elastomeric materials.

2.1. BIOLOGICAL PROCESSES IN SOIL IMPROVEMENT

A bio-mediated soil improvement system refers to a chemical reaction network that is managed and controlled within soil through biological activity and whose byproducts alter the engineering properties of soil. An overview of these types of systems is presented schematically in figure 2.1.

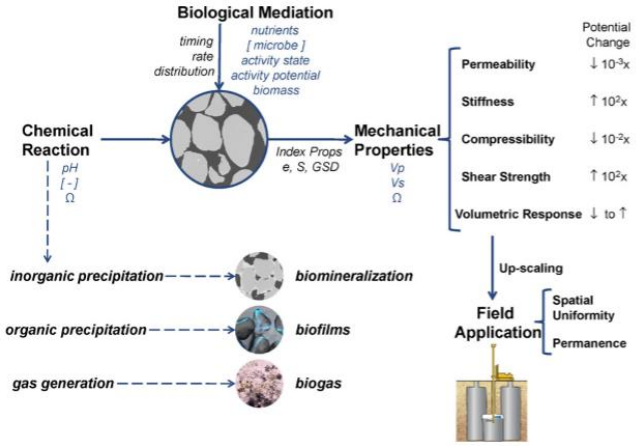

FIGURE 2-1 Synthesis of the bio-mediated soil improvement systems. ([-]=chemical concentration, Ω=resistivity, Vp=compression wave velocity, Vs=shear wave velocity) [1]

Biomediated geochemical processes have the potential to modify physical properties (density, gradation, porosity, saturation), conduction properties (hydraulic, electrical, thermal), mechanical properties (stiffness, dilation, compressibility, cementation, friction angle), and chemical composition (buffering, reactivity, cation exchange capacity) of soils [2]. The most used involve the processes of biomineralization, biofilm formation, EPS production and biogas generation.

Biofilm formation, and the production of other extracellular polymeric substances (EPS), is responsible for the generation of organic solids that occupy a portion of the pore space with a soft, ductile, elastomeric-like material that reduces pore size, reduces rearrangement of particles during soil deformation, and increases ductility [2]. Biofilms form when microorganisms adhere to a surface and excrete EPS as part of their metabolism. This substance enhances further attachment of more microorganisms and other particles, thereby forming a biofilm that can affect the physical properties of soils However, property changes due to biofilm and EPS production may be lost, and thus be applicable only for short-term ground modification, as these living systems must be continuously nourished [11]. Close to the surface in riverine and marine environments, biofilms play an important role in trapping and stabilizing sediments, and increasing the resistance to erosion [12]. In the subsurface, it was observed that water losses from rice fields were limited, owing to bacterial clogging [13].

Biological activity in the subsurface is frequently accompanied by the development of discrete gas bubbles in otherwise saturated environments. A variety of gases can be produced by microbial processes (e.g. carbon dioxide, hydrogen, methane and nitrogen). Biogas generation may enable long-term reduction in the degree of saturation of a soil which increases pore space compressibility [2].

Biomineralization processes that precipitate inorganic solids (including microbially induced calcite precipitation, or MICP) usually have a mechanical effect like reduction in pore space and increased stiffness. These effects will then result in reduced hydraulic conductivity, increased large-strain strength, and increased dilative behavior. Microbially induced calcite precipitation, or MICP, is one of the most emerging and promising biological soil improvement techniques. In MICP the biologically driven precipitation of calcium carbonate (calcite or $CaCO_3$) occurs. Calcite precipitation may be achieved by many different processes, including urea hydrolysis, denitrification, sulfate reduction, among others [2]. The urea hydrolysis is the most used process since the enzymatic activity of urease, the enzyme responsible for the urea hydrolysis, is the most energy efficient, with around 90% conversion in a time period of 24 hours [14], but also because it’s a straightforward and easy controllable reaction [15].

2.1.1. MICP BY UREA HYDROLYSIS

The mechanism of $CaCO_3$ precipitation by urea hydrolysis can be categorized into two stages: (1) urea hydrolysis and (2) CaCO3 precipitation. In the first stage, urease hydrolyses the substrate urea, generating ammonia and carbamate (Eq. 2.1). Carbamate spontaneously decomposes to produce another molecule of ammonia and carbonic acid (Eq. 2.2). The two ammonia molecules and carbonic acid subsequently equilibrate in water with their deprotonated and protonated forms, resulting in an increase in the pH (Eq. 2.3 and Eq. 2.4) [16].

$$CO(NH_2)_2 + H_2O \xrightarrow{Urease} NH_3 + CO(NH_2)OH \quad (2.1)$$

$$CO(NH_2)OH + H_2O \longrightarrow NH_3 + H_2CO_3 \quad (2.2)$$

$$H_2CO_3 \longleftrightarrow HCO_3^- + H^+ \quad (2.3)$$

$$2NH_3 + 2H_2O \longrightarrow 2NH_4^+ + 2OH^- \quad (2.4)$$

A schematic model describing the role of ureolytic bacteria on calcium carbonate precipitation is illustrated in figure 2.2.

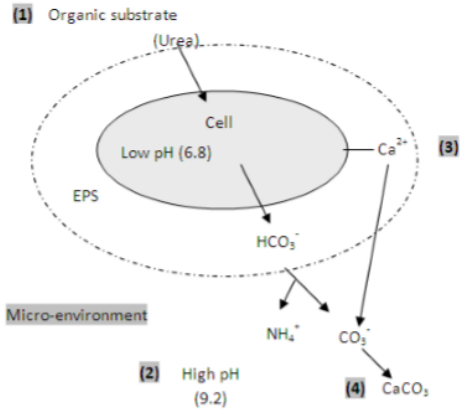

FIGURE 2-2 Schematic model summarizing the role of ureolytic bacteria in $CaCO_3$ precipitation in the presence of Ca^{2+} ions. The processes involved in the precipitation are: (1) Hydrolysis of urea (Eq.2.1-Eq.2.3), (2) Increasing the alkaline of the microenvironment (Eq.2.4), (3) Surface adsorption of Ca^{2+} ions (Eq.2.6), (4) Nucleation and crystal growth (Eq.2.7-Eq.2.8) [14]

There are two metabolic pathways for bacterial carbonate formation. These pathways are autotrophic and heterotrophic pathways. In the autotrophic pathway, CO_2 is used as a carbon source causing its depletion in the microenvironment. In the presence of Ca^{2+} ions, such depletion enhances the production of $CaCO_3$. In the passive heterotrophic pathway, bacteria can precipitate $CaCO_3$ due to the production of CO_3^{2-} is originated from ammonification of amino acids or degradation of urea or uric acid (Eq.2.5-Eq-2.7). In all cases, ammonia as a metabolic end product is produced which induces a pH increase [17]. Alkaline pH is the primary means by which microbes promote calcite precipitation [16].

$$Ca^{2+} + Cell \longrightarrow Cell - Ca^{2+} \quad (2.5)$$

$$Cl^{-} + HCO_3{}^{-} + NH_3 \longleftrightarrow NH_4Cl + CO_3{}^{2-} \quad (2.6)$$

$$Cell - Ca^{2+} + CO_3{}^{2-} \longrightarrow Cell - CaCO_3 \quad (2.7)$$

$CaCO_3$ precipitates as crystals which are formed in three stages: (1) the development of supersaturated solution, (2) nucleation at the point of critical saturation (i.e. the supersaturation at which $CaCO_3$ actually initiates), and (3) spontaneous crystal growth on the stable nuclei [18]. These stages are crucial for soil stabilization. The saturation level (S) of a solution with respect to $CaCO_3$ can be defined by the Eq.2.8, where (Ca^{2+}) and (CO_3^{2-}) represent the concentration of the dissolved Ca^{2+} and CO_3^{2-} respectively and K_{sp} is the calcite solubility product. When the concentration of Ca^{2+} and CO_3^{2-} exceeds the solubility product (K_{sp}), supersaturation of solution is reached. The higher the supersaturation is the more likely precipitation of $CaCO_3$ is to take place [14].

$$S = \frac{[Ca^{2+}][CO_3{}^{2-}]}{K_{sp}} \quad (2.8)$$

The rate of $CaCO_3$ precipitation is, in general, a linear function of the ion concentration product of (Ca^{2+}) and (CO_3^{2-}) (Eq.2.9) hence obeying 2nd order kinetics or 1st order kinetics if one of the reactants (e.g. calcium) is in excess [19].

$$G = k[Ca^{2+}][CO_3{}^{2-}] + C \quad (2.9)$$

Where G is the calcification rate in mmol $CaCO_3$ $m^{-2}d^{-1}$ and k is a factor that would depend on the areal biomass of the calcifying organisms and physical environmental conditions such as temperature, light, and flowrate. C does not have any biological significance.

2.1.2. MICROORGANISMS IN MICP

The preferred bacteria for MICP is *Bacillus pasteurii* or *Sporosarcina pasteurii*, mainly because of their ability to produce high amount of precipitates within a short period of time due to their high urease activity [20]. *B. pasteurii* is a type of aerobic bacteria that is able to hydrolyze urea to produce carbonate by the generation of adenosine triphosphate (ATP) through the secretion of urease enzyme.

Being that a high urease activity is desired, and that this is only achieved by cultivating pure ureolytic bacteria strains under sterile conditions to prevent any contamination and growth of urease-negative bacteria in the culture, this represents a major cost factor of MICP application [20]. One option is the *in situ*

enrichment of indigenous urease active microorganisms using medium containing urea, sodium acetate trihydrate, ammonium chloride and yeast extract [21].

2.1.3. BIOCEMENTATION

The biomineralization of the precipitated $CaCO_3$ crystals links the soil particles together through an effective bridging that is predominantly concentrated at the point of contacts [20]. An example of a scanning electron microscopy (SEM) image that verifies the effective bridging phenomenon is shown in figure 2.3.

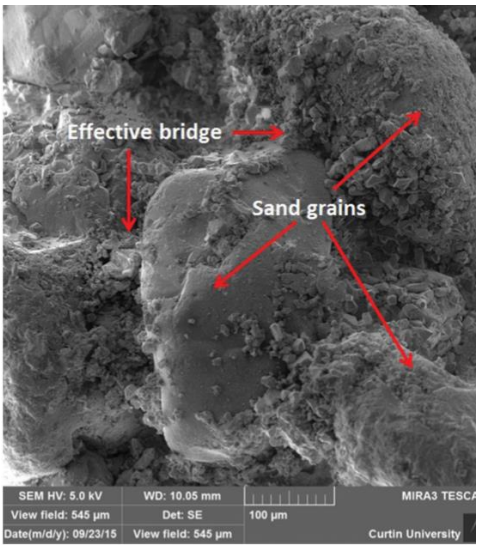

FIGURE 2-3 SEM image showing the effective bridging phenomenon [20].

2.1.4. UREASE IN UREOLYTIC BACTERIA

Urease was the first enzyme to be isolated in its crystalline form from *Canavalia ensiformis* (jack bean). The enzyme urease consists of four domains, one of which contains an active site with a bimetallic Nickel center. The urease from different genus of bacteria possess identical structures, which is the case between urease of *Klebsiella aerogenes* and *Sporosarcina pasteurii* [22]. Urease is synthesized under conditions of nitrogen starvation. The location of urease in the bacterial cells is considered contradictory since the literature as reported urease as a cytoplasmic protein and as protein located in the membrane and periplasm of *Staphylococcus* sp. *and Protus mirabilis* [16].

The urease activity of both plant and bacterial origin can be seen in figure 2.4.

Type of reaction	Urea (mM)	Ca (mM)	Urease activity	Maximum Strength(MPa)	Depth of Penetration(mm)	Reference
Bacterial Urease	100-1250	100-1000	11-28 mM urea.min^{-1}	0.6-30	1000	(Al-Thawadi, 2008)
Bacterial & plant urease	1500	1500	4-18 mM urea.min^{-1}	1.8 (3 applications)	170	(Whiffin, 2004)
CIPS	ND	ND	ND	0.679-3.8 (1 application)	179	(Harkes et al., 2010)
Plant urease	200	600	0.3 g.L^{-1}	NM	300	(Van Meurs et al., 2006)

ND: Not Defined, Property to Calcite Technology Pty Ltd (Perth, Australia)
NM: Not Measured.

FIGURE 2-4 Urease activity from different sources and respective biocementation conditions [14].

2.1.5. APPLICATIONS AND LIMITATIONS

About 1–100 m^3 of sand were treated in a laboratory by van Paassen [23], which found that the strength of biocemented sand was significantly increased upon MICP treatment with the limitation of spatial heterogeneity being present. Field-scale biocementation tests were performed by Gomez *et al.* [24]. The study focused on the surficial application of MICP to provide surface stabilization of loose sand. An improvement of approximately 28 cm near the targeted depth of 30 cm was observed.

As opposed to other soil improvement techniques involving the use of cementation agents, the initial cost of MICP installation is still costly, although it could become the cheaper treatment in the long run since the enzyme can be reused in subsequent applications of treatment using the same cementation solution. Another limitation of the MICP technique is that it can only be utilized for specific soil sizes, with particle sizes between 0.5–3 mm. Also, the end product of MICP urea hydrolysis, ammonia, is a substance which has a repugnant odor and can be considered detrimental to the health, making it a disadvantage [20].

2.2. BIOSENSORS

A biosensor is a sensing micro-device that consists of a biological sensing element and a physicochemical detector that enables sensing of molecular interactions between the biocomponent and the desired analyte. The classical approaches for detection of analytes, such as high-performance liquid chromatography and gas chromatography, are usually accompanied by an extensive processing time and trained personnel requirements. Biosensor-based devices are then able to offer several advantages such as high sensitivity and selectivity to its target, rapid processing period, user-friendly, easy to implement, and being cost-beneficial [25].

Biosensors have been widely used in different scientific fields. They can be used in medical care for an accurate detection of tumors, pathogens, elevated blood glucose levels in diabetic patients. In the food industry, biosensors could be used for detection of food contamination or for checking and minimizing the growth of bacteria or fungus in fresh food [26]. From environmental point of view, these biosensors could be enhanced to detect pollution in air and presence of any pathogens, heavy metals [27]. And in military defense systems, they can be used to detect the presence of any harmful biological materials, like *Bacillus anthracis*, Ebola, hepatitis C viruses, etc. [28].

2.2.1. Architecture of Biosensors

The Biosensors usually have 3 components (figure 2.5): (i) a biological entity (e.g. DNA, microorganisms, antibodies, nucleic acids, proteins, etc.) that recognizes the analyte under study; (ii) a transducer or a detector element that transforms the signal resulting from the interaction of the analyte with the biological element into a signal that can easily be measured and quantified. Can be optical, piezoelectric, electrochemical, etc.; (iii) biosensor display device and the associated signal processors, which are primarily responsible for displaying the analyzed results in a user-friendly manner [29].

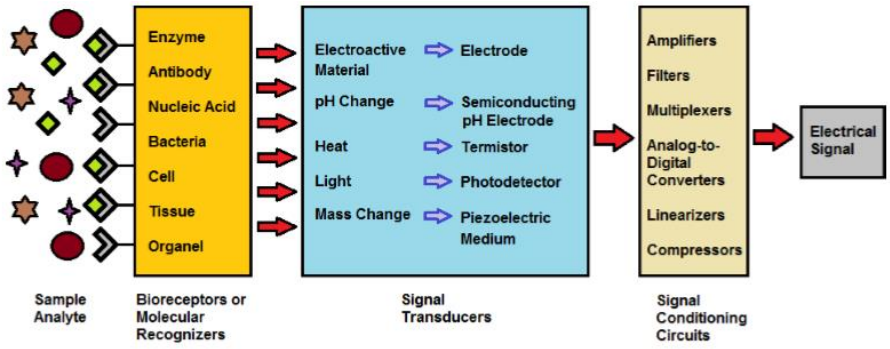

FIGURE 2-5 Operating principles of biosensors showing their three main components [29].

2.2.2. Classification

Biosensors can be classified according to their transduction principle, the nature of their bioelement or the nature of the analyte to be detected, the most used being the first classification [27]. Depending on their transduction principle, biosensors can then be divided in 4 classes:

Electrochemical biosensors - Electrochemical sensors work by reacting with target analytes to produce an electrical signal that can be correlated to the concentration of the target analyte in the given phase (figure 2.6a). The typical electrochemical sensor setup consists of a working electrode, counter electrode, reference electrode, and the electrolyte medium. This type of biosensors is preferred for fast, accurate, and

continuous measurements for on-site monitoring of analytes. They have the disadvantage of requiring a means for electron transfer between the biomolecule and the electrode upon which they are supported. These devices are also prone to fouling and are considered high cost [30].

Mechanical biosensors - Mechanical biosensors have advantages over other types of biosensors as they have great sensitivity and selectivity with regard to a wide variety of analytes and have been used to detect analytes such as DNA strands, bacteria, explosives, hazardous gases. The most common types of nanomechanical sensors are of the cantilever type, which have emerged from the AFM technique. A mechanical biosensor consists of a micromachined cantilever beam (figure 2.6b-c). The transducing effect in such a system can be attributed to the bending of the cantilever due to changes in mass, stress, temperature, frequency. Selectivity toward the target molecules is achieved by the use of target specific molecules that include enzymes, polymers, antibodies, or other moieties that can bind to the metalized surface of the cantilevers [30].

Optical biosensors - Optical biosensors consist of transducers in nanoscales which rely on the measurement of photons for detecting the presence of biological analytes (figure 2.6d). Light from a light-source (e.g. lasers) is transmitted to a sensing layer composed of biorecognition molecules. The output light is then guided to a detector (e.g. spectrophotometer, photodiodes) where the reflected, scattered, emitted, or absorbed light is measured and interpreted. Optical biosensors have many advantages over classic analytic methods, such as a high signal to noise ratio, accuracy, fast and reversible sensing, multiplexing and biodegradable sensing mechanism [30].

Magnetic biosensor - The basic principle of a magnetic biosensor is based on the interaction between biomolecules at the nanoscale and a magnetic field (figure 2.6e). Usually, biomolecules to be detected are immobilized on a magnetic label and passed over on-chip magnetic sensor. The sensor senses the presence of magnetic labels by the alteration of magnetic field due to their inherent properties. Based on their working mechanism the magnetic biosensors can be divided in 4 types: (i) Hall effect biosensor (ii) Magnetoresistance (MR)-based biosensors (iii) Magneto-impedance biosensors (iv) Flux gate biosensor [30]. Only the magnetoresistance based biosensors will be discussed in this thesis as they were the chosen biosensors of work.

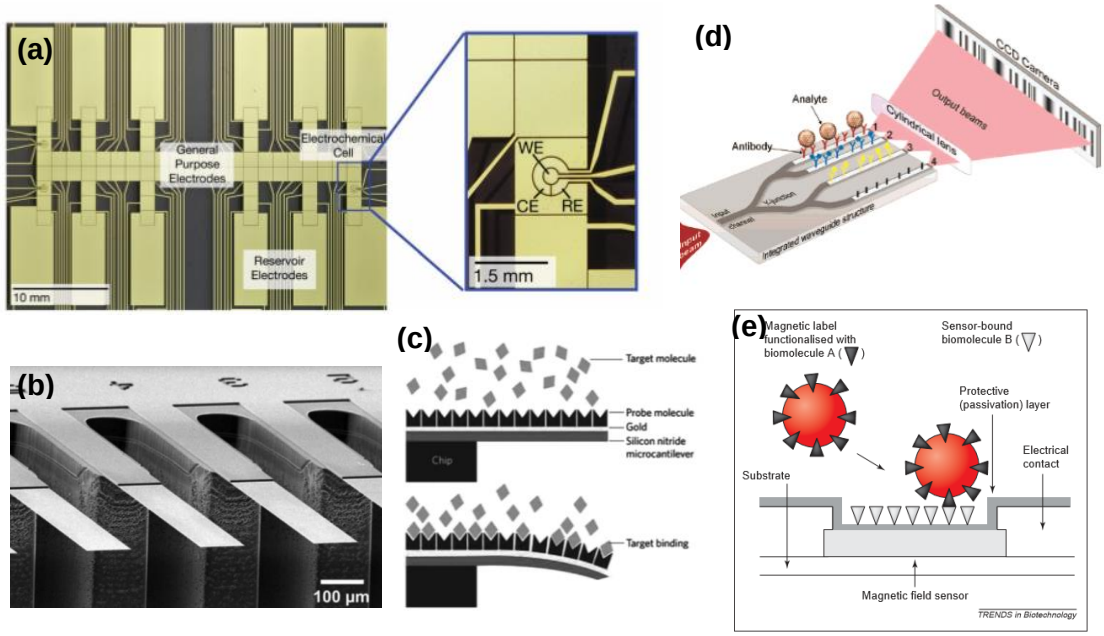

FIGURE 2-6 The four different types of biosensors according to their transduction principle: (a) Electrochemical biosensor. Photos and schematics of a three-electrode electrochemical cell (WE-working electrode, RE- reference electrode, CE- counter electrode) [31]. (b) Micromachined mechanical sensor array [32]. (c) Illustration of working principle of a cantilever sensor [32]. (d) Illustration of a four-channel integrated optical sensor [33]. (e) Illustration of the working principle of the detection of magnetic labelled biomolecules using magnetic biosensors [34].

2.2.3. (MR)-BASED SENSORS

The basic principle of the magnetoresistance (MR) is the variation of the resistivity of a material or a structure as a function of an external magnetic field, as generally described by the following general equation [35]:

$$R = f(B) \tag{2.10}$$

Magnetoresistive sensors have a wide range of industrial applications due to their simplicity of design, low cost, robustness, and temperature stability. In automotive and consumer electronic applications, MR sensors are used for current, position, speed and angle sensing as well as Earth's magnetic field sensing in compass applications. In biotechnology, MR sensors are used for bimolecular detection in protein assays using magnetic tags or in microfluidic systems for magnetic bead manipulation [36].

The anisotropic magnetoresistive (AMR) effect was first described in 1856 by William Thomson [37]. Thomson observed that the resistivity of ferromagnetic materials depended on the angle between the direction of electric current and the orientation of magnetization. In the following years, AMR sensors were

primarily used as read heads in magnetic hard disk drives. Another magnetoresistive effect was discovered in 1988 in thin ferromagnetic films by Grünberg, Binasch *et al.* as well as Fert, Baibich *et al*. [35]. This effect was denominated giant magnetoresistive effect (GMR), because the measured change of magnetoresistance largely exceled that of the AMR effect. They demonstrated that the electric resistance in a magnetic multilayer consisting of a sequence of thin magnetic layers separated by equally thin non-magnetic metallic layers was strongly influenced by the relative orientation of the magnetizations of the ferromagnetic layers (about 50% at 4.2 K). When aligning the magnetization directions of the ferromagnetic layers from the initial antiparallel state to a parallel configuration by applying an external magnetic field, the electrical resistance of the layer stack decreased [35], [36]. The reason for the changing electrical resistance is the spin dependence of electron transport, which affects the scattering rates at film interfaces for spin-up and spin-down electrons. In case of film thicknesses smaller than the mean free path of the electrons, which is in the order of nanometers, they move through all layers. For electrons passing the interface between the non-ferromagnetic layer and the ferromagnetic layer with its magnetization antiparallel to the electron spin, the scatter rate is higher than for the electrons passing through the interface between the non-ferromagnetic layer and the ferromagnetic layer with the magnetization parallel to the electron spin [35].

Although observed at first in multilayered thin films with interlayer exchange coupling, any material combination with interfaces between a ferromagnetic and a nonmagnetic metal is theoretically able to display GMR. Such is the case of spin valve structures, granular GMR where ferromagnetic granular particles are embedded into a nonmagnetic conductive matrix, and magnetic tunnel junctions (MTJs) (figure 2.7) [35].

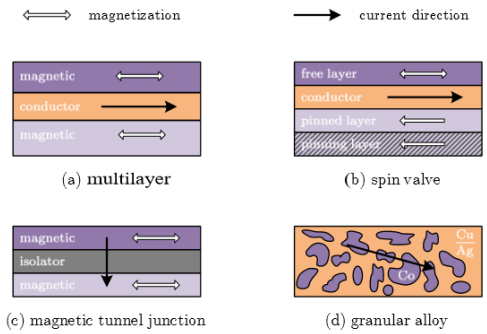

FIGURE 2-7 Schematics of the different GMR structures: (a) Multilayer structure, (b) Spin valve, (c) Magnetic tunnel junction (MTJ) and (d) Granular GMR structure [36].

The spin valve structure was first purposed in 1991 by Dienly and coworkers [38]. In spin valves, an additional antiferromagnetic (pinning) layer is added to the top or bottom part of the structure. A ferromagnetic layer is then pinned by exchange of the antiferromagnetic layer, while the other ferromagnetic layer remains free to rotate. A typical spin valve structure consists then of two ferromagnetic layers, separated by a Cu spacer (figure 2.8) [39].

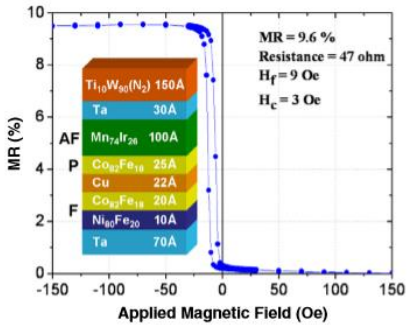

FIGURE 2-8 Typical spin valve stack and respective magnetoresistance varying with magnetic field. (AF- antiferromagnetic layers, P- Pinned layer, F- Free layer) [39].

Typical MR values displayed by spin valves are 4%–20% with saturation fields of 0.8–6 kA/m [40].

2.2.4. MAGNETORESISTIVE BIOCHIPS

The biochip consists of an arrangement of single or multiple biosensing elements in a series of sensing zones, designed and fabricated on-chip. The chip dimensions (usually mm scale) are defined and the available chip surface is used as efficiently as possible, in such a way as to maximize the active sensing area within each sensing zone, to incorporate appropriate reference sensors and to avoid electrical, magnetic or thermal crosstalk between sensors or on-chip structures [34]. For static detection with magnetic microarrays, a passivation layer for a sensor chip is vital for the device sensitivity. The most widely demonstrated passivation layers include Si_3N_4, Al_2O_3/SiO_2 bilayers, and polymers. Si_3N_4 is a good isolation layer and is often used for passivation, because a very thin layer down to 30 nm can be obtained allowing for the sensitive detection of superparamagnetic nanoparticles [41].

These biochips are used in bioassays where a recognition biomolecule (antibody, DNA probe, and so on) is immobilized on the surface of the sensor and a medium containing the target molecule (DNA strand, antigen protein) labeled with a magnetic particle is in contact with the sensor surface. If there is biorecognition between target molecule and the one immobilized, binding of the molecules will occur. Washing of the biochip will remove all unbound particles and non-specific interactions. Then, applying an external magnetic field, the magnetic labels attached to the target molecule will create a fringe field that is detected by the magnetoresistive sensor.

2.2.5. MAGNETORESISTIVE STATIC PLATFORM

A magnetoresistive platform adapts the format of conventional optical microarrays that rely on patterning different types of capture molecules on the surface of a substrate for multiplexed immunoassays. Instead of using a laser and fluorophores for detection and labelling, magnetic microarrays use magnetic sensor arrays and magnetic particles as detectors and labels, respectively. Some of the existent prototypes implement biochips integrated with a microfluidic channel on a printed circuit board (PCB), measurement electronics, signal communication modules, and magnetic coils (figure 2.9 a-c) [41]. An ultraportable handheld MR diagnostic prototype was also made (figure 2.9 d-f) [42].

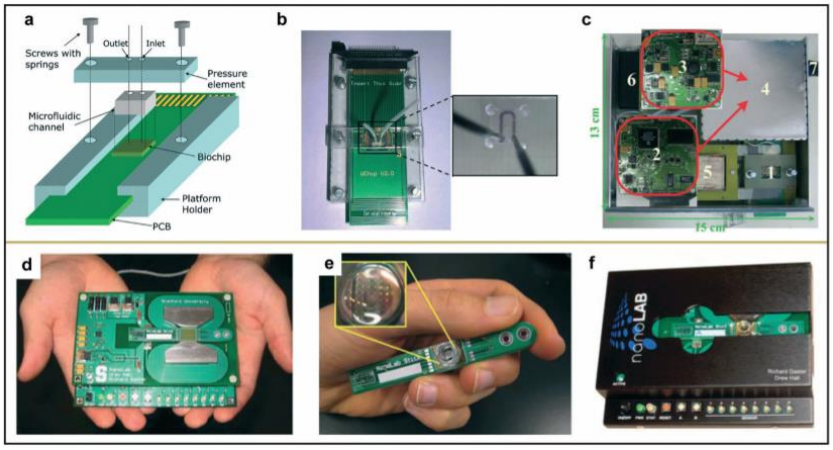

FIGURE 2-9 Some platform prototypes: (a) Schematic showing the assembly of a biochip aligned with a microfluidic structure [43]. (b) Photo of a biochip in a PCB assembled with PMMA plates and a PDS channel [43]. (c) Photo of the prototype system: (1) Biochip on a PCB, (2) Processing unit, (3) Signal communication module and magnetic drive circuits, (4) Noise shielding enclosure, (5) Magnetic coils, (6) Powering unit, (7) USB connector [43]. (d) Photo of a hand-held MR diagnostic device [41]. (e) Photo of a disposable stick with a reaction well attached on top of the sensor [43]. (f) Photo of a diagnostic device with a case and test stick [41].

Figure 2.9c shows a picture of the complete platform prototype. An important feature of the measurement system is the usage of a PCB as chip carrier, since this can be fully customized and is not expensive, which is an important aspect since the biochip is disposable. However, the cryptographic module and fluid controller module remained to be implemented [43]. This platform will be further discussed in the next chapter as it was used in the quantification of urease.

2.3. MICROFLUIDICS

Microfluidics deals with the science and technology of fluid flow over micron or sub-micron length scales, pertaining to the passage and manipulation of small volumes of liquids or gases (commonly, in femto-liter to micro-liter scale) through miniaturized conduits of varied geometrical shapes and practical functionalities.

Traditionally, silicon micromachining methods have been used to fabricate microfluidic channels from silicon and glass. In more recent years other types of materials such as Polydimethylsiloxane (PDMS) and Polymethyl methacrylate (PMMA) have been successfully employed for generating microfluidic structures. To understand microfluidics, one has to learn the basic principles revolving around the transport phenomena and flow physics in micro and nanoscale systems [44].

2.3.1. Fundamental Principles

The momentum equation that governs fluid dynamics is one of the most important equations of fluid mechanics. The momentum equation is essentially Newton's second law applied to a continuum. The momentum equation states that the time rate of change of linear momentum of a continuum is equal the sum of the forces acting on the continuum. Two types of forces are typically present: body forces that act on the bulk material inside the continuum and surface forces that act at the boundary surface. The differential momentum equation is written as the following equation:

$$\rho \frac{\partial \mathrm{V}}{\partial \mathrm{t}} + (V.\nabla)V = \rho F - \nabla p + \nabla \tau \tag{2.11}$$

where ρ is the fluid density, V is the fluid velocity vector, t is time, p is pressure, F is the external force vector and τ is the shear stress tensor. These are also known as Navier-Stokes equations [45].

The Navier–Stokes equations apply to numerous flow situations and are based on assumption of the continuum model for fluid. The continuum model ignores the molecular nature of gases and liquids and regards the fluid as a continuous medium describable in terms of the spatial and temporal variations of density, velocity, pressure, temperature, and other macroscopic flow quantities. The equations are greatly simplified when applied to incompressible flows in which variations in fluid viscosity can be neglected. Under these conditions, the equations reduce to Eq.2.12 [45].

$$\rho \frac{\partial \mathrm{V}}{\partial \mathrm{t}} + (V.\nabla)V = \rho g - \nabla p + \mu \nabla^2 V \tag{2.12}$$

where ρ is the fluid density, V is the fluid velocity vector, t is time, p is pressure, g is gravitational force, and μ is the fluid viscosity. These are also known as Navier-Stokes equations [45].

2.3.2. Laminar, Turbulent, and Creeping Flow

In many problems the flow pattern in a certain channel geometry or around an obstacle needs to be determined, either experimentally (by performing flow observations), theoretically (by solving the Navier-

Stokes equation), or numerically (by modeling it). The middle alternative is usually hard to solve for, and very rarely a complete solution to the Navier-Stokes equation can be found by theoretical means. In fact, only a few parameters are actually needed to characterize the flow, the so called dimensionless parameters [46].There are several dimensionless groups of parameters that are very important in assessing the state of a fluid in motion in a microfluidic system, one of those being the Reynolds number (Re), that correlates inertial forces to viscous forces[45]. The Reynolds number can be calculated by Eq.2.13.

$$Re = \frac{\rho V D_h}{\mu} \tag{2.13}$$

where ρ is the fluid density, V is the characteristic velocity of the fluid, μ is the fluid viscosity, and D_h is the hydraulic diameter. The hydraulic diameter depends on the channels cross-sectional geometry and can be calculated with the Eq.2.14.

$$D_h = \frac{4 \times cross - sectional\ area}{wetted\ perimeter} \tag{2.14}$$

The Reynolds number can, in the absence of external forces, uniquely characterize the solution to the flow equations. In other words, two problems at completely different scales may have identical solutions provided they have equal Reynolds numbers [46]. For Re < 1, the velocity field is time-independent, fully laminar, and completely reversible. As the Reynolds number starts to grow the flow becomes unsteady, with a somewhat cyclic time dependence. As Re increases further, there start to appear regions of turbulence and the flow starts to become chaotic [46]. The Reynolds number of a fluid flow can then describe its flow regime, laminar or turbulent (figure 2.20).

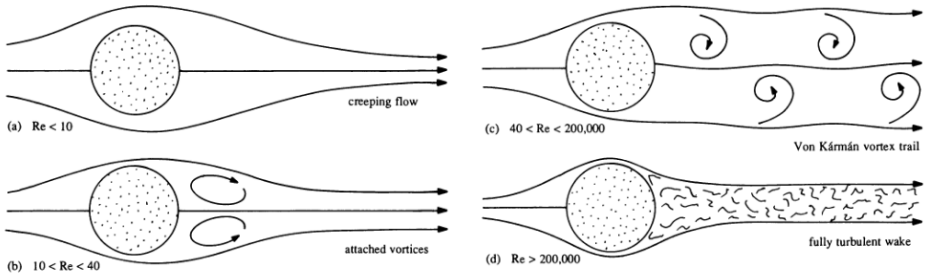

FIGURE 2-10 Schematics of different flow regimes with respective Reynolds numbers [47].

Laminar flow is described as smooth or streamlined flow, while Turbulent flow is chaotic. Re < 2300 generally indicates a laminar flow. As Re approaches 2300, the fluid begins to show signs of turbulence, and as Re becomes greater than 2300, the flow is considered to be turbulent. Microfluidics can be a special

case since one can be dealing with relatively small Reynolds numbers, Re < 1. It represents a limiting case of laminar flow and occurs when viscous forces completely dominate inertia forces. In these conditions, instead of the Navier-Stokes equation, the Stokes equation is used [46]. This type of flow is known as Creeping flow.

2.3.3. Interfacial Boundary Condition in Liquids: Slip and No-slip

The traditionally applied no-slip boundary condition at the fluid–solid interface is an idealized paradigm, which assumes moderately strong attractive forces between the fluid and wall. However, effects of surface tension, liquid evaporation, porosity, osmotic transport, van der Waals forces, electrostatic forces, etc. may potentially result in deviations from this classical notion [44].

It has been hypothesized by many researchers that the no-slip boundary condition arises because of the microscopic asperities on the surface. The liquid molecules may get locally trapped in the surface asperities and thus may not be able to escape from the contact with the solid boundary because of their otherwise compact intramolecular packing. In this logic, it makes sense that a molecularly smooth boundary would allow the liquid to slip, because of the non-existence of the surface asperity barriers. This is confirmed by recent studies which have demonstrated that the assumption of 'no slip at the boundary' can fail greatly not only when the fluidic substrates are sufficiently smooth, but also when they are sufficiently rough. The reasons behind such anomalous behavior lies in fundamental interfacial interactions (such as wettability) [44].

2.3.4. Drive of the Fluid flow

There are many ways to drive the fluid flow through a microfluidic device, which include the classical driving fluid method relying on the action of pressure difference and the more recently introduced methods use phenomena on the basis of electrokinetic and capillary forces. The search for new principles to drive the fluid flow through a microfluidic device has continued since at microscales there is an increase in magnitude of required pressure difference. With very small cross sections, the necessary fluid pressure may often reach inconvenient levels endangering the mechanical integrity of the devices [45].

2.3.5. Materials

The choice of materials for microfluidics is critical, especially considering the application in biosensors. A broad range of materials have been demonstrated as viable compatible materials for creating advanced

and low-cost microfluidic devices. They can be divided in 4 categories: i. Inorganic materials ii. Elastomers and plastics iii, Hydrogel iv. Paper. A description of each is given bellow.

Inorganic Materials – In these types of materials are included silicon and glass, which were the first materials to be used for microfabrication. The silicon's surface chemistry, based on the silanol group (─Si─OH) is well developed and modification can be easily accomplished via silanes. For example, nonspecific adsorption can be reduced, or cellular growth improved through chemical modification of the surface. Due to its intrinsic properties, silicon is transparent to electromagnetic wavelengths in the infrared spectrum but not to wavelengths in the visible light spectrum, making typical fluorescence detection or fluid imaging challenging. Silicon possesses good thermal conductivity and is resistant to high temperatures; therefore, it is suitable for applications requiring a relatively high operating temperature, such as polymerase chain reaction (PCR). However, silicon substrates are relatively expensive when compared with other materials, such as glass and polymers. Furthermore, the fabrication process for silicon-based microfluidic devices involve substrate cleaning, resist coating, photolithography, development, and wet/dry etching which are time consuming and costly [30]. An example of a microfluidic device using silicon can be seen in figure 2.11a.

Several types of glass are used in microfluidic devices such as soda lime, quartz, and borosilicate. In relation to silicon, glass has the advantage of being transparent and chemically stable. It's also an ideal material for working with biomolecules since glass has the property of relatively low nonspecific adsorption. It has, however, the disadvantage of not being suited for complex multilayered devices because bonding glass-based device layers to create sealed channels often needs high temperatures and/or large electric fields [30].

Elastomers and Plastics - Polymer-based microfluidics were introduced after silicon/glass chips, though they have since become the most commonly used microfluidic materials. This is because, compared to inorganic materials, polymers are easy to access and inexpensive. Based on their physical properties, polymers can be classified into three groups: elastomers, thermoplastics, and thermosets.

Elastomers consist of cross-linked polymer chains that can stretch or compress when external force is applied and return to their original shape when the external force is removed (figure 2.11b).

One of the most know elastomer is PDMS. This type of material offers some advantageous features compared to the inorganic materials, such as having a shear modulus of 0.25 MPa and a Young's modulus of roughly 0.5 MPa which allows it to conform to a surface and achieve atomic-level contact, a feature that is useful in forming and in sealing microfluidic systems. Besides this, PDMS is optically transparent, readily available from commercial sources at decent prices (~$80/kg) and can sustain a large temperature range, from 100 to 300 ºC. Despite all of this, PDMS has a hydrophobic surface (due to the repeating $Si(CH_3)_2O$) that can lead to nonspecific adsorption of proteins and other molecules. However, the hydrophobic surface of the PDMS (with a water contact angle of ~110) can be modified to be hydrophilic (with a water contact

angle around 10) by brief exposure to oxygen plasma. Other disadvantages account for the fact that PDMS polymer network sometimes absorbs small molecules, leaches uncured monomers, and swells in solvents. Therefore, applications for PDMS devices are restricted to aqueous solutions [30].

Thermoplastics are a class of synthetic polymers that exhibit softening behavior above a characteristic glass transition temperature (Tg), while also allowing them to return to their original chemical state upon cooling. The most common examples of thermoplastics used in the microfluidic design are PMMA, polycarbonate (PC), and cyclic olefin polymers (COP) or copolymers (COC) (figure 2.11c). PMMA has the advantages of being biological compatible and gas impermeable. Covalently modified surfaces are also, generally more stable in thermoplastics than in PDMS. For example, after treatment with oxygen plasma, the surface of PMMA retains hydrophilicity for up to a few months [48]. They show a slightly better solvent compatibility than the PDMS elastomer, however, they are incompatible with most organic solvents, such as ketones and hydrocarbons [30].

Thermosets are covalently cross-linked polymers and thus do not melt. From a manufacturing point of view, thermosets are shaped during the polymerization and cross-linking process. Because of the covalent bond formation, thermosets exhibit higher residual stress, shrinkage and crack-formation compared to thermoplastics. Their main advantages rely on their geometrical stability and solvent resistance. Common thermosets used in microfluidics are the SU-8 photoresist (MicroChem, USA), and the optical glue NOA81 (Norland Products, Inc, USA) [30]. The last one has been used for solvent resistant microfluidics (figure 2.11d) [49].

Hydrogel- Hydrogels are a class of crosslinked hydrophilic polymer networks that can change their volumes reversibly by more than one order of magnitude due to small changes of certain environmental parameters, such as pH, glucose temperature, electric field, light, as well as by the carbohydrates and antigens present [50]. Hydrogels can be natural (e.g., collagen, gelatin, and fibrin, and polysaccharides) or synthesized in a laboratory (e.g., polyethylene glycol, polyacrylic acid, and polyvinyl alcohol) (figure 2.11e). Jinseok et al. described a microfluidic biosensor that uses an array of hydrogel-entrapped enzymes to quantitatively determine the concentration of an analyte and simultaneously detect multiple analytes [51].

Paper- Paper has recently become an alternative material to inorganic or polymeric materials for fabricating microfluidics devices (µPADs) due to the fact that it is a ubiquitous and inexpensive cellulosic material, it's compatible with many biochemical and medical applications and that it transports liquids using capillary forces without the assistance of external forces. Filter paper (Whatman Grade 1) and chromatography paper are the most widely used substrates for µPADs. They are composed of pure cellulose, which has abundant hydroxyl groups (—OH) and a few carboxylic acid groups (—COOH) on the fiber surface. Since cellulose has a slightly anionic surface, it can serve as a scaffold for immobilizing positively charged biomolecules. The fundamental working principle of this technology is to create hydrophobic barriers onto the sheet of hydrophobic cellulose matrix, which will constitute the micron-sized capillary channels. µPADs

have some disadvantages, namely the low efficiency of sample delivery to the sensing surface due to the retention of samples within the paper fluidic channels (less than 50%) [30]. An example of a microfluidic paper structure can be seen in figure 2.11f.

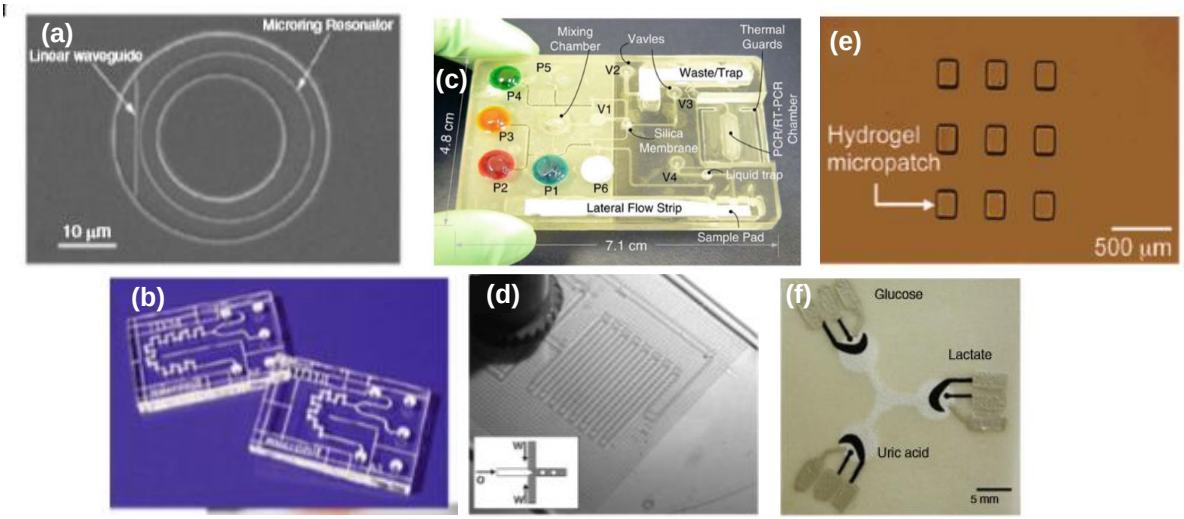

FIGURE 2-11 Different types of materials to be employed in microfluidics: (a) Top-view SEM image of a microring resonator made from silicon [30]. (b) Commercial elastomer-based microfluidic devices [30]. (c) Photo of the PMMA nucleic acid cassette [30]. (d) Photo of a flow focusing drop emitter made with a NOA 81 sticker [49]. (e) Image of an array of hydrogel micropatches confined to the surface of a modified glass [51]. (f) Three-electrode paperfluidic device [30].

2.3.6. MICROFABRICATION TECHNIQUES FOR ELASTOMERS AND PLASTICS

It will only be discussed microfabrication techniques for two types of materials, PDMS and thermoplastics, since they are the most used. Figure 2.12 shows the polymer microfluidics fabrication procedures and selection strategies associated with PDMS (blue line) and thermoplastics(redline).

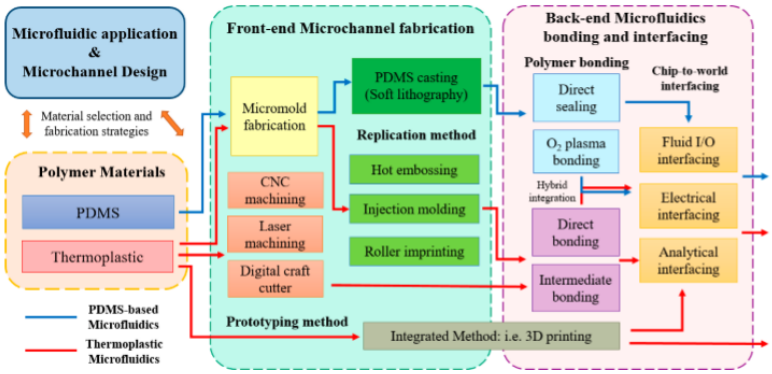

FIGURE 2-12 Representation of the various microfluidic fabrication Processes for PDMS (blue line) and Thermoplastics (red line) [52].

PDMS microchannels are mostly fabricated by a simple soft lithography (figure 2.13) process in which the PDMS reagent is directly cast onto a master mold, followed by a bonding process. The typical PDMS casting procedure is performed by mixing a PDMS base with a curing agent, followed by curing. The PDMS layer is then released from the mold to complete the casting procedure. SU-8 resin and standard photoresist (PR) can be used as molds in PDMS procedure [52].

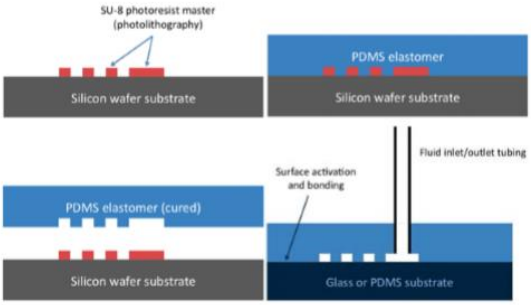

FIGURE 2-13 Typical PDMS molding process. Top left: SU-8 mold is prepared by photolithography to provide a negative of the desired surface topography. Top right: The PDMS is and cured. Bottom left: The cured PDMS stamp is separated from the master template. Bottom right: Holes are poked for the fluid inlet and outlet, and the PDMS is bonded to either a glass slide or another PDMS substrate [46].

Since the casting process is such a simple process and the layer is easily released from the mold, PDMS casting is a reliable and high yield procedure. A PDMS layer can be directly sealed to another PDMS or glass substrate via van der Waals forces without the need for further fabrication procedures. To meet high bonding requirements however, the PDMS bond strength can be enhanced by using oxygen plasma treatment to form an O–Si–O covalent bond at the PDMS interface [53]. More details on the microfabrication of PDMS molds can be found in chapter 3.

For the thermoplastic microfluidic channels fabrication, various fabrication options can be used, the most utilized being hot embossing, and injection molding. Hot embossing involves pressing a microstructured material into a preformed plastic part at a temperature close to the glass transition of the polymer [46]. In Injection molding the plastic is heated above its glass transition temperature (or its melting point, in the case of a crystalline polymer), and then injected into a multiple-part metallic mold. The assembly is then cooled, the mold is opened, and the part is separated from the mold. Injection molding can be a very fast fabrication with one part taking as little as a few seconds [46].

In the thermoplastic fabrication process, bonding is a critical last step that determines the bonding strength, geometry stability, optical transmissivity, and surface chemistry of the produced microfluidic device. Thermal methods are the most common techniques for bonding thermoplastics. In the classical bonding process, the two plastic parts are brought into contact in a hot press, and heated close to the melting

temperature. The increased mobility of the polymer chains results in enhanced diffusion across the interface, effectively bonding the chips. The pressure and temperature need to be carefully controlled, or else the devices will be damaged during the process. The heat for thermal bonding methods can also be provided locally by a laser which allows significantly more complicated geometries to be built [46].

Recently, 3D printing technologies have become a popular prototyping method for fabricating the polymer microfluidic devices [54], [55].

2.3.7. Microfluidics and Biosensors in Diagnostics

According to a recent National Institute of Health (NIH) report, point-of-care (POC) testing has the potential to introduce a paradigm shift into personalized medicine by creating a link between disease diagnoses and the ability to tailor therapeutics to the individual [56]. Being a technique that primes of being near-patient, the POC sensors are built around the idea that they should operate as lab-on-a-chip devices, implying that they are miniaturized automated laboratories. The only way to achieve this and surpass the need for lab techniques that require culture bottles, petri dishes, and microtiter plates is to employ microfluidics. Analysis rates for POC devices integrated with microfluidic channels are usually shorter and several assays can be integrated in a single system without extending the size and complexity of the device [30]. A variety of samples including blood, urine, saliva, stool, and plasma, amniotic and cerebral fluids have been used for diagnosis in POC devices.

2.3.8. Biological Applications

In the last decade, the applications for microfluidic devices have proliferated at an explosive rate similar to the revolution brought in the field of microelectronics by the invention of the integrated circuit [57]. The similarity in the dimensions of cells and microchannels (10–100 μm widths and depths) plays a crucial role in modifying the procedures of molecular biology for enzymatic analysis, DNA analysis, and proteomics [30].

Jung et al. [58] performed flow-based sorting of human mesenchymal cells by using optimally designed microfluidics chips based on the principle of hydrodynamic filtration.

In the neurological realm, microfluidics is employed for both in vivo deliveries of drug solutions from on-chip reservoirs situated on neural implants as well as in vitro studies of neuronal cells via highly precise delivery growth and inhibitory factors by the use of gradient-generating devices [59].

Mauleon et al. [60] developed an microfluidic system that allows diffusion of oxygen throughout a thin membrane and directly to the brain slice via microfluidic gas channels. The device consists of four independent parts: the perfusion chamber, the PDMS layer, the PDMS microfluidic channel, and a glass slide.

Caviglia et al. [61] developed a microfluidic cytotoxicity assay for studying the impact of anticancer drugs doxorubicin and oxaliplatin. The targeted drug delivery tested the cytotoxicity and was evaluated using real-time impedance monitoring.

A microfabricated lung mimic device was created which uses compartmentalized PDMS microchannels to form an alveolar capillary barrier on a thin, porous, flexible PDMS membrane coated with extracellular matrix (ECM) [62].

3. MATERIALS AND METHODS

3.1. MAGNETIC LABELS

Diverging from the conventional ELISA (enzyme-linked immunosorbent assay), the reporter group used in this work is not biological in nature. Instead, nanometer sized magnetic particles (MP) (250 nm, Nanomag-D, Micromod, Germany) will be used. These particles are 75-80% (w/w) magnetite, coated with dextran (40 kD) and modified with streptavidin proteins that will specifically bind to the biotin modification present in the target biomolecules used, with the streptavidin-biotin being the strongest non-covalent biological interaction known. These nanoparticles are superparamagnetic, meaning they have zero magnetization in the absence of a magnetic field. When superparamagnetic nanoparticles are immersed in a magnetic field, they become uniformly magnetized.

The magnetization (M) of monodisperse non-interacting magnetic nanoparticles under an applied external field H can be modelled by a Langevin-like function:

$$M = M_s \left[\coth\left(\frac{\mu_0 m_p H}{k_B T}\right) - \frac{k_B T}{\mu_0 m_p H} \right] \tag{3.1}$$

where m_p is the magnetic moment of the nanoparticles inside the matrix and M_s is the saturation magnetization [63]. Micromod 250 nm particles magnetization in function of an external magnetic field was measured in a vibrating sample magnetometer (VSM) system (DSM 880 VSM). A volume of 20 µL of nanoparticles at the stock concentration was injected in a recipient and was then measured. The measured moment in the VSM system corresponds to the sum of the magnetic moments of each particle. To be able to compare susceptibility between different particles, the magnetization of each particle had to be calculated. As such, the measured magnetic moment was divided by the number of particles in the sample (known from the data given by the supplier) and by the particle volume.

Figure 3.1a shows the magnetization curve obtained for the Micromod 250 nm particles, measured in the range of -3000 to +3000 Oe. The Langevin-like function describes relatively well the magnetization curve. However, in the electronic set-up used to magnetize the magnetic particles, the magnetic field varies between a lower range. Analyzing a low field regime (between-50 Oe and 50 Oe), the 250 nm particles

magnetization did not show a good fit (figure 3.1b). An excess of susceptibility is observed in this field range indicating that the nanoparticles inside the label polymeric matrix may be interacting [63].

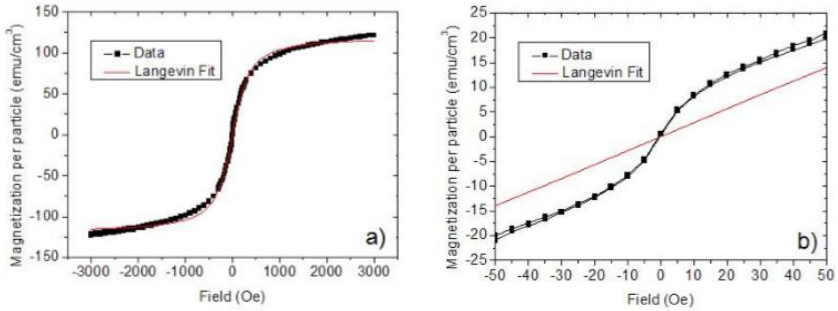

FIGURE 3-1 (a) Magnetization of Micromod 250nm particles in function of an external magnetic applied field. Fit was done using Langevin-like model. (b) Low field magnetization of Micromod 250nm particles in function of an external magnetic applied field. Figures taken from [63].

The Micromod 250 nm particles have a magnetic moment of 1.6 x 10-16 $A.m^2$ for a 1.2 kA/m magnetizing field and a susceptibility of $\chi \sim 5$ [64].

3.2. DETECTION METHODS

3.2.1. DIRECT ELISA

ELISA (enzyme-linked immunosorbent assay) is a method designed for detecting and quantifying substances such as peptides, proteins, antibodies and hormones. In an ELISA, an antigen must be immobilized on a solid surface and then complexed with an antibody that is linked to another molecule, usually an enzyme. The most commonly used enzyme labels being horseradish peroxidase (HRP) and alkaline phosphatase (AP). In this thesis however, a magnetic label conjugated to an antibody via streptavidin-biotin interaction will substitute the enzyme. Although in conventional ELISA the detection is accomplished by assessing the conjugated enzyme activity via incubation with a substrate to produce a measurable product, the detection with the magnetic particles will occur by measurement of the fringe field produced by those while subjected to an external magnetic field. In figure 3.2 the schematics of Direct ELISA is presented.

FIGURE 3-2 Illustration of the direct ELISA detection method on the left accompanied by the typographical illustration on the right. The colors of the components on the left correspond to the words in the same color on the right [10].

The direct ELISA assays were first performed on gold substrates which have the same composition of the covering layer of the biosensors on the chips surface. In the last stages they were performed on the Biochip sensors.

The gold coated substrates used had dimensions of 5 x 7 mm^2 and had been previously covered with photoresist for surface protection. The gold layer consists of 5 nm titanium plus 40 nm of gold, sequentially sputtered (Alcatel, SCM-450) over a 6-inch silicon wafer. At first, the photoresist was stripped from the substrates using Microstrip 3001 solution supplied by FujiFilm electronical materials. After two hours of immersion on this solution, the substrates were rinsed with isopropanol (IPA) and deionized water (DI), and blown-dried with a compressed air gun. After this, the gold coated substrates were exposed to ultraviolet light/ozone plasma for 11min at 28mW/cm^2 inside an UVO cleaner machine from Jelight, USA. This UVO cleaner cleans the surface by exciting and/or dissociating contaminant molecules of photo resists, resins, human skin oils, cleaning solvent residues, silicone oils, etc. The same cleaning treatment, inclunding the ultraviolet light and ozone plasma, was given to the biochips before usage.

Gold was the chosen metal to act as a surface for the immobilization of biomolecules due to the electrostatic interactions, hydrophobic or hydrophilic molecules interactions established with proteins. However, the resulting layer is likely to be heterogeneous and randomly oriented, since each molecule can form many contacts in different orientations. A crosslinker is then a reagent that chemically joins two or more molecules by a covalent bond, as it contains two or more reactive ends, which are capable to chemically attach to specific functional groups of proteins or other molecules. The crosslinker used in this work is the one proposed by Cardoso [9], the Sulfo-LC-SPDP (Sulfosuccinimidyl 6-(3'-[2-pyridyldithio]-propionamido)hexanoate). This linker is a water-soluble long-chain molecule. It binds to the gold through the thiol (SH) group. This formation of chemical bonds between gold and sulfur is very strong, with the Au\S bonds having been extensively used in the formation of self-assembled monolayer (SAM) films. SAMs using Au\S bonds have been used for the immobilization of sulfur-terminated organic molecules on gold surfaces [65]. The aliphatic chain end links to lysines present in the protein via an amide bond [66]. A scheme of this process is represented in figure 3.3.

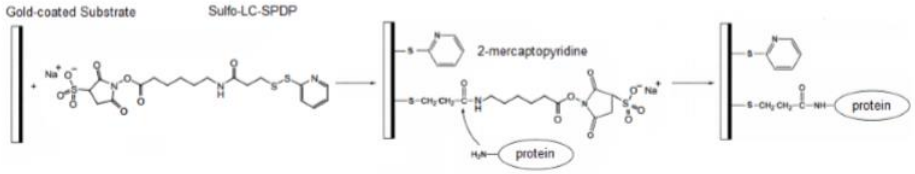

FIGURE 3-3 Schematics of the interaction between the Sulfo-LC-SPDP, the gold surface and the protein of interest. The linker binds to the gold through a thiol group while the end of the aliphatic chain in the former forms an amide bond with the protein. Figure taken from [9].

The working solution of antibody used in ELISA was a rabbit polyclonal biotin conjugated anti-*C. ensiformis* urease from Rockland diluted in PBS 0.1 M pH 7.4 (40g NaCl, 1g KCl, 7.2g $Na_2HPO_4.2H_2O$, 1.2g KH_2PO_4 in 500 mL of H_2O) with a concentration of $1.32x10^{11}$ particles/µL. The urease used is from *C. ensiformis* (Jack bean) from Sigma-Aldrich and was prepared by dilution in PBS 0.1 M pH 7.4 at the desired

concentrations varying between 0.1 and 100 mg/mL. Although *C. ensiformis* is not the microorganism used in field applications of biocementation, it's more commercial available. A protein Basic Local Alignment Search Tool (BLAST) was made between urease from *C. ensiformis* and the urease from *B. pasteurii*, obtaining 59% of identity (see Appendix A.1). Urease produced from *Bacillus pasteurii* in a laboratory was also used (see subchapter 3.3).

The experimental assay for the Direct ELISA follows similar guidelines as the ones used by Sara [9] and Valentim [10]. It starts by manually spotting 1 µL of the crosslinker agent prepared with a concentration of 2.23 $x10^{15}$ particles/µL in PBS 0.1 M pH 7.4 on top of the sample. After a waiting period of 20 minutes, the sample is washed with PBS buffer 0.1 M pH 7.4 to remove any unbound crosslinker molecules. The sample is left to dry at room temperature. A volume of 1 µL of urease in PBS is then spotted on top of the sample and stored inside a Petri dish in a humid atmosphere to prevent evaporation and at room temperature (24 ºC). The immobilization of the urease to the linker takes 1 hour. In the meantime, the magnetic particles solution should be prepared. This solution is composed of streptavidin coated magnetic nanoparticles and antibodies in a volume ratio of 1:1 (10 µL of solution with $4.9x10^{8}$ magnetic particles to 10 µL of working antibody solution), and PBS Tween 20 0.02% (v/v) as a solvent. The magnetic particles, antibodies and PBS Tween-20 are present in the solution in a ratio of 1:1:10, respectively. One begins by pipetting 10 µL of magnetic nanoparticles from the stock solution to an empty Eppendorf. The Eppendorf is then placed in contact with a magnetic concentrator (DynaMag-2 invitrogen). Attracted to the magnet, the particles will group together and stick to the side of the Eppendorf that is in contact with the magnet. This allows the collection, and subsequent discarding, of the suspension medium. This step is necessary since the magnetic particle solution has sodium azide 0.02% that can denature the antibodies. The Eppendorf is then taken away from the proximity of the concentrator and the pellet of magnetic nanoparticles is resuspended in 10 µL of PBS Tween 20. This process is repeated two times more. At the fourth time, instead of adding 10 µL of buffer, 10 µL of antibody solution are added. The solution is left mixing for 45 minutes in a rotator stirrer (model 3000445, JP SELECTA) after which the Eppendorf is put in contact once more with the magnetic concentrator for one last medium substitution. This ensures that the only antibodies in the solution are the ones coupled to a magnetic nanoparticle. With the magnetic particles solution prepared, and after the urease waiting time is over, 1 µL of the former solution is spotted on the sample surface. The sample should be left to settle for 30 minutes in a humid environment at room temperature. After, the samples should be manually washed with PBS Tween 20 and observed under an optical microscope (DFC 300 FX, Leica) after it has dried. To be noted that this process was done in gold dies and biochip sensors. An image of this process is seen bellow (figure 3.4).

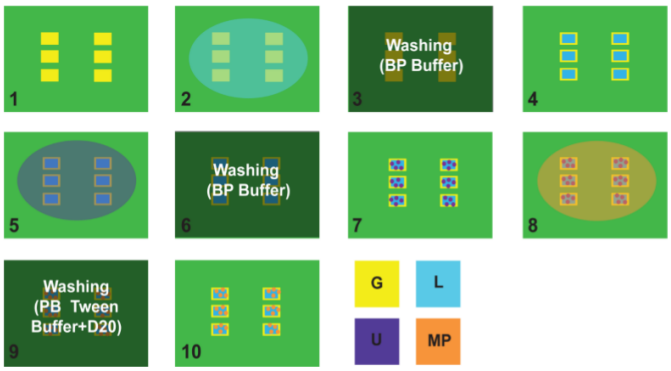

FIGURE 3-4 Scheme for the experimental procedure using the direct ELISA method. (1) Sensors covered with gold (2) Solution of linker is spotted over the sensors (3) Washing step with PBS 0.1 M pH 7.4 (4) The linker is now covering the sensors (5) A solution of urease is spotted over the sensors (6) After an hour, another washing step with PBS buffer (7) The sensors should now be covered with urease enzyme (8) The solution with magnetic particles conjugated to antibodies is spotted over the sensors (9) After 30 minutes the sensors are washed with PBS Tween 20 followed by DI water (10) The urease present in the sensors is now conjugated to the Ab-magnetic particles complex that should be seen under a microscope. G-Gold substrate; L-Crosslinker; U- Urease solution; MP- Magnetic particles solution. Figure was taken from [10].

Alongside the standard assays, a negative control ELISA was also performed. This assay follows the same protocol of the standard ELISA with the difference of PBS being spotted instead of urease.

Another experimental method for the ELISA assay was also tried. This assay proceeded in the exactly same way as the one above described with the difference that the urease in varying concentration was pre-recognized with the antibody (Ab)-conjugated magnetic particles solution (with concentration used in conventional direct ELISA assay previously described) in a volume ratio of 1:1. This solution was then left for 1 hour in moderate agitation, after which 1 µL of it was spotted in the sample.

3.2.2. SANDWICH ELISA

The sandwich ELISA differs from the Direct ELISA by using two antibodies (capture and detection antibody) instead of one. The capture antibody adsorbs to the surface and captures the target while the detection antibody conjugated with magnetic particles binds to the target (figure 3.5).

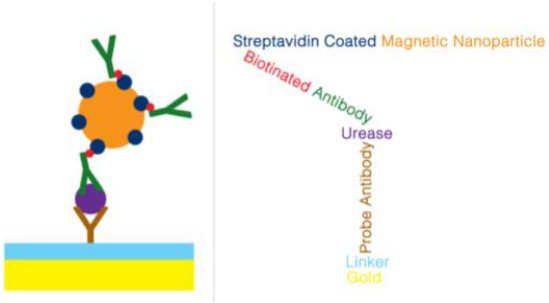

FIGURE 3-5 Illustration of the sandwich ELISA detection method on the left accompanied by the typographical illustration on the right. The colors of the components on the left correspond to the words in the same color on the right [10].

Antibody adsorption on a solid surface occurs through hydrophilic and/or hydrophobic interactions between antibodies and target solid substrates. If the antibodies are randomly oriented on the surface, nonspecific binding can occur through protein–protein (hydrophobic/hydrophilic and electrostatic) interactions. These nonspecific binding will reduce the number of available binding sites and might be a problem in an immunoassay. To obtain a more arranged and stronger attachment to the surface, the linker molecule Sulfo-LC-SPDP was used as proposed by Sara [9].
The antibodies recognize the epitope on the antigen present in the target molecule via the Fab regions located on the tips of the Y branches. As such, the antigen to be measured must contain at least two antigenic epitopes capable of binding to the antibody, since at least two antibodies act in the sandwich. While it is common to use two different antibodies for the capture and detection, in this thesis the same antibody was used as both. Since the antibody used is polyclonal, it recognizes various epitopes in the target, so the two layers of antibodies should be formed around the protein. The advantage of Sandwich ELISA is that the sample does not have to be as purified before analysis, with the assay being up to 2 to 5 times more sensitive than direct ELISA.

The experimental assay for Sandwich ELISA is similar to the Direct ELISA, differing in the urease immobilization to the surface. After spotting the linker and cleaning the sample with PBS, 1 µL of antibodies working solution are spotted and left to settle for 1 hour inside a Petri dish in a humid environment. After another cleaning step using PBS buffer, 1 µL of 0.1% (m/v) bovine serum albumin (BSA) is spotted on the sample for 1 hour. This step serves as a blocking step where the remaining nonspecific active sites in the antibody should be blocked by the BSA protein. The sample is again washed with PBS and the antigen is spotted on top of the antibody layer and left to settle in a humid atmosphere for 1 hour. From this point onwards, both tests proceed in the same manner.
Alongside the standard assays, negative controls were also performed consisting of spotting PBS instead of urease.

In the sandwich ELISA assay the method of immobilizing the urease on the surface after the binding of the complex Ab-magnetic particles to its epitopes was also performed. This assay proceeded in the exactly the same way was the one already described for the direct ELISA.

3.3. *BACILLUS PASTEURII* GROWTH

3.3.1. CULTURE GROWTH

Cultures of *B. pasteurii* previously grown by Pedreira [67]were stored at -80°C in 2 mL cryovials. For the preparation of the pre-inoculum, the 5 mL of the cultivation medium were inoculated with 50 µL (1% v/v) of

the thawed cultures. The cultivation medium was adopted from [68] and [5] and prepared by mixing the compounds listed in Table 3-1 in 5 mL of distilled water. Six falcons (sextuples) with 5 mL were prepared in total. All the medium components were sterilized in separate by autoclaving at 121°C for 20 minutes.

TABLE 3-1 Culture medium components used in the growth of *B. pasteurii* and their respective concentrations, brands, and purity.

COMPOUND	FINAL CONCENTRATION	BRAND	PURITY
Yeast extract (YE)	20 g/L	Liofilchem	-
$(NH_4)_2SO_4$	10 g/L	Panreac	>99%
$NiCl_2.6H_2O$	1 mM	-	-
Urea	0.5 M	-	-
Tris-base	0.13 M	Eurobio	-

After autoclaving, the bacteria cells were then added to the medium under sterile conditions. This procedure was performed under aseptic conditions (sterilization under UV light for 15 minutes) in a laminar flow chamber (BIOAIR Instruments aura 2000 MAC 4 NF, Italy) using sterile material. The pre-inoculum was incubated at 30°C in an orbital incubator (AgitorB 200 ABALAB) at 250 rpm for approximately 12 hours.

Afterwards, all six pre-inocula were put together in a 50-mL flask, obtaining a total of 30 mL of medium. Cellular growth was monitored offline by measuring the optical density (OD) of samples at 600 nm in a double beam spectrophotometer (Hitachi U-2000), using 3 mL glass cuvettes with an optical path length of 1 cm. For the OD determination, an aliquot of the culture sample was diluted with deionized water in order to obtain an absorbance value lower than the threshold (ca. 0.5-0.6), usually 1:10 dilution. Culture medium not inoculated was used as reference.

The OD of the 30 mL medium was measured and the volume necessary to achieve an OD of 0.1 was pipetted from the medium and diluted with culture medium not inoculated in a flask. In total, three flasks with OD of 0.1 were prepared and incubated at 30°C in an orbital incubator at 250 rpm. OD measurements were made during the growth until a desired OD of 1 was reached and the culture growth stopped.

The resulting culture medium was then centrifuged in Centrifuge 5810 R from Eppendorf at 6000xg, 4ºC and for 5 minutes. The supernatant was discarded, and the pellet was kept at 4ºC overnight.

3.3.2. Sample Preparation and Concentration

For further use of the obtained urease in the cell lysate, a step was needed to increase the concentration of urease in the sample while removing other unwanted proteins and debris. Since urease is an intracellular protein, the first step is to disrupt the membrane of the bacteria and release the enzyme. First, the pellet is resuspended in 4 mL of PBS 50 mM pH 7.4, after which this solution was sonicated for 10 minutes with the settings of 24.650 kJ, 60s ON, 60s OFF, 45 W, MS 72 in a sonicator from Bandelin. Afterwards, 2.5 mL of

the sample are centrifuged using Amicon Ultra-0.5 mL 100 kDa (Merckmillipore) at 4000xg, 4ºC and for 15 min. A temperature of 4ºC was employed since proteins are more stable at this temperature. A concentrated solution was obtained. The last step was only performed for samples that didn't undergo colorimetric assays

3.4. COLORIMETRIC ASSAYS

3.4.1. BCA PROTEIN ASSAY

In order to measure the concentration of total protein in the solution, a Pierce TM BCA Protein Assay kit was employed. This kit uses a method that combines the biuret reaction (Cu^{+2} to Cu^{+1} by presence in an alkaline medium) with the highly sensitive colorimetric detection of the cuprous cation (Cu^{+1}) by using a reagent containing bicinchoninic acid (BCA). The chelation of two molecules of BCA with Cu^{+1} forms a purple-colored product. This product exhibits a strong absorbance at 565 nm that is nearly linear with increasing protein concentrations over the range 20-2000 µg/ml. The protein concentrations are determined with reference to standards of BSA. A series of dilutions of known concentration of this protein are prepared and assayed alongside the samples with unknow concentration. The concentration of the standard solutions were 2000, 1500, 1000, 750, 500, 250, 125, 25 µg/ml and a blank. Following the kit procedure, 25 µL of each sample and standard were added to an 96-well microplate, followed by the addition of 200 µL of working reagent composed by two reagents present in the kit. The plate is incubated at 37ºC for 30 minutes, after which the absorbances of the wells are read at 562 nm in the SpectraMax Plus Microplate Reader (Molecular devices).

3.4.2. UREASE ACTIVITY ASSAY

For the measurement of the urease activity, the Urease Activity Assay kit (Sigma) was used. In the method provided by the kit, urease catalyzes the hydrolysis of urea resulting in the production of ammonia. The ammonia is then determined by the Berthelot method resulting in a colorimetric product measured at 670 nm, proportionate to the urease activity present in the sample. One unit of urease is the amount of enzyme that catalyzes the formation of 1.0 mmole of ammonia per minute at pH 7.0.

However, the presence of ammonia in samples will result in assay background. As such, ammonia in the samples was removed by filtration with an Amicon Ultra-4 Centrifugal Filter Unit with 10 kDa Molecular Weight Cut-Off (MWCO) membrane (Merckmillipore). The amicon was centrifuged at 3320 g and 16ºC for 40 minutes using a swinging-bucket rotor. In the end, each amicon (two in total) had a concentrate of approximately 70 µL. These solutions were each diluted with 130 µL of PBS pH 7.4 buffer. In this assay, standards were also needed. Standards using concentrations of 500, 400, 300, 200, 150, 100, 50 and 0

µM of Ammonium Chloride were prepared. A volume of 90 µL of both standards and samples were pipetted into separate wells of a 96 well plate, after which 10 µL of urea (according to the supplier information) were also added to each well. The mircroplate is then Incubated for 30 minutes at 30ºC. In the next step, 100 µL of Reagent A are added to each well to terminate the urease reaction, the plate is mixed, and then 50 µL of Reagent B are added. Finally, the plate is incubated for 30 minutes protected from light at 37ºC, and its absorbance is measured at 670 nm.

3.5. PROTEIN GEL ELECTROPHORESIS IN POLYACRYLAMIDE GEL

3.5.1. POLYACRYLAMIDE GEL ELECTROPHORESIS

In order to separate the urease from the pool of proteins obtained in the cell lysis, a protein gel electrophoresis was run with both the cell lysate and the pure urease from *C. ensiformis*. A polyacrylamide gel at 12% was prepared, where denatured samples were posteriorly loaded. The denatured conditions cause the alteration of the native conformation of the protein and allow the separation to occur by their size. This gel was formed by two parts with different composition. The upper one, stacking gel, where the samples were loaded and whose function was to line up the bands so that all the bands started at the same point. And the lower one, named resolving gel, where the samples run and separate in order of their molecular weight. In the Table 3-2 the composition of each buffer can be seen.

TABLE 3-2 Composition of the resolving gel (12%) and stacking gel (4%) necessary to make three 12% polyacrylamide gels.

Component	Volume needed for 3 gels (mL)	
	Resolving gel (12%)	Stacking gel (4%)
Acrylamide/bisacrylamide 40% (29:1, BIO RAD)	6.000	0.500
Resolving buffer, 4x (1.5M TrisHCl, 0.4% SDS, pH 8.8)	5.000	-
Stacking buffer, 4x (0.5M TrisHCl, 0.4% SDS, pH 6.8)	-	1.250
Milli-Q water	8.890	3.200
TEMED (99%, Sigma)	0.010	0.005
APS	0.100	0.025

A volume of 20 mL of the Resolving Gel were prepared, with the ammonium persulfate (APS) being added last since it's responsible for the polymerization. After, 5 mL of the mixture were pipetted to the gel support carefully so as not form air bubbles, with water being added on top of the gel. After it polymerizes (1-2 hours) the water was removed and the stacking gel 4% was prepared with 1 mL being pipetted into the gel, covering it. Combs are inserted in the gel and before continuing one has to wait for the gel to polymerize. After, the gel is removed from the support and, if needed, stored in water in the fridge for future use (up until 2 weeks).

The buffer used on the electrophoresis came from the dilution of running buffer 10x pH 8.3, which was made with 1 L of Milli-Q water, Tris with a final concentration of 25 mM, glycine with a final concentration of 192 mM and SDS with a final percentage of 0.1%. The samples to be loaded were prepared by adding 20 µL of the solution to be analyzed, 25 µL of Loading buffer (2x Alemmli Sample Buffer, BIO RAD) and 5 µL of DTT 1M that's responsible for denaturing proteins. The samples were then heated in water at 100ºC for 10 minutes in order to activate the denaturation action of DTT. The gel was mounted in the support and placed in the container. Running Buffer (1x) is poured inside the container and outside of the gel until the 2gel mark and inside the gel support until it's filled. The combs from the gel are carefully removed and 3 µL of the protein ladder PageRuler Plus Prestained Protein Ladder (Thermo Fisher Scientific) (see Appedinx A), as well as 25 µL of the samples, are pipetted into their respective wells in the gel. After loading the samples, a constant voltage of 80 V was applied so as to allow a better separation of proteins. When the front reached the intended point, the electrophoresis was stopped.

3.5.2. Coomassie Blue Staining

The polyacrylamide gel obtained after electrophoresis could be immediately stained or could be used for a western blot and then stained. After running the gel, it was disposed in a Coomassie bath for 1 hour at 25ºC and 60 rpm using an Agitorbb 200 incubator (aralab) in order to stain the bands of the protein in blue, after which they were washed with distilled water. The gels were then put in a bath with Destaining solution (30% ethanol, 10% acetic acid) at 25ºC, 60 rpm for 20 minutes (repeated at least 3x or until most of the blue color was stripped). Afterwards, the gel was scanned using a GS-800 Calibrated Densitometer (BIO RAD).

3.5.3. Silver Staining

For a more sensitive staining protocol, silver staining was performed after Coomassie Blue staining. The stained gel starts by being washed with ethanol 30% for at least 10 minutes, after which it's washed 2 times for 10 minutes each with Milli-Q water. The sensibilization happens next, consisting of a bath in 0.02% Sodium Thiosulfate for 1 minute, followed by 30 second wash with Milli-Q water, repeated 3 times. The gel is stained for 30 min with a 0.15% Silver Nitrate solution and then washed for 1 min with Milli-Q water. The next step is the development. One should always prepare a fresh development solution: 3% Sodium Carbonate and 0.05% Formaldehyde. The solution is poured until a brown precipitate appears in the gel. The solution is discarded, and fresh solution is added again. When the bands are sufficiently discretized, the gel is washed with 5% acetic acid for 15 minutes in order to stop the reaction, after which it is washed 2 times with Milli-Q water. In the end, the gel is scanned.

3.6. WESTERN BLOT

For the western blot, filter papers (Thermo Scientific), polyvinylidene difluoride (PVDF) Western Blotting Membranes (BioRad), and transfer buffer were prepared. The goal of the transfer of the proteins from the gel to the PVDF membrane was to allow their detection by antibodies by turning the proteins accessible. The PVDF membrane is characterized by its capacity to bind proteins by hydrophobic and dipole interactions, which makes it advisable to moisten the membrane with methanol before starting the transference.

The composition of the transfer buffer, as well as other buffers needed in the next steps can be seen in Tables 3-3 and 3-4.

TABLE 3-3 Concentrations and brands of the components used to prepare both the transfer buffer and TBS solutions necessary for the western blot immunoassay.

TRANSFER BUFFER			TBS (1X)		
Compound	**Concentration**	**Brand**	**Compound**	**Concentration**	**Brand**
Tris	25 mM	Eurobio	Tris	20 mM	Eurobio
Glycine	192 mM	-	NaCl	500 mM	Panreac
Methanol	20%	Fisher Scientific			

TABLE 3-4 Concentrations and brands of the components used to prepare both the blocking solution and detection solution necessary for the western blot immunoassay.

BLOCKING SOLUTION (IN TBS)			DETECTION SOLUTION (IN TBS)		
Compound	**Concentration**	**Brand**	**Compound**	**Concentration**	**Brand**
Nonfat dried milk	5%	Bio-Rad	3,3'-Diaminobenzidine (Dab)	0.5 g/l	-
Tween 20	0.1%	Acros Organics	Hydrogen Peroxide	30%	Sigma

The process starts with the gel being washed with transfer buffer and incubated for 5 minutes at 25ºC, 60 rpm. The PDVF membranes are then incubated in methanol for 15 minutes at room temperature, after which the methanol is removed, and the membrane is washed with transfer buffer. The membrane is then incubated with transfer buffer for 5 minutes at 25ºC, 60 rpm. The set up was mounted in the transfer system (Enduro Electrophoresis Systems) with the following order: filter, gel, membrane, and filter again. The system is immersed in transfer buffer and run at 250 mA for 90 minutes. The transfer buffer in the container is kept in agitation and in a low temperature so as to assure that there's an even mixture and that the temperature doesn't rise with the current applied. After the transfer is finished, the membrane is removed

from the sandwich and washed for 2 minutes with transfer buffer. The regions that were not linked to urease were blocked, in order to avoid unspecific linkage to the primary antibody. This process used a blocking solution and took place in an incubator for 1 hour at 25ºC and 60 rpm. The membrane is washed in the end with TTBS (0.05% Tween 20 in TBS) and incubated for 15 minutes with TTBS at 25ºC and 60 rpm. The next step was the incubation with agitation of the membrane with a primary antibody during the night at 4 ºC. As primary antibody, an anti-urease rabbit antibody diluted 1:1000 (0.09 mg/mL) in a mixture of 2 mL of TBS and 0.25% nonfat milk was used. This anti-urease antibody is specific for the detection of urease, due to what it should only bind with this protein. After the incubation, the incubation solution was removed, and the membrane washed with TTBS during 10 min for three times at 25ºC and 60 rpm. In order to detect the protein of interest, a mixture containing 40 mL of TBS, 0.02% nonfat milk, 0.05% Tween 20 and anti-rabbit secondary antibody at 1:2000 was added. This antibody, which comes from goats, will be able to recognize the rabbit antibody (the primary), bind to it, and due to its conjugation with HRP, its detection will be possible. The incubation takes place for 2 hours at 25ºC and 60 rpm. To eliminate the excess of the secondary antibody, the membrane is washed with TTBS for 30 minutes. The last step involves the exposure of the membrane. A volume of 100 mL of the detection solution was poured over the membrane and it was left immersed until the bands appeared. This reaction is only possible since the HRP enzyme conjugated with the secondary antibody catalyzes the conversion of DAB to an insoluble brown reaction product in the presence of hydrogen peroxide. The reaction is stopped by removing the detection solution and washing with water. The membrane is then scanned.

3.7. MICROFABRICATION OF MAGNETORESISTIVE SENSORS

3.7.1. MICROFABRICATION

The fabrication of the spin valve magnetoresistive biochip compromises several steps of fabrication, mainly photolithography, etching and lift-off techniques. Due to the small dimensions of the structures being fabricated when compared to impurities and microorganisms, the sensors are fabricated inside of a clean-room, where there are no dust particles. The process was carried out at INESC-MN 250 m^2 clean-room facilities (class 100 and class 10 areas). After microfabrication and characterization, the chip is bonded to a chip-carrier and ready to be used.

The process steps are listed in run sheet (see Appendix B.1). This run-sheet accompanies the microfabrication of the 6-inch wafer substrate along the process, and in there all details and conditions used are written down. The spin valve MR biochip used in this work thesis compromised the fabrication steps detailed bellow.

STEP 1: SPIN VALVE DEPOSITION

After sample cleaning with IPA, DI water and blow-dried with a compressed air gun, the spin valve stack is deposited inside Nordiko 3600, an ion-beam deposition system. The deposition occurs under an external magnetic field so as to define an easy axis for the magnetization of the ferromagnetic layers. The stack structure of the spin valve deposited is Ta 15 Å /NiFe 28 Å /CoFe 28 Å /Cu 27 Å /CoFe 33 Å /MnIr 75 Å /Ta 50 Å.

STEP 2: 1ST EXPOSURE: SPIN VALVE DEFINITION

The sample was submitted to a pretreatment of 30 minutes in a vapor prime machine under vacuum and temperature of 130ºC, where the deposition of an organic compound, Hexamethyldisilane (HDMS) occurred. This treatment helps to improve adherence of the photoresist. After, the sample was spin coated with a positive photoresist (PFR 7790G 27cP, JSR Electronics). This photoresist is composed by a polymer, a sensitizer (control of the chemical reactions in polymeric phase) and a casting solvent. A photoresist is a light-sensitive material that is used to form a patterned coating on a surface. There are two types of resist tones, positive and negative. In a positive photoresist the photochemical reaction during exposure to radiation of a resist weakens the polymer by rupture of the main and side polymer chains. The exposed resist then becomes about 10 times more soluble in developing solutions than the non-exposed counterpart. If a PR has a negative tone, the photochemical reaction strengthens the polymer by random cross-linkage of main or pendant side chains, becoming less soluble than the non-exposed parts [69]. Figure 3.6 illustrates the two types of photoresists manufacturing techniques.

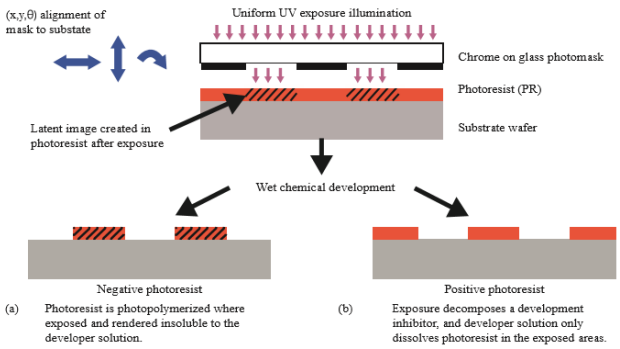

FIGURE 3-6 (a) Negative photoresist and (b) positive photoresist exposure, development, and pattern transfer [69].

The spin coating is made in a Silicon Valley Group (SVG) coating system at a rotation speed of 2500 rpm for 30 seconds. The final thickness of PR obtained for these conditions is 1.5 µm. After spin coated, the PR is soft-baked at 85ºC for 60 seconds so as to remove solvents and promote photoresist adhesion.

The PR layer is then exposed by a direct write laser machine (DWL 2.0, Heidelberg Instruments) using a 442nm wavelength HeCd laser, as defined in the biochip mask. This system is capable of resolving structures down to a dimension of 0.8 µm.

After the exposure, the sample is baked at 110ºC for 60 seconds to stop ongoing PR photochemical reactions. A suitable developer (JSR Micro PTH70EG solvent) is used to remove the exposed PR. The developing of the sample occurs for 60 seconds in the SVG tracks. The substrate is then washed with DI water and dried by high speed spinning.

STEP 3: ION MILLING: SPIN VALVE ETCHING

The etching process consists in the removal of unprotected material. Three types of techniques were used for etching in the fabrication of the MR biochips: ion milling, reactive ion etch (RIE) and wet etch. In this step the ion milling technique was used. In this technique the ions of an inert gas (Ar) are accelerated from a wide beam ion source into the coated surface of a substrate under vacuum in order to remove material to some desired depth. The etching was carried out in Nordiko 3000, with the Ar gun set at an angle of 70º relatively to the sample surface. The etching rate of ion milling is approximately 1 Å/s.

The spin valve material not protected by the photoresist mask are etched away, leaving the sensor shape structures well defined.

STEP 4: RESIST STRIP

After etching, the remaining photoresist on top of the sensor structure is removed. This is accomplished by immersing the sample in an organic solvent (Microstrip 3001, Fujifilm) in a hot bath at 65ºC and with ultrasounds. The sample must stay in solution until all the PR is removed. The sample is then washed with IPA, rinsed with DI and blow-dried with a compressed air gun.

STEP 5: 2ND EXPOSURE – CONTACTS DEFINITION

Similar steps to the 1st exposure are taken. Vapor prime for 30 minutes at 130ºC, followed by resist coating with 1.5 µm thickness. A pre-development step is needed which helps in the lift-off process and serves to prevent the occurrence of the ‘rabbit ears’. The developer is dispensed for 20 seconds into the substrate, with no bake in the SVG tracks. The contacts will be exposed using the DWL.

The mask is then developed in the SVG developer track as in STEP 3.

STEP 6: CONTACTS DEPOSITION

In this step, a 3000 Å thick layer of aluminum is deposited over the photoresist layer. The aluminum structures compromise the metal contacts for the sensors as well as the associated current lines. The deposition of Al occurs at Nordiko 7000, a sputtering machine. In this step a 150 Å titanium-tungsten layer is also deposited over the spin valve in Nordiko 7000. This layer protects the spin valve from oxidation and corrosion, also acting as an anti-reflective layer for good mask exposure.

STEP 7: ALUMINUM LIFT-OFF

A lift-off process is used to obtain the required structures for the sensor contacts and current lines by removing the excess Aluminum. This process uses a solvent that dissolves the positive photoresist underneath the deposited metal, starting at the edge of the unexposed photoresist, lifting off the metal. The thin film of metal remains where there was no PR (Figure 3.7). The sample is immersed in a resist strip solution (Microstrip 3001, Fujifilm) in a hot bath at 65ºC and applying ultrasounds. In the end, the sample is rinsed with IPA, DI and blow-dried with a compressed air gun.

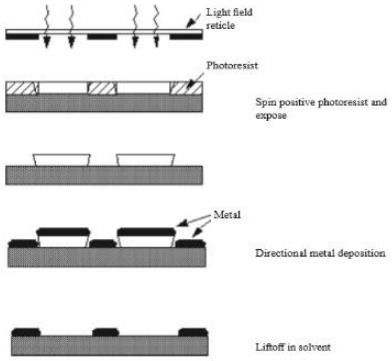

FIGURE 3-7 Schematics for a lift-off process using a positive photoresist [69].

STEP 8: PASSIVATION LAYER – 3000 Å SIN

A 3000 Å thick layer of silicon nitride is deposited over the surface of the sample by plasma-enhanced chemical vapor deposition (PECVD). The deposition takes place in a Electrotech machine. The SiN acts as a diffusion barrier against water molecules and ions, preventing corrosion from solutions.

STEP 9: 3RD EXPOSURE – PASSIVATION LAYER

The same procedure as STEP 2. In this step exposure of the pads will happen so as to allow outside contact to the sensors to be made.

STEP 10: REACTIVE ION ETCHING

In this step RIE was used to open the pads. This technique combines physical and chemical etching. A plasma of CF_4 and Ar is used for selectively and anisotropically (etch rate much higher in vertical direction than in the lateral) remove SiN. The RIE is performed in a LAM Rainbow 440 system, with an etch rate of approximately 5.47 Å/s.

STEP 11: RESIST STRIP

After etching, the remaining photoresist on top of the sensor structure is removed as seen in STEP 4.

STEP 12: 4TH EXPOSURE – AU PAD FOR CHEMISTRY

The same procedure as STEP 5. In this step exposure of the structures used for biomolecule immobilization happens. The gold is utilized due to it being biocompatible.

STEP 13: AU PADS DEPOSITION

In this step, a 50 Å thick layer of titanium is deposited to promote the adhesion capacity of the 400 Å thin film of gold deposited. This is performed by sputtering in Alcatel SCM 450 machine.

STEP 14: AU LIFT-OFF

The patterning of the gold is accomplished by lift-off in a Microstrip bath at 65ºC.

STEP 15: DICING

Before dicing the final sample into individualized dies, coating with 1.5 µm photoresist is done to protect the chips in the process. An automatic dicing saw (Disco DAD 321) was used to cut the sample dies. The chips are then cleaned in a hot-bath of Microstrip 3001 at 65ºC.

STEP 16: ANNEALING

Each die is annealed at 250ºC for 30 minutes under a magnetic field of 1 T. The annealing is done in order to improve the exchange magnetic field in the pinned layer so that it can be sufficiently high to use the pinned layer as a reference layer [63].

STEP 17: WIRE BONDING

The chips were mounted on a PCB and the electrical connections made via wire bonding of the contact pads. This technique uses ultrasonic vibrations to weld a thin aluminum wire interconnecting the metal contact on the chip and the PCB contacts.

After wire bonding, the wires were protected from external damage by a layer of silicone gel (Elastosil E41) deposited over the wires (figure 3.8) and it was left to dry for some hours at room temperature.

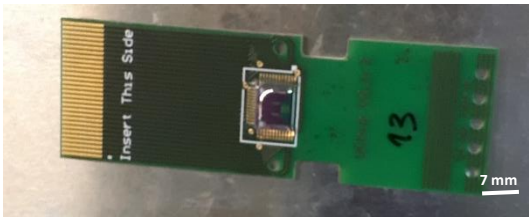

FIGURE 3-8 Biochip mounted on a PCB and wired bonded. The wires are protected by a layer of silicone gel.

3.7.2. BIOCHIP MASK

The chip layout used has 30 U-shaped spin valve sensors arranged in 6 distinct sensing regions (figure 3.9a-b). Each region compromises 4 biological active sensors plus a reference sensor. The biological active sensors are surrounded by aluminum current lines and are coated with a gold film (Ti 5 nm/ Au 40 nm). Sensor area is described in [70].

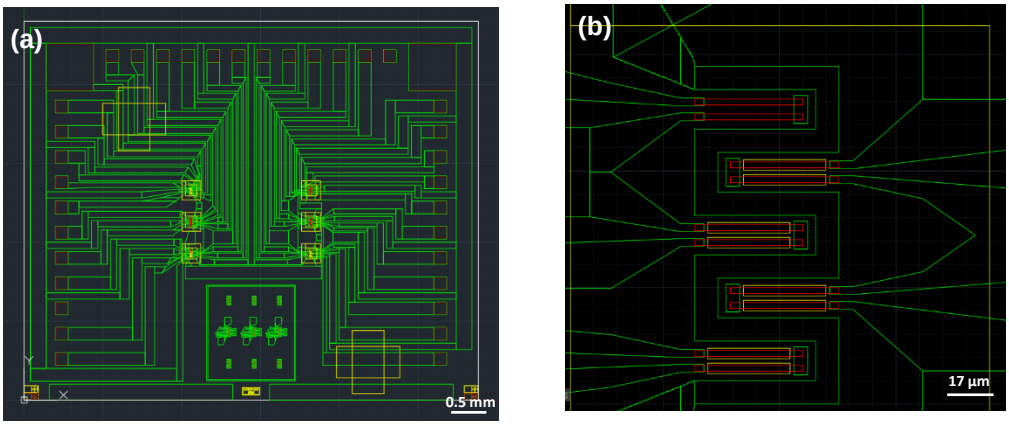

FIGURE 3-9 (a) Schematic layout of the Biochip mask made with AutoCAD and with dimensions of 6.0x7.2 mm^2. (b) Sensing region amplified with 4 biological active sensors and a reference sensor.

3.8. CHARACTERIZATION OF THE MR SENSORS

The characterization of the biochips when under an external magnetic field was performed as figure 3.10. The MR sensor is biased by a current source (Keithley 220) and the voltage is measured by a voltmeter (Keithley 182). The spin valve measurement is done using 2 probes. The magnetic field is created by two Helmholtz coils connected in series and supplied by a current source (Kepco Bipolar operational power supply). Both current sources are controlled by a computer (GPIB connection). The voltage data is sent by the voltmeter to the computer using also a GPIB connection [63].

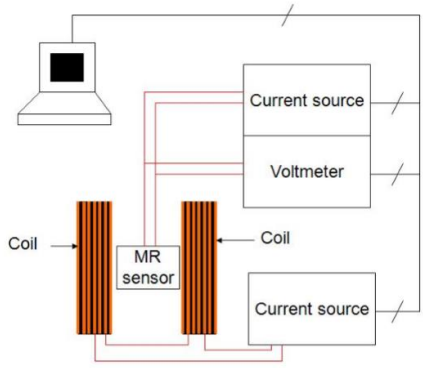

FIGURE 3-10 Set up for the characterization of the magnetoresistive sensors. Figure taken from [63].

A representative transfer curve for the fabricated biochips can be seen in figure 3.11. The spin valve sensor has a minimum resistance of 390-440 Ohm and a magnetoresistance of ~8 %.

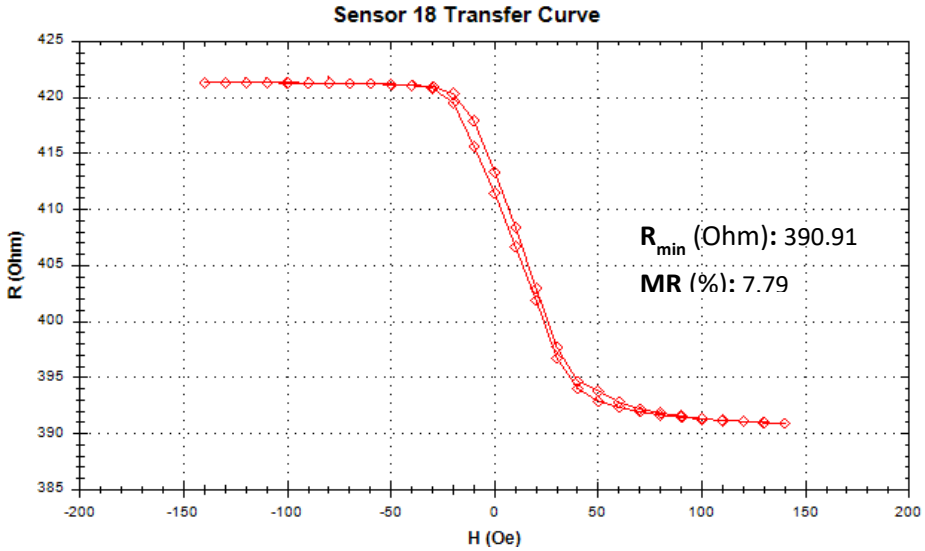

FIGURE 3-11 Transfer curve of a biochip obtained using the setup from figure 3.10. (R_{min}= minimum resistance; MR= Magnetoresistance)

3.9. MAGNETORESISTIVE PLATFORM

The electronic read-out set-up used in this thesis was the one represented by Martins et al. [43]. This platform compromises three different parts (figure 3.12a): 1. a power supply /battery; 2. a control and acquisition board which serves to encrypt the data collected from the sensors and to act as a bridge between the device and the user interface; 3. a magnetic field generator/inductor. There is a slot for the biochip mounted on a PCB to be inserted in the platform. The complete architecture of the platform is schematized in figure 3.12b.

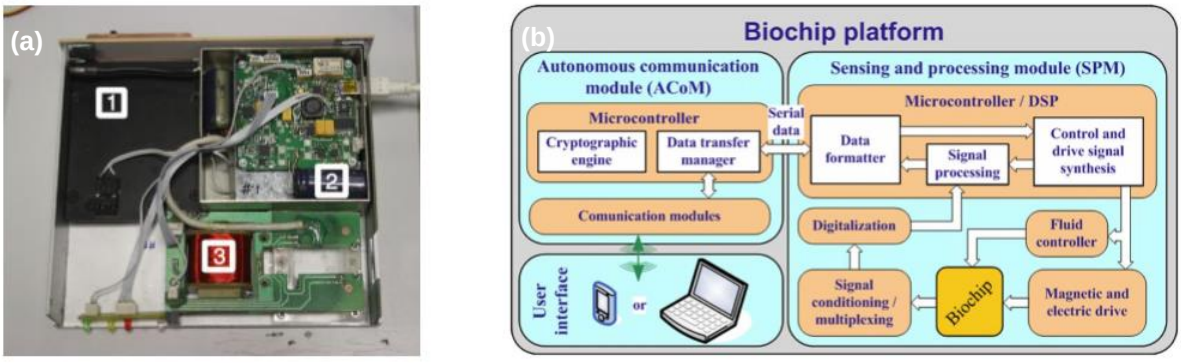

FIGURE 3-12 (a) Photo of the magnetoresistive platform: (1) Battery, (2) Control and acquisition board, and (3) Magnetic field generator. Figure was taken from [10]. (b) Architecture of the portable platform for biochip readout. Figure taken from [43].

The biochip is located in the sensing and processing module (SPM). The module provides the signals required to perform the magnetic and electric drive of the biochip sensors, to perform multiplexing of the sensor signals, and to acquire the conditioned signal in order to perform digital signal processing in a DSP (16-bit digital signal processor). The autonomous communication module (ACoM) is then responsible for encrypting the data collected at the SPM and for its transmission to the device responsible for the user interface, using an USB port [43].

The magnetic drive circuit is one of the critical parts of the measurement system. To avoid low-frequency noise the measure is performed in AC, requiring an AC magnetic field. Using a GUI, it is then possible to automatically measure the transfer curves of all the biochip sensors. The user only needs to define the biochip type, the sensor bias current and the measurement range in the software used [43]. One important aspect of this platform is that the sensors signals are processed in real time and displayed in a PC. The user interface also allows full control over the assay. Besides this, the acquired data can be stored in extensible markup language (XML) or comma separated value (CVS) file format, allowing deeper analysis of the data using other applications [71].

For the Biochips experimental set-up, the detection of the magnetic particles was done by using a DC+AC external magnetic field. The AC field is used to magnetize the nanoparticles while the DC magnetic field is superimposed to the AC field in order to properly bias the sensor transfer curve [71]. The parameters used were 1 mA DC current and 13.5 Oe rms. The DC field for which the maximum sensor response appears is 30 or -30 Oe, depending on the sensors. A bandwidth of 4 Hz and a magnetic AC drive type were used.

An example of the data acquired by the biochip platform in real time can be seen in figure 3.13.

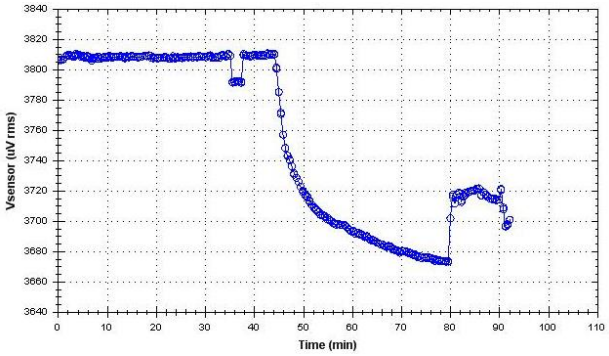

FIGURE 3-13 Example of a biosensor read-out using the MR platform: (1) Until 40 minutes, baseline acquisition; (2) From 42 to 80 minutes, Injection of magnetic particles solution and letting it settle over the sensors; (3) At 80 minutes washing with PBS Tween 20 occurs; (4) Acquisition of binding signal happens between 80 and 90 minutes.

In the first moments, the system starts acquiring a baseline (5 to 10 min). Then, the magnetic nanoparticle solution is spotted over the biochip and the sensor responds by showing a shift in the acquired baseline. This shift is caused due to the fringe field resulting from the interaction between an external magnetic field and the magnetic nanoparticles and that is picked up by the sensor. The more particles there are immobilized over the sensor, the bigger the fringe field produced, the bigger the signal detected. The signal

will then continue to move until it settles on a new value that corresponds to a saturation of the signal, where all the magnetic particles over the sensors are being read. This saturation line gives the user a visual cue to start the washing phase. After each consecutive wash, the unbound particles that didn't have an affinity to the recognition biomolecule are washed away leaving the sensors no longer saturated. The signal starts to shift once more. After some time has passed, the biochip reaches its final stage with the signal from the biosensor settling in the binding signal.

3.10. MICROFLUIDICS

For building PDMS structures one needs a mold, which can be made of different materials. In this work both PMMA molds and SU-8 molds were used. The PMMA molds were used for the casting of the U-chip channels used in the biochip platform for passage of the magnetic particle solution over the sensors. These molds were already fabricated from previous work from Valentim [10]. The SU-8 molds were fabricated for the casting of a micromixer and magnetic separator used for urease sample preparation. In the case of the SU-8 molds an additional step involving the exposure of an aluminum mask is necessary for patterning. This last process is described in the Run sheet (see Appendix B.2). The micromixer module will serve to mix the solution of magnetic particles conjugated with antibodies and the sample containing urease. The separator will use a magnet in a lateral location for separating the magnetic particles attached to the urease from possible impurities in the solution.

3.10.1. AUTOCAD MASK

Six different structures were designed (figure 3.14). Two micromixers and two filtration units only differing in size and two different sets of magnetic separators. In this work, however, only the large micromixer structure and the symmetric magnetic separator were employed. The others were made for different work, so they will be discarded in this thesis.

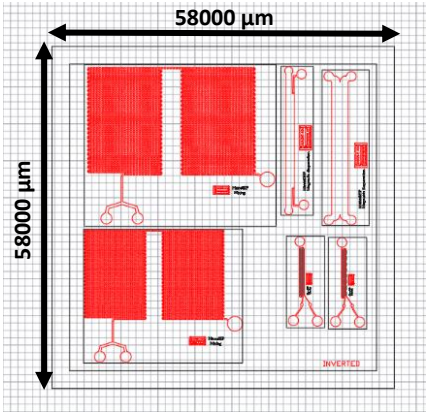

FIGURE 3-14 AutoCAd mask of the microfluidic structures: micromixers on the left, magnetic separators on the top right and filtration units on the bottom right. Only the largets mixer and magnetic separator were used.

The micromixer has a design similar to the one in [72]. In the mixing operation there are two types of mixers that can be used: active and passive micromixers. Since the active mixers require external forces, they tend to require complex fabrication processes. The passive mixers are easier to fabricate, but they need longer mixing lengths. A passive mixer will be used in the present work, more specifically, ones that are less complex but with satisfactory mixing indexes/ degrees. In the obstruction micromixer, to enhance particle mixing and reduce mixing time and length, transverse components of velocity are used to force particles to move laterally in the microchannels. Transverse particle flows are created in the channels by adding, in this case, obstacles at 45 degrees angle so as to physically guide particles into the other half of the microchannel. The obstacles also stir the fluid, creating lateral mass transport that enhances fluid mixing. The dimensions of the mixer are represented in figure 3.15.

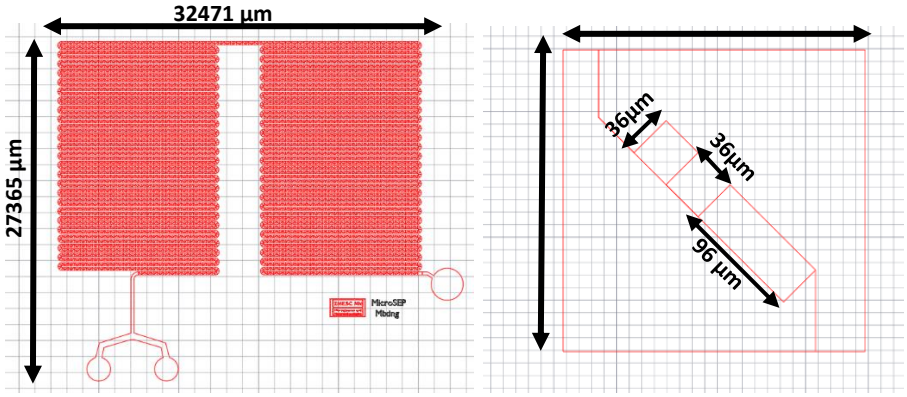

FIGURE 3-15 AutoCAD design for the micromixer with a close-up of the individual units containing the obstacles on the right. The inlets have a diameter of around 1800 µm and the outlet a diameter of 2500 µm.

The magnetic separator layout was taken from [73]. In this layout the channel contains two flow streams (figure 3.16a). The stream opposite to the magnet will have the magnetic solution entering while the stream near the magnet will have a buffer passing through. The magnet provides sufficient magnetic field to attract the particles laterally into the buffer flow stream. As such, the particles move out of the sample flow stream and into the buffer stream, while carrying the bound target analyte with them. Movement of other molecules across this interface is limited by diffusion due to the low Reynolds number (laminar) fluid flow. The dimensions of the separator can be seen in figure 3.16b.The magnet (Q-12-08-02-N from supermagnete)

used in this work was made from NdFeB and had dimensions of 12x8x2 mm. Three of these magnets were coupled together and used in the experimental set up.

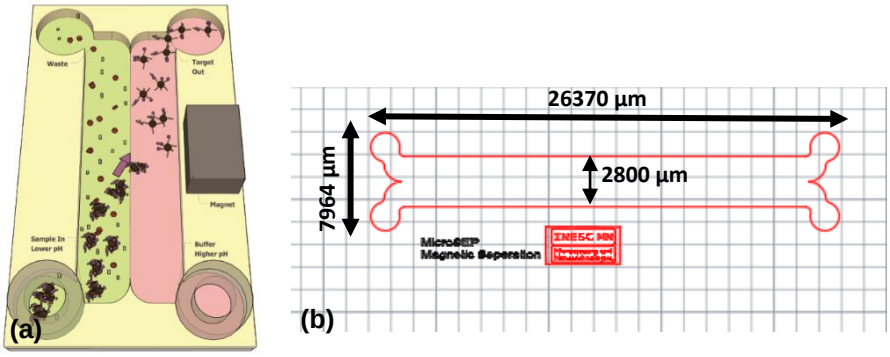

FIGURE 3-16 (a) Target analyte separation in a microfluidic. The channel contains two flow streams. The left stream (green) is the sample that has been pre-incubated with MPs. A rare-earth magnet provides Sufficient magnetic field to attract the aggregates laterally into the pink flow stream. The aggregates then move out of the sample flow stream and in to the pink stream, carrying the bound target analyte with them. The figure was taken from [77]. (b) AutoCAD design for the magnetic separator. The inlets and outlets have a diameter of around 1600 µm.

3.10.2. COMSOL MULTIPHYSICS SIMULATIONS

Simulations for fluids in the micromixer, with and without obstacles, were carried out using COMSOL Multiphysics 5.3. The studies made were for laminar flow and transport of diluted species.

Some parameters were initially imposed, including the Inlet flow rate of 0.1 µL/min in order to have a residence time of approximately 11 minutes, the inflow urease concentration was calculated based on the average concentration of the concentrate solution obtained after filtration with amicon MWCO of 10 kDa, obtaining the value of 0.108 mol/m^3. This value was calculated assuming that bacteria have an average protein with 267 amino acids and that an amino acid has an average molecular weight of 100 Da [74], after which the average weight for a protein was determined to be 29.37 kDa. Assuming the concentration of the solution already described, the final value of 0.108 mol/m^3 was obtained by using a conversion calculator [75]. The inflow MNP concentration was calculated to be approximately 8.136x10^{-7} mol/m^3, which was obtained considering the use of 10 µL per assay and that there are 4.9x10^{11} particles per mL of solution.

3.10.3. ALUMINUM MASK

A glass substrate of 5x5 cm is washed with IPA, DI water and blow-dried with an air gun. In the next step, a 1500 Å thick layer of aluminum is deposited over the glass. The deposition of Al occurs at Nordiko 7000. The sample is then submitted to a pretreatment of 30 minutes in a vapor prime machine under vacuum and temperature of 130ºC. After, the sample was spin coated with a positive photoresist. The PR layer is then exposed in DWL to pattern the mask containing the mixer and magnetic separator. After the exposure, the sample is baked at 110ºC for 60 seconds. A suitable developer is used to remove the exposed PR. The developing of the sample occurs for 60 seconds in the SVG tracks. The substrate is then washed with DI

water and dried by high speed spinning. After, a wet etch is performed on the mask. Wet etch is a technique that uses a chemical solution for material removal. The chemical solution used in this work was prepared for etching an Al thin film (Aluminum etchant: solution phosphoric, nitric and acetic acid). This etching is isotropic meaning that the same amount of material is removed in all directions [63]. The substrate is immersed for around 3 minutes in this solution, after which the photoresist is stripped in a Microstrip hot bath at 65ºC for 20 minutes.

3.10.4. SU-8 MOLD

SU-8 is a negative photoresist, meaning that the area exposed to light will crosslink causing the unexposed part to dissolve faster in a solvent. SU-8 has excellent sensitivity, high resolution, high aspect ratio and good thermal and chemical stability. It is an acid-catalyzed negative photoresist. On average, a single molecule contains eight epoxy groups [69]. The SU-8 used to achieve a height of 50 µm was the SU-8 50 from Microchem. Silicon was used as a substrate. The sample is washed with IPA, rinsed with DI water, and blow-dried with a compressed air gun. It is then left in the UVO cleaner for 20 minutes, after which it's heated at 100ºC for 10 minutes in a hotplate in order for the water molecules to evaporate, and increasing the SU-8 adhesion as such. The sample is placed in a spinner (Model WS-650Mz-23NPP from Laurell) located inside a laminar flux chamber. SU-8 is manually poured in the sample, and is let to rest for 30 seconds before spinning. The sample is spinned at 500 rpm for 10 seconds with 100 rpm/s acceleration, followed by spin at 2000 rpm for 37 seconds and 300 rpm/s acceleration. The next step involves soft-baking and serves to evaporate the solvent and increase the rigidity of the SU-8. This step involves a pre-bake for 3 minutes at 65ºC followed by 8 minutes at 95ºC in a hotplate. The substrate is let to cool-down for 5 minutes. The SU-8 coated substrate is then put in contact with the aluminum mask, the closest as possible, and exposure to UV light is performed with 600 mJ/cm^2 for 20 seconds. After, the post exposure bake (PEB) is done by baking the substrate for 1 minute at 65ºC in a hotplate followed by a bake at 95ºC for 7 minutes. This step is when the polymerization of the SU-8 occurs and causes solidification, after the epoxy groups being protonated by the UV light. Finally, the photoresist is developed using propylene glycol methyl ether acetate (PGMEA) (Sigma-Aldrich). The substrate is immersed for 6 minutes in the developer with strong agitation. The sample is then rinsed with IPA and blow-dried.

After the mold fabrication, the final heights were measured using a profilometer (Tencor Instruments).

3.10.5. PMMA MOLDS

The PMMA molds used for the casting of PDMS to make the U-channels were fabricated by Valentim [10]. It consists of three molds: the bottom part of the mold (figure 3.17a) consists of twenty-four squares (0.9 by 0.9 cm) with a U-shaped salience, with a 0.3 mm height; the middle part (figure 3-17b) has twenty-four squared holes that align over the saliencies of the bottom mold; the top part (figure 3.17c) contains twenty-four sets of two holes (forty-eight holes total, in pairs) with a 0.8 mm diameter, that make up the inlets and outlets. The three PMMA plates (2 mm thick) with 15x15 cm were micromachined using a CNC milling machine (TAIG Micro Mill from Super tech & Associates).

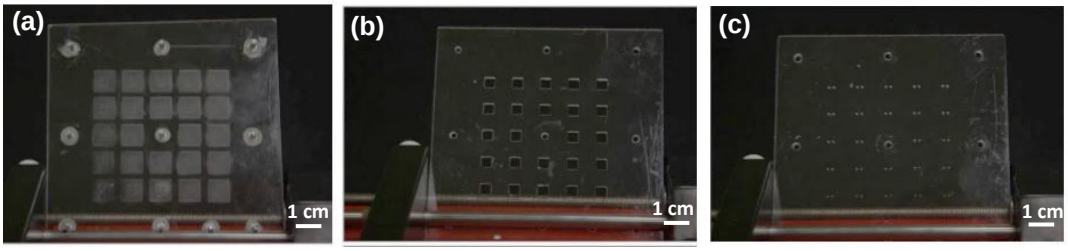

FIGURE 3-17 (a) Bottom part of the PMMA mold with the 24 U-shaped saliences. (b) Middle part of the mold with 24 squared holes to align over the sequences. (c) Top part of the PMMA mold with 24 sets of two holes that make up the inlets and outlets of the channels. Photo taken from [10].

3.10.6. PDMS STRUCTURES

PDMS (Sylgard 184-Dow Corning) was prepared by mixing the curing agent and the base in a 1:10 mass ratio in an analytical balance (SA 80 Scientech). This step was followed by a 1hour degassing step to remove all air bubbles, which occurs in an exicator (Bel-Art). The PDMS is then poured over the SU-8 mold inside a petri dish or injected in the PMMA molds whose holes are then plugged with hollow tubes (SC22/15, instech). The molds are then cured in an oven (Memmert) at 70ºC for 1 hour. After baking, the PDMS is released from the mold. In the PDMS casted over the SU-8 molds, the inlets and outlets are made by manually perforation with a syringe tip (LS22 22ga x 12mm, instech).

For the microfluids used in the urease sample preparation, the PDMS had to be bonded to a substrate of boroaluminosilicate (CORNING 1737 AMLCD Glass substrates) of 0.7 mm thickness (2 x 2 in). PDMS was then immersed in water for 30 minutes at 65ºC while the glass was submerged in IPA (30 minutes in the bath at 65°C) followed by rinsing with DI water. Afterwards, both glass and PDMS are placed in an oxygen plasma chamber for 1 min. In the final step, glass is immediately placed over the PDMS. Since the surfaces become highly hydrophilic, a permanent bonding occurs.

3.11. BIOLOGICAL ASSAYS USING THE PLATFORM AND INTEGRATED MICROFLUIDICS

For the platform testing, a syringe is loaded with PB-Tween 20 buffer, enough to fill the syringe while leaving enough free space to pull the piston, then drawing into the inlet tube 20 µL of the magnetic particles solution (described in materials and methods) from an Eppendorf. The syringe is placed in the syringe pump (NewEra), the inlet tube (polyethylene tubing, BTPE-90 with 0.86 x 1.27 mm, instech) connected to the first inlet hollow tube (SC22/15, instech) of the PDMS U-channel, finishing the set-up (figure 3.18a).

After the biochip is inserted inside the biochip platform and the system is turned on and let to acquire a baseline for 5-10 minutes, the syringe pump (New Era Pump systems) is set to run at the same flow rate of 5 µL/min until the magnetic nanoparticle solution covers all the PDMS channel. The pump flow rate is then set to zero until the resistance signal read by the platform stabilizes in the saturation signal, after which the pump flow rate is set to 10 µL/min in order for the PBS Tween 20 to wash the sample until the binding signal is achieved. After that, the syringe, which should still have some buffer solution inside, is replaced by one with DI water and then one with just air inside. Using a flow rate of 5 µL/min, air is pushed through the tubing and U channel until there are no more droplets inside the tubing. This process is summarized in figure 3.18b.

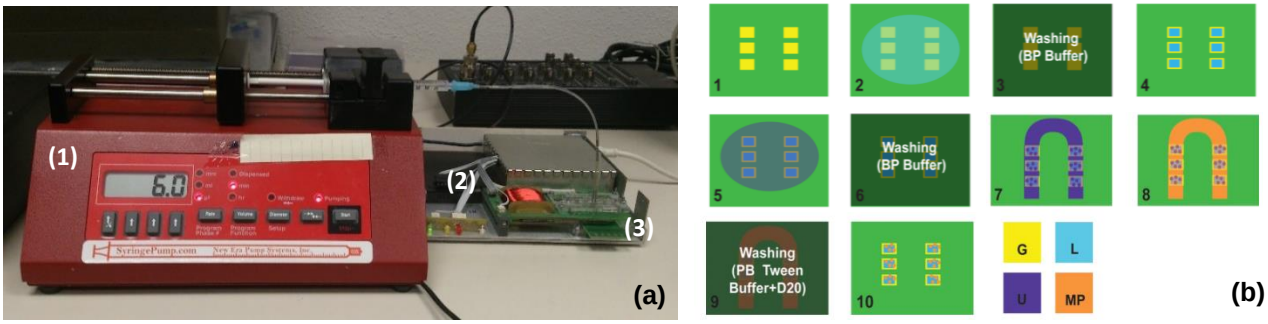

FIGURE 3-18 (a) Platform and Microfluidics system setup: (1) Syringe Pump (2) Platform (3) Biochip slot. (b) Scheme for the experimental procedure using the direct ELISA method and platform integrated with microfluidics: (1) Sensors covered with gold (2) Solution of linker is spotted over the sensors (3) Washing step with PBS 0.1 M pH 7.4 (4) The linker is now covering the sensors (5) A solution of urease is spotted over the sensors (6) After an hour, another washing step with PBS buffer (7) The biochip is inserted in the platform with the microfluidic U-channel covering the sensors(8) Passage of the magnetic particle solution through the channel (9) After 30 minutes the sensors are washed with PBS Tween 20 followed by DI water (10) The urease present in the sensors is now conjugated to the Ab-magnetic particles complex and the biochip is removed from the platform. Figure was adapted from [10].

4. RESULTS AND DISCUSSION

4.1. JACK BEAN UREASE ASSAYS IN GOLD SURFACES AND BIOSENSORS

Direct ELISA assays were performed on gold pads and biochips with varying concentrations between 0.1 and 100 mg/mL (figures 4.1a-b and 4.2a-d). A negative control was also made. In these assays urease was immobilized on the surface first, and then the magnetic particles solution with antibodies was added.

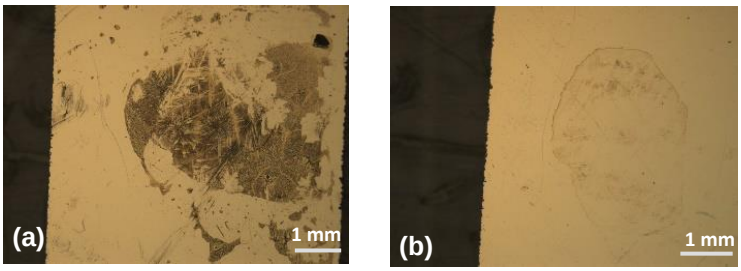

FIGURE 4-1 (a) Direct ELISA using 50mg/mL of urease and spotted on a Gold die. (b) Negative control (no urease) direct ELISA assay on gold die.

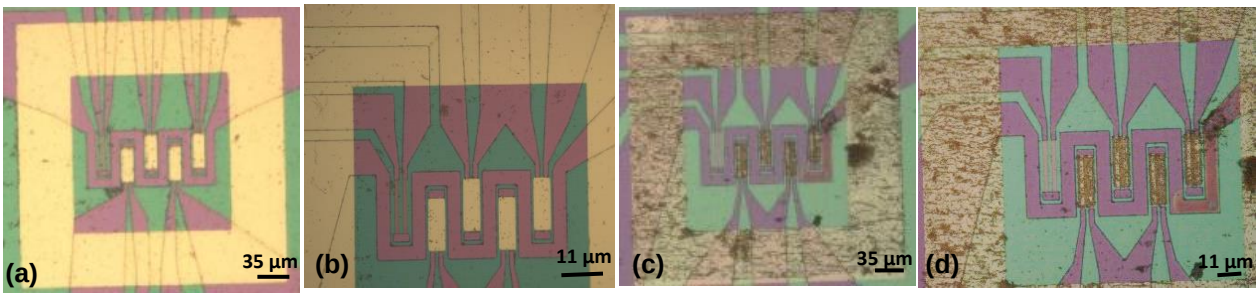

FIGURE 4-2 (a) Negative control (no urease) direct ELISA assay on a biochip (40x magnification). (b) Negative control (no urease) direct ELISA assay on a biochip (200x magnification). (c) Direct ELISA using 60mg/mL of urease and spotted on a biochip (40x magnification). (d) Direct ELISA using 60mg/mL of urease (200x magnification).

Even though some particles are still observable in the negative control, the difference between the control and bioactive substrate is clearly notable. The fact that some of the particles still attach to the surface despite not existing urease in the negative control, might be due to the free cysteine residues present in the antibody that bind to the linker via amide bonds. However, there are much less free groups to attach to the linker in the antibody that there are in urease, the latter forming a stronger bond.

The functionalized biosensors where also read in the magnetoresistive platform. An example of a resistance curve is seen in figures 4.3a-b, for both a negative control, and one with 50 mg/ml of jack bean urease.

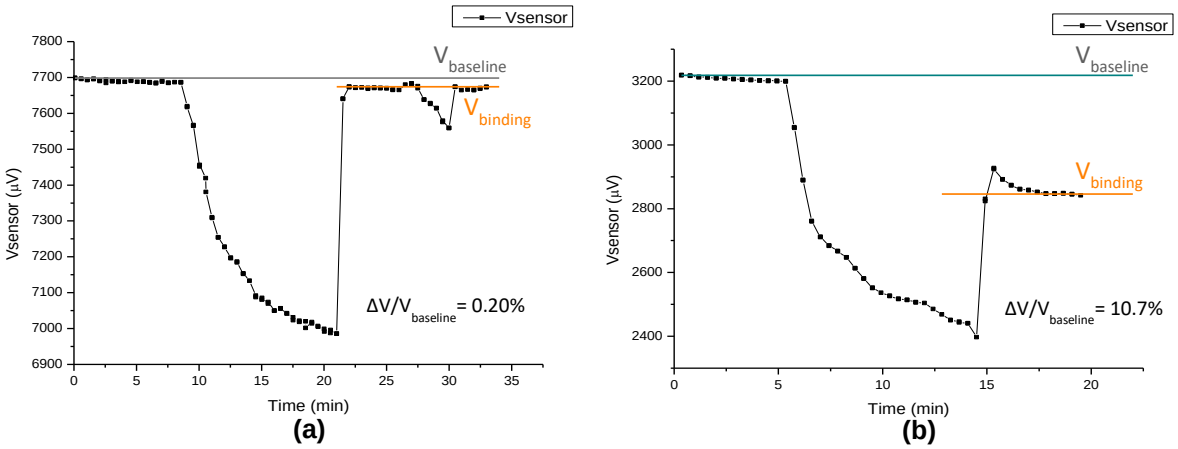

FIGURE 4-3 (a) Voltage signal acquired from a negative control direct ELISA assay by the MR platform. (b) Voltage signal acquired from a direct ELISA assay with 50 mg/mL urease immobilized. ($V_{baseline}$= resistance value from the initial baseline; $V_{binding}$= resistance value obtained correlated to the number of magnetic particles remaining in the sensor surface after washing; ΔV= Resistance difference between $V_{baseline}$ and $V_{binding}$)

While in the negative control the signal obtained after washing practically returns to the previous baseline, the one with urease has a greater difference between the initial and final resistance values due to the immobilization of the magnetic particles. The Δ V values are normalized by dividing it with the resistance value of the starting baseline. In the negative control the binding signal doesn't completely return to the starting state probably due to the small quantity of particles that get attached to the surface by antibody-linker interactions.

Using concentrations of urease between 0.5 mg/ml and 70 mg/ml, a calibration curve for quantification of urease was obtained (figure 4.4).

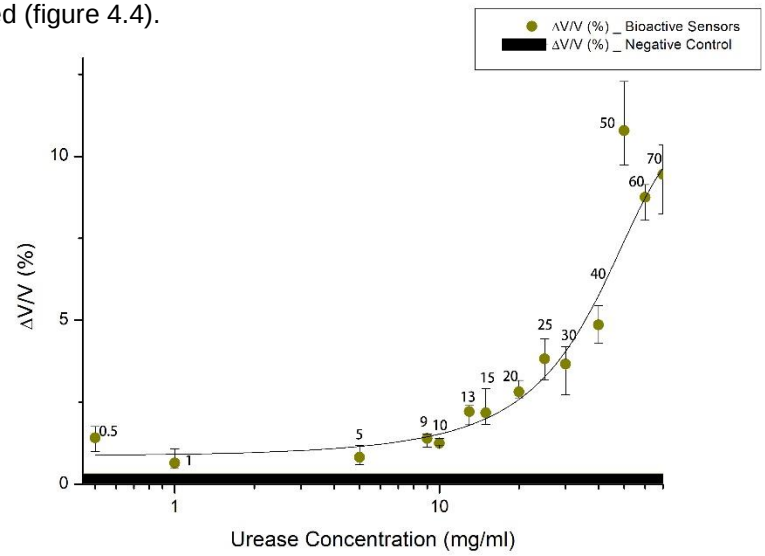

FIGURE 4-4 Calibration curve for urease quantification using the MR platform. Concentrations between 0.5 mg/mL and 70 mg/mL were measured. A fitting using a logistic equation (y=a/(1+b*exp(-k*x)) was made, obtaining the following parameter values: a=10.861; b=11.613; k=0.064 and a R^2=0.951. (ΔV= Resistance difference between $V_{baseline}$ and $V_{binding}$, V= $V_{baseline}$)

Since no information was known about the concentration of urease in the field, the range was chosen by taking into account that at 70 mg/ml the urease starts to precipitate in solution giving very inconsistent results, and that 0.5 mg/ml seem to be the detection limit. One way to decrease the sensitivity of detection is by enabling particle attraction during the assay which will guarantee that the particles are attracted to the sensors. This wasn't done in this thesis but is something to consider if field values are of low concentration.

In the calibration curve a stabilization seems to be occurring around 60 mg/ml, meaning the saturation of the sensors is being reached.

Finally, sandwich ELISA assays were also performed to see if less non-specific binding occurred. Direct ELISA with the same urease concentration was used as positive control and no urease was used as a negative control.

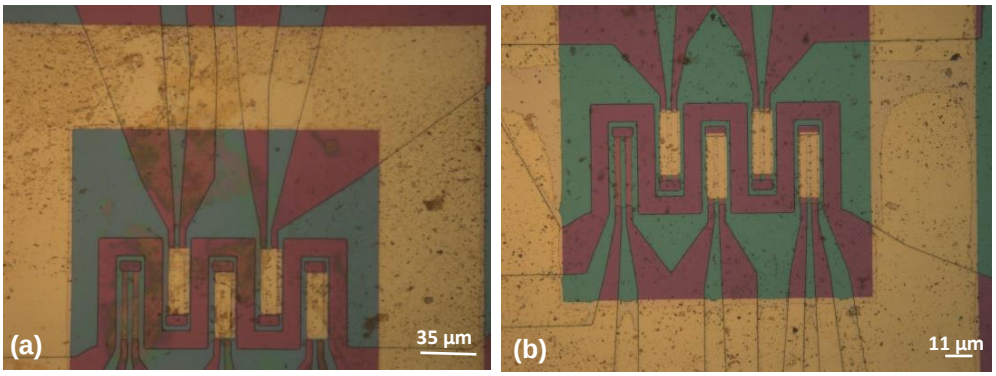

FIGURE 4-5 (a) Direct ELISA using 40mg/mL of urease and spotted on a biochip (200x magnification). (b) Sandwich ELISA using 40mg/mL of urease (200x magnification).

The difference between the two detection methods didn't seem to yield different results, meaning urease is still attaching to the surface in the sandwich ELISA methodology. With a sample containing other proteins other than urease, in the sandwich ELISA they would less likely attach to the surface since they aren't recognized by the immobilized antibody while in the direct ELISA they would most likely attach, preventing urease from doing so as efficiently.

For more quantifiable information, the biochips functionalized with sandwich ELISA should be read in the platform for future work.

One thing that is important to note is that during some of the assays using the platform, some sensors were short circuited with resistance values tending to zero in the middle of the assay (figure 4.6a-b). The short circuit can be explained by the holes seen in the aluminum. If the passive layer covering them was too thin or degraded, an ionic solution coupled to current being passed could lead to corrosion of the current lines, eventually leading to the short circuits. The condition of the surface of the chips is then important for conducting assays with good resistance responses and no corrosion.

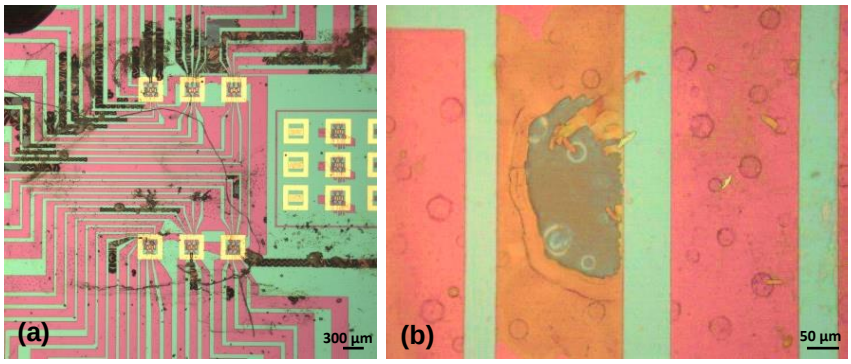

FIGURE 4-6 (a) Biochip surface after doing a direct ELISA assay on the MR platform with short circuited current lines (10x magnification). (b)Close-up of corrosion in the aluminum current lines (200x magnification).

4.2. *B. PASTEURII* UREASE GROWTH

The growth curve obtained by measurements of the cultivation medium inoculated with *B. pasteurii* absorbance at 600 nm is represented in figure 4.7. Triplicates were made.

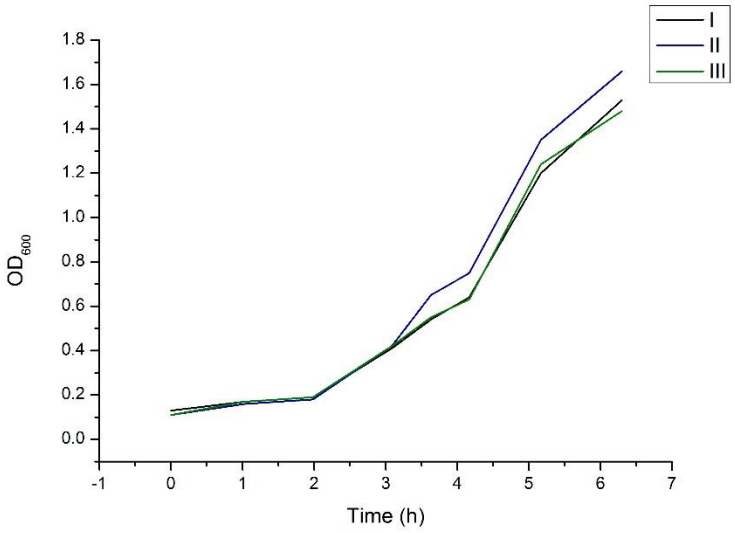

FIGURE 4-7 *B. pasteurii* growth curve in the culture medium described in table 3.1 using an inoculum cultivated in the same medium. Triplicates were made.

The growth curve can be divided in the three distinct phases, consisting of a lag phase, exponential phase and stationary phase. In the first two hours a lag phase can be observed where the bacteria were still adapting to the fresh medium. The exponential phase, where the most cell growth is observed, occurs until approximately 5 hours, after which a decrease in growth is seen with a stabilization in the OD. This indicates that the nutrient supply is depleted, causing the number of viable bacteria to stay the same, with rate of bacterial cell growth equal to cell death. Using the Eq.4.1 from [68] and considering usage of similar culture medium it's possible to convert the OD read at 600 nm for the *B. pasteurii* to concentration of cells.

$$Y = 8.59 \times 10^{7} X^{1.3627} \tag{4.1}$$

Where X is the OD value obtained at 600nm and Y is the concentration of cells per mL. Knowing the volume present in the flask is then possible to obtain the total number of cells. Doing the calculations an average value of 1.38×10^{8} cells is obtained for the start of the growth and an average value of 2.52×10^{8} cells is obtained for the last OD measured, meaning the number of cells almost doubled during the assay.

4.3. TOTAL PROTEIN QUANTIFICATION

Using the calibration curve obtained by the BSA standards (see Appendix A.3, fig.A.3), it was possible to obtain the corresponding protein concentration in the different samples, as seen in Table 4-1. To be noted that only two of the three triplicates were subject to protein quantification. Each one of those culture mediums was measured in triplicates, after which an average was calculated.

TABLE 4-1 Average absorbance values measured at 565nm for total protein quantification in the samples previously filtrated with amicon 10 kDa. The BCA kit was used for the quantification and the values calculated with the calibration curve (see Appendix A.3, fig.A.3). All the measurements taken from samples centrifuged with amicon with MWCO of 10 kDa were diluted initially with a dilution factor of 1:2.86 that is already taken into account here.

	Absorbance (565nm)	Protein Concentration (mg/mL)
I	1.157±0.015	3.176
II	1.190±0.092	3.280

Besides the above measurements, culture medium that had not been previously subjected to a centrifugation using Amicon with a MWCO of 10 kDa, but instead using an Amicon with a MWCO of 100 kDa, were measured. Both the filtrate and concentrate were analyzed, with the latter having been diluted with a dilution factor of 1:100.

TABLE 4-2 Absorbance values measured at 565nm for total protein quantification in the samples previously filtrated with amicon 100 kDa. The BCA kit was used for the quantification and the values calculated with the calibration curve (see Appendix A.3, fig.A.3).

	Absorbance (565nm)	Protein Concentration (mg/mL)
III. concentrate	0.9095	83.62
III. filtrate	0.665	0.565

The concentrate has very high protein concentration compared to the filtrate, which is to be expected since most of the solution passed through with the 100 kDa molecules. These samples were the ones used in the Western blot for immunodetection of urease.

4.4. UREASE ENZYMATIC ACTIVITY AND SPECIFIC ACTIVITY

A linear equation from the calibration curve of the ammonium chloride standards (see Appendix A.3, fig.A.4) was obtained with a R^2 coefficient of 0.986. The absorbance of samples with different concentrations of the culture medium were analyzed. The measured absorbance and respective conversion to urease activity is present in Table 4-3. The specific activity of an enzyme is an important factor that can give insight about the purity of the sample. It's calculated by diving the enzymatic activity by the total number of proteins present in the sample.

TABLE 4-3 Absorbance values measured at 670nm for urease activity quantification in the samples previously filtrated with amicon 10 kDa. The urease activity was calculated with the calibration curve obtained with urease activity assay kit (see Appendix A.3, fig.A.4). The specific activity of urease was obtained by dividing the urease activity by the total protein present in the sample and presented in table 4.1. The values in the table are already being multiplied by the dilution factor. All the measurements taken from samples centrifuged with amicon with MWCO of 10 kDa were diluted initially with a dilution factor of 1:2.86 that is already taken into account here.

	Dilution Factor	Absorbance (670nm)	Urease Activity (U/L)	Specific Activity (U/mg)
I	1:1	1.137	12.72	0.004
I.1	1:5	1.999	150.95	0.048
I.2	1:25	2.358	936.6	0.295
I.3	1:50	2.897	2419	0.762
I.4	1:100	3.034	5116	1.611
I.5	1:200	2.635	8615	2.713
I.6	1:1000	2.778	45975	14.48
II	1:1	0.563	1.092	3x10-4
II.1	1:5	1.830	133.8	0.041
II.2	1:25	2.316	915.3	0.279
II.3	1:50	2.342	1857	0.566
II.4	1:100	2.380	3791	1.156
II.5	1:200	2.777	9191	2.802
II.6	1:1000	3.017	50818	15.49

The first thing to be noted is that both mediums (I and II) show similar values for the same solutions, except for the sample II, which has a very low value compared to it's I counterpart, and as such it is counted as a pipetting error on the user part. Observing the data, it is clearly noticeable that the urease activity is increasing with the dilution factor, which is unexpected. Various tests were repeated with the same results, indicating it wasn't a manual error. According to Sumner and Howell [76] urease activity increases with increasing buffer dilution until a point is reached beyond which further dilution may cause the activity to decrease. In this case, the biggest jump in urease activity is seen from 1:200 to 1:1000 dilution factor. Further dilutions should be made to see if a stabilization occurs as expected. The fact that the dilution of the sample increases urease activity means there is some type of inhibition occurring in the solution. Sunmer and Howell [76] found that urease can be inhibited by urea. This effect depends upon the pH of the buffer, for when the pH is below pH 6.0 there is no inhibition of urease activity when as much as 10 per cent urea is used, while if the pH of the buffer is above pH 6.0 the amount of urea required to inhibit urease activity decreases with decreasing acidity. At pH 7.9 the optimum urea concentration with phosphate buffer is calculated to be about 0.7 per cent. Considering that the initial medium contained a little above 1% of urea and the pH of the medium was 9, it is possible that the urease is being in fact inhibited by urea. Deasy [77] proposed that the urease was not inhibited by urea itself but by the complex ammonia-urea whose formation is favored in alkaline solutions with high urea concentrations.

In the same manner as done in the protein quantification assay, measurement of the concentrate and filtrate obtained after centrifugation using an amicon with MWCO of 100 kDa instead of 10 kDa was performed. In addition of a dilution of 1:100, the concentrate was also diluted with the factors of 1:1000 and 1:10000 in order to observe if the enzymatic activity continued to increase with dilution like the previous assays demonstrated.

TABLE 4-4 Absorbance values measured at 670nm for urease activity quantification in the samples previously filtrated with amicon 100 kDa. The urease activity was calculated with the calibration curve obtained with urease activity assay kit (see Appendix A.3, fig.A.4). The specific activity of urease was obtained by dividing the urease activity by the total protein present in the sample and presented in table 4.2. The values in the table are already being multiplied by the dilution factor.

	Dilution Factor	Absorbance (670nm)	Urease Activity (U/L)*	Specific Activity (U/mg)
III. concentrate	1:100	1.843	946.4	0.011
III. concentrate_2	1:1000	2.563	14567	0.174
III. concentrate_3	1:10000	2.226	121766	1.456
III. filtrate	-	0.11	-2.830	-0.005

The negative value obtained for the urease activity in the filtrate indicates there is no urease present in the sample, which is to be expected since urease has a molecular weight of around 300 kDa making it too large to pass through the amicon membrane.

From the urease activities of the concentrate samples there is a ten time increase in activity to one sample to another, suggesting that the inhibition of urease is occurring like it was seen for previous assays.

4.5. POLYACRYLAMIDE GEL ELECTROPHORESIS

The scan of the polyacrylamide gel taken after silver staining can be seen in figure 4.8a with the lanes labeled. In this gel duplicates of concentrate after amicon 100 kDa filtration with a dilution of 1:100 and filtrate were run.

In the filtrate lane, lane 5 in figure 4.8a, we can see that there aren´t any proteins above the 100 kDa molecular weight, which is expected due to the separation previously made with amicon 100 kDa MWCO. On the other hand, protein bands with a molecular weight lower than 100 kDa are obtained in lanes 2 and 3, in spite of the filtration. This happens due to the denaturation of proteins and separation into their subunits. Urease has a high molecular weight, but, due to denaturation, it breaks into its subunits, varying their weight depending of the nature of the urease, bacterial or plant. Urease from Jack bean is made up of identical subunits, its molecular mass without Ni(II) ions amounting to 90.77 kDa, assembled as hexamers, having a total of 545.34 kDa (the 12 nickel ions included). Unlike plant and fungal, bacterial ureases, like the one produced by *Bacillus pasteurii*, are composed of three distinct subunits, one large (αβγ, 60–76 kDa) and two small (β, 8–21 kDa and γ, 6–14 kDa), commonly forming $(\alpha\beta\gamma)_3$ trimers, resulting in the enzyme molar masses between 190 and 300 kDa [78].The denaturation into smaller units makes it hard to distinguish the possible urease band from the gel.

Another gel was run (figure 4.8b), this time with duplicates of concentrate (after amicon 100 kDa filtration) with a dilution of 1:100 and filtrate and pure urease from Jack bean at 40 mg/ml concentration.

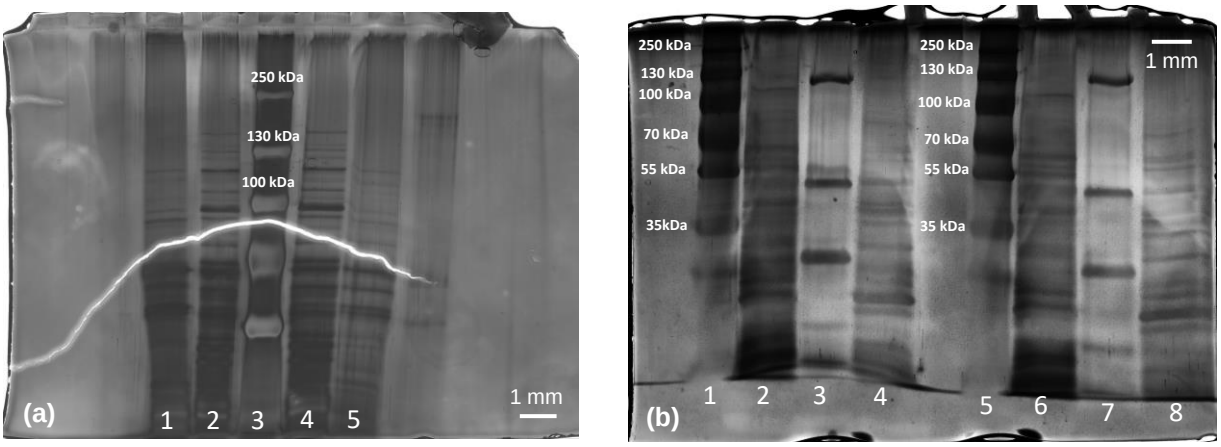

FIGURE 4-8 (a) Scanned 12% polyacrylamide gel after electrophoresis. The samples in the lanes are: (1) Protein ladder, (2) Concentrate with dilution factor of 1:100, (3) Protein ladder, (4) Concentrate with dilution factor of 1:100, and (5) Filtrate. Some of the molecular weights of the protein ladder are represented in lane 3. (b) Scanned 12% polyacrylamide gel after electrophoresis. The samples in the lanes are: (1) Protein Ladder, (2) Concentrate with dilution factor of 1:100, (3) Jack bean urease with 40 mg/mL, (4) Filtrate, (5) Protein ladder, (6) Concentrate with dilution factor of 1:100, (7) Jack bean urease with 40 mg/mL, and (8) Filtrate. Some of the molecular weights of the protein ladder are represented in lanes 1 and 5.

Even though the bands of the ladder in this gel are harder to discretize, the bands of jack bean urease are very prominent (indicating very high concentration). Strangely, three distinct bands with despairing weights appear in the pure urease lane, when supposedly only one should appear. The top band seems to have a weight of around 100 kDa which is the expected for this urease. The other bands could be explained if there was a possible contamination by other proteins.

4.6. WESTERN BLOT

While doing the detection of the HRP present in the second antibody attached to the primary antibody which should be conjugated to the urease, some issues arouse. In the first assays no bands were being detected. To see if it was an issue with the western blot protocol or if the antibody just wasn't binding to the urease from *B. pasteurii*, since it's a specific antibody for the urease from jack bean urease, a gel with both concentrate samples and pure urease samples was transferred to a PDVF membrane. If the band from urease didn't show in the membrane after revelation, the issue provided from the protocol, since it is known from the biological assays done in the gold surfaces that the primary antibody is binding to the jack bean urease. No bands, including the ones from pure urease, were obtained during exposure of the membrane. Another assay using a fresher reagent of hydrogen peroxide was then performed. This time the top urease bands, as seen in figure 4.9, appeared in the membrane. The fact that only the 100 kDa bands appeared in the pure urease lane may explain that the remaining bands not revealed might indeed be part of protein contaminants.

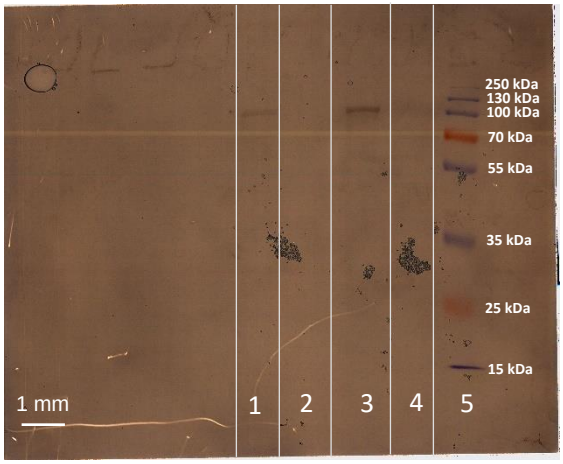

FIGURE 4-9 Photo of a PDVF membrane after revelation step in a western blot. The samples in the lanes are: (1) Jack bean urease at 40 mg/mL, (2) Concentrate with dilution factor of 1:100, (3) Jack bean urease at 40 mg/mL, (4) Concentrate with dilution factor of 1:100, and (5) Protein ladder. Some of the molecular weights of the protein ladder are represented in lane 5.

No bands from the urease present in the concentrate were revealed. This can both mean that either the antibody doesn't bind strongly enough with this urease, or that it was present in very small quantities that couldn't be detected using a western blot, although the last one is extremely unlikely since the technique as a sensitivity of 0.1 ng [79]. Another possible cause is that the dab may not be working properly which explains why the jack bean urease band has so little intensity for a band that contains approximately 1 mg of protein. Although no more western blots were done, in the future one should be done using fresh reagents and seeing if there is a change in intensity and appearance of bands.

The gels used for western blot were also stained with Coomassie blue and silver nitrate to see if there was a difference in bands between them and the gels that had no protein transferred, but since no visual difference was seen in the gels, they weren't displayed in here.

4.7. *B. PASTEURII* ASSAYS IN GOLD SURFACES AND BIOSENSORS

After obtaining samples containing urease from *Bacillus pasteurii*, tests using direct ELISA and sandwich ELISA in the biosensors were employed (figure 4.10a-f). Positive controls using jack bean urease and negative controls were also performed.

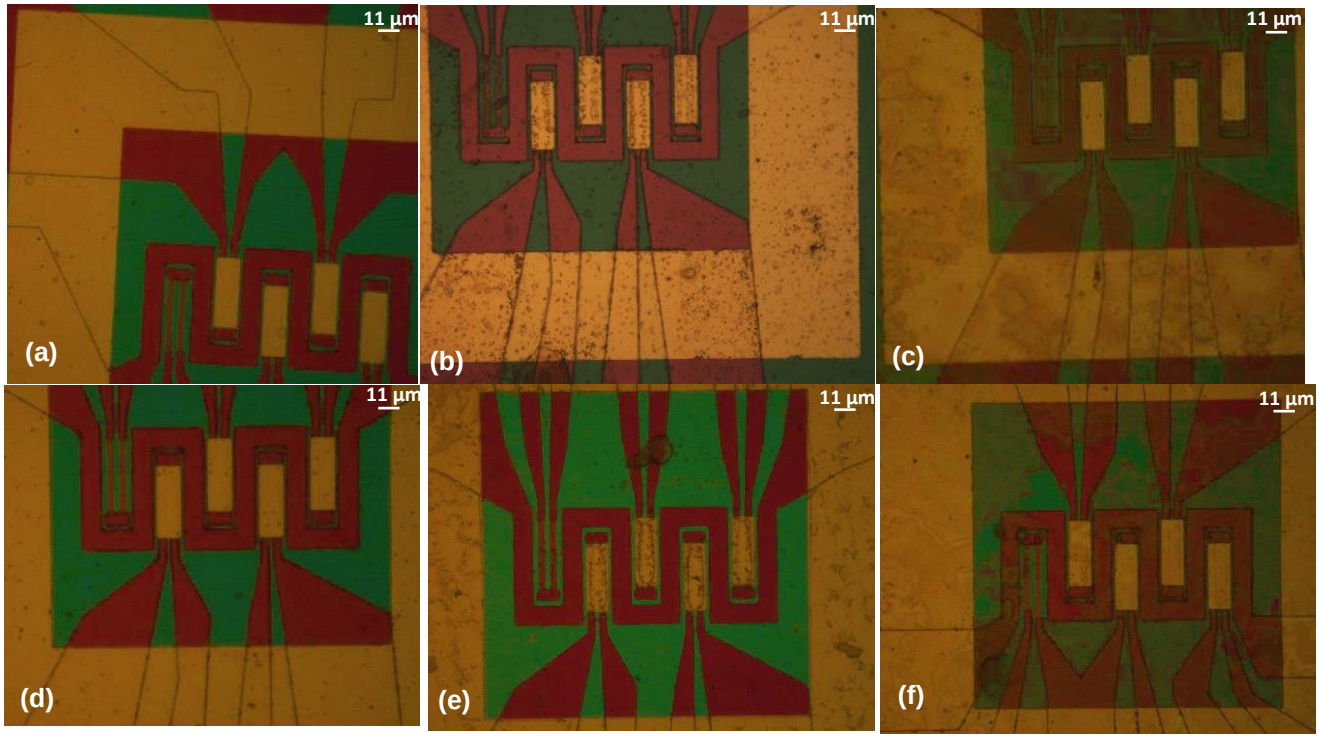

FIGURE 4-10 (a) Negative control (no urease) direct ELISA assay on a biochip (200x magnification). (b) Direct ELISA using 60mg/mL of jack bean urease (200x magnification). (c) Direct ELISA using the concentrate solution after filtration with 100 kDa amicon and containing the *B. pasteurii* urease (200x magnification). (d) Negative control (no urease) sandwich ELISA assay on a biochip (200x magnification). (e) Sandwich ELISA using 60mg/mL of jack bean urease (200x magnification). (f) Sandwich ELISA using the concentrate solution after filtration with 100 kDa amicon and containing the *B. pasteurii* urease (200x magnification).

As previously seen, both direct and sandwich ELISA show similar levels of surface particle concentration. In the assays using the concentrate undiluted, no particle attached to the gold is observed. Instead, the sensor seems to be covered in a layer, possible of proteins, that were at different depths than the gold, and as such couldn't be easily focused in conjunction with surface. It was hypothesized that this layer could be preventing the attachment of the urease to the linker. As such, assays where the urease was pre-recognized by the antibody-magnetic particle complex before surface immobilization were conducted. These tests showed similar results as the ones with urease directly immobilized on the surface, with no *B. pasteurii* urease being detected, thought the layer was no longer present. The fact that no *B. pasteurii* urease was detected despite the layer, that was possibly preventing the attachment, being no longer present during immobilization, could mean that the antibody isn't' recognizing the urease or that the enzyme is present in an extremely low amount. These results are in accordance to the ones obtained by the immunodetection through western blot.

A biosensor functionalized with *B. pasteurii* urease using the sandwich ELISA detection method was read in the platform, with no shift in the baseline being observed, meaning no urease particles were attached to the surface, or they were so but in quantity lower than the sensitivity limit. Again, the use of particle attraction

during the assay could potentially solve the problem if the low concentration is the issue preventing the reading.

One of the other possible explanations for *B. pasteurii* urease not being detected might be that the antibodies conjugated to the magnetic particles are not recognizing the enzyme. This can be explained by the fact that the high concentration of other proteins makes it difficult for the diffusion of recognition complexes to diffuse in the sample and bind to urease, which could be solved by increasing the ratio of Ab-magnetic particles complexes to the concentration of solution. Other explanation could be that are proteins interfering with urease, inhibiting it from interacting with the antibodies. To test this hypothesis assays samples containing urease from *B. pasteurii* were diluted in jack bean urease solution (figure 4.11a-d).

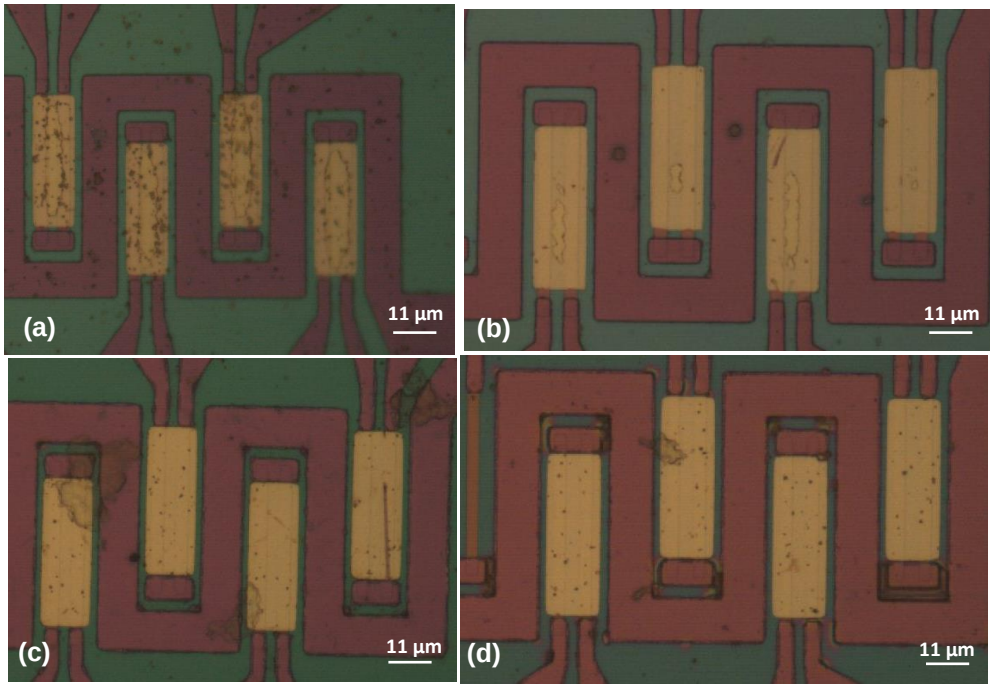

FIGURE 4-11 (a) Positive control assay with direct ELISA using a 50 mg/mL concentration of urease (200x magnification). The next photos pertain to Direct ELISA assays using the concentrate solution with *B. pasteurii* urease diluted in a 50 mg/mL jack bean urease solution with different dilution factors: (b) Dilution factor of 1:4 (200x magnification), (c) Dilution factor of 1:20 (200x magnification), and (d) Dilution factor of 1:100 (200x magnification).

A positive control using urease from jack bean immobilized in the surface via direct ELISA was performed. Comparing it with the other assays, where a small volume of the concentrate solution was diluted in it, a significant decrease in the amount of particles present in the surface is observed. This means that some sort of inhibition of both ureases is occurring that is caused by a protein present in the concentrate solution. By further diluting the urease from *B. pasteurii*, an increase in particles interacting with the urease is seen, though not quite as many as in the control (final concentrations of jack bean urease stayed approximately the same at 37.5, 47.5 and 49.5 mg/mL). Further dilutions should be performed to see if the number of magnetic particles in the surface increases.

These results corroborate what was seen in the colorimetric assays, with the urease enzymatic activity increasing with dilutions. However, the urea that was hypothesized to be causing the inhibition shouldn't be causing the inhibition here since it's very unlikely that the molecule is present in the solution after the amicon with 10 kDa MWCO was used.

4.8. COMSOL SIMULATIONS

Comsol simulations for the mixer considering laminar flow and transport of diluted species were first carried out. By analyzing the results, it is seen that around the obstacles there is a great increase in fluid velocity as it is to be expected, varying one order of magnitude (figure 4.12a-c).

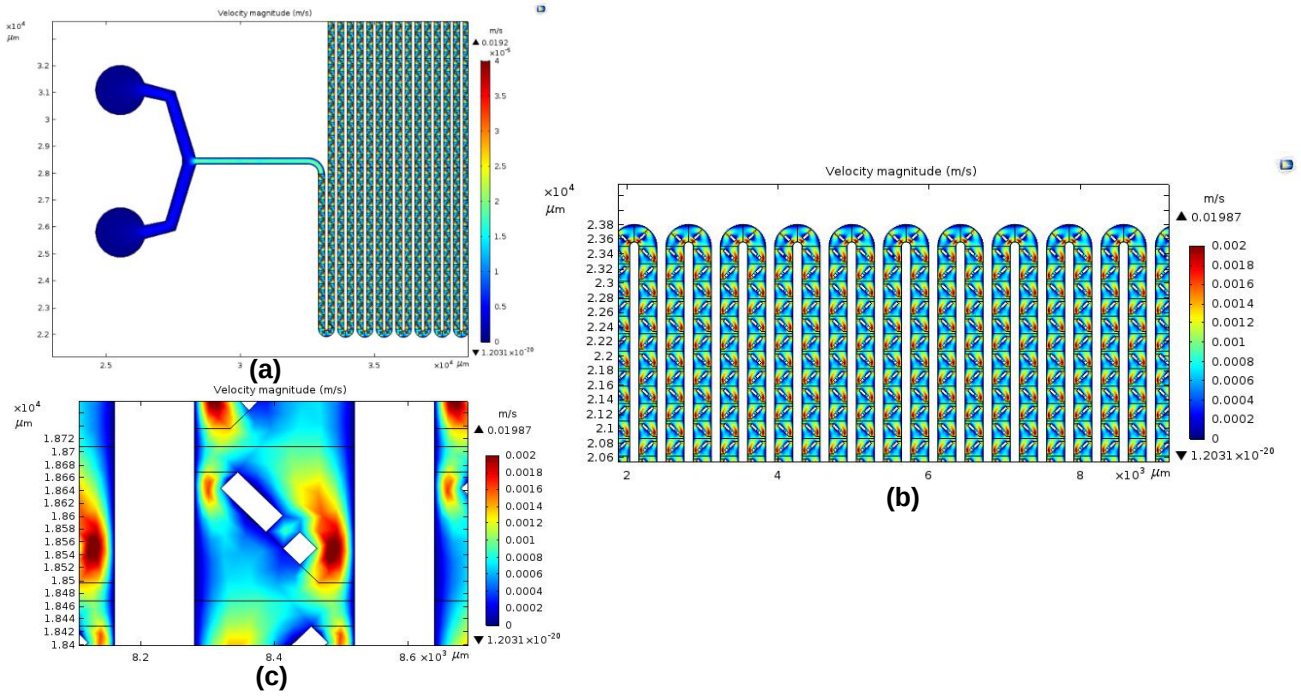

FIGURE 4-12 COMSOL simulation results for the Velocity magnitude (m/s) observed along the (a) inlets of the mixer, (b) Serpentine, and (c) the obstacles in the micromixer. For the simulation laminar flow was considered. Other inputs: Inlet flow rate of 0.1 µL/min; average concentration of the concentrate solution of 0.108 mol/m^3; inflow MNP concentration of 8.136x10^{-7} mol/m^3.

By studying the mass transport in the mixer, it was concluded that, since the urease solution has a much higher concentration than the particles, the concentration of the mixed solution achieves, right at the beginning, a mixed state with a stable concentration between 0.05 and 0.06 mol/m^3. The fact that there are so many proteins in the solution of the urease for so few magnetic particles can difficult the conjugation of the complex Ab-magnetic particles to the urease, since the path to urease is blocked. As such, using a concentrate solution with purified urease or a more diluted solution overall is recommended.

Using the simulations, the Reynolds number, as well the Péclet (Pe) number were calculated. Two cut lines (figure 4-13a-b) were made in the smaller unit constituent of the micromixer in order to simulate the profile of the velocity (figure 4.13c) and of the Reynolds number (figure 4.14) between the walls and the obstacles.

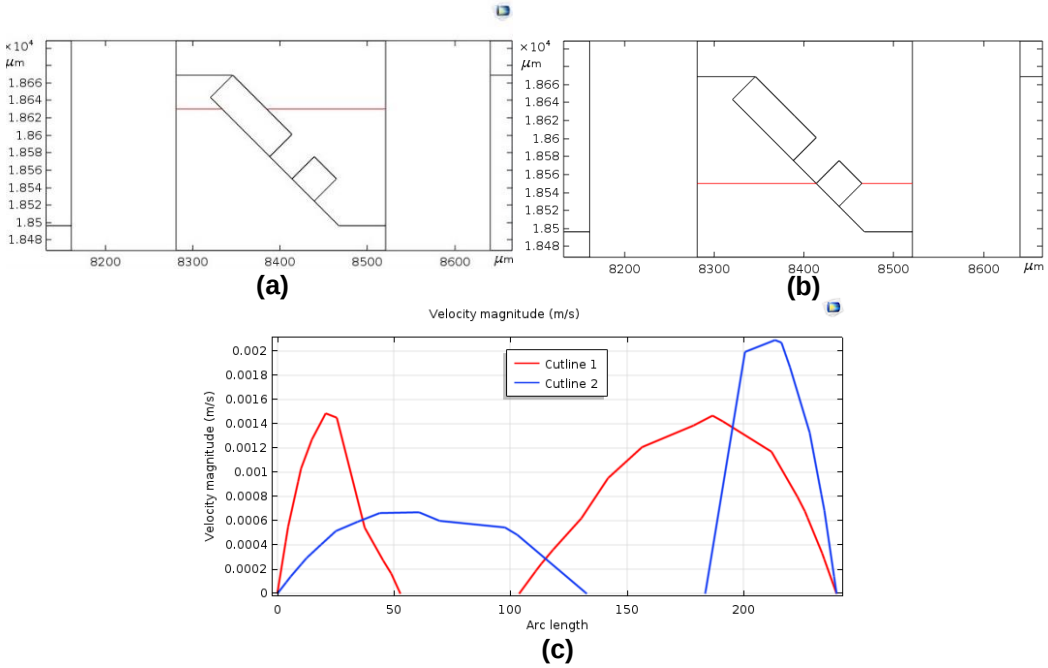

FIGURE 4-13 (a) Cutline 1 made in the smaller units of the micromixer. (b) Cutline 2 made in the smaller units of the micromixer. (c) Velocity profile for both the cutlines made.

To calculate the Reynolds Number, the equation $Re = \frac{uL}{v}$ was employed, with u being the velocity of the fluid (m/s), L being the characteristic linear dimension (m) and v being the kinematic viscosity of the fluid (m^2/s). The Reynolds number was plotted as a function of the velocity of the fluid between the micromixer walls, along different cut lines. The L was assumed to be the smallest dimension, in this case the width of the channel through which fluid can pass. For cut line 1 and cut line 2 we then have a L of approximately 1.9×10^{-4} and 2.22×10^{-4} m, respectively. The kinematic viscosity of the fluid was obtained by the following expression: $v = \frac{\mu}{\rho}$, where μ is the dynamic viscosity (kg/m.s) and ρ is the density (kg/m^3). Considering the fluid as a PBS solution at 25°C, the μ is 0.001 kg/m.s and the ρ is 1006.2 kg/m^3. The value obtained for v was 9.94×10^{-7} m^2/s.

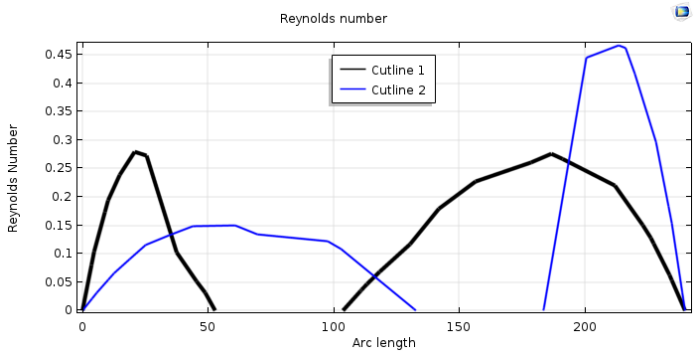

FIGURE 4-14 Reynolds number profile for both the cutlines described in figure 4.13a-b. The Reynolds number was calculated using the equation $\boldsymbol{Re} = \frac{\boldsymbol{uL}}{\boldsymbol{\nu}}$, with the following parameter values: L=1.9x10^{-4} and 2.22x10^{-4} m for the cutline 1 and 2, respectively; $\boldsymbol{\nu}$ of 9.94x10^{-7} m2/s.

Reynolds number below 1 is typical for microfluidic devices, indicating creeping flow.

The Péclet number was calculated using the equation $Pe = \frac{uL}{D}$, with D being the diffusion coefficient (m^2/s) and u the average velocity of the fluid (m/s). This last parameter was acquired in COMSOL after integration of the velocity function in all the domains (7.25Ex10^{-4} m/s). The diffusion coefficient was obtained with the *Stokes-Einstein* relation: $D = \frac{kT}{3\pi d\mu}$, with k = *Boltzmann* constant (1.38065x10^{-23} m^2.kg.s^{-2}.K^{-1}), T = temperature (293 K) and d=particle diameter (250 nm). The value calculated was 1.717x10^{-12} m^2/s. Having the diffusion coefficient D, the Péclet number was calculated, obtaining a Pe of 9.33x10^4. This high Péclet number indicates that the diffusion of the species occurs slowly, as opposed to the phenomenon of advection. As such, the interfaces between flow streams are dictated only by the flow rate in the inlets.

The same simulations were made for the mixer without the obstacles in order to compare their relevance in the mixing (figure 4.15a-b). The simulation for mass transport is not represented since it yields the same results as the mixer with obstacles, having achieved stable concentration in the initial zone of the structure.

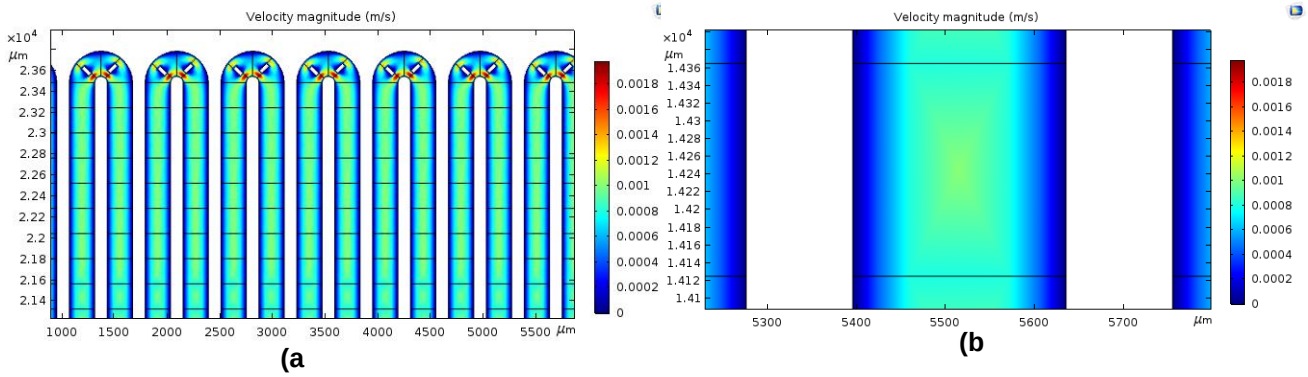

FIGURE 4-15 COMSOL simulation results for the Velocity magnitude (m/s) observed along the micromixer without obstacles. (a) Serpentine close-up. (b) Close-up of the individual units constituent of the micromixer. For the simulation laminar flow was considered. Other inputs: Inlet flow rate of 0.1 µL/min; average concentration of the concentrate solution of 0.108 mol/m^3; inflow MNP concentration of 8.136x10^{-7} mol/m^3.

Similar to what was done previously, a 1D cutline (figure 4.16a) was made to analyze the velocity profile (figure 4.16b) and the variation of the Reynolds number (figure 4.16c) along the walls of the mixer.

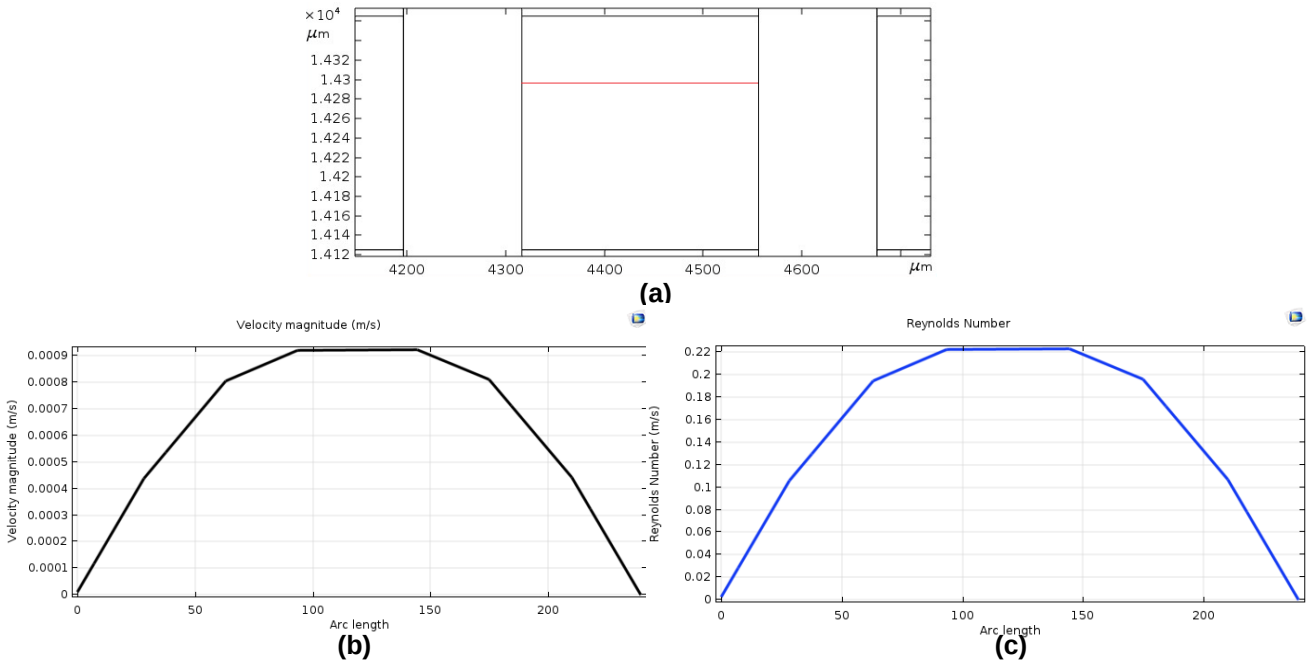

FIGURE 4-16 (a) Cutline made in the smaller units of the micromixer. (b)) Velocity profile for the cutline made. (c) Reynolds number profile for the cutline. The Reynolds number was calculated using the equation $\boldsymbol{Re} = \frac{\boldsymbol{uL}}{\boldsymbol{\nu}}$, with the following parameter values: L=2.40x10^{-4} m and $\boldsymbol{\nu}$ of 9.94x10^{-7} m2/s.

The Reynolds number was calculated like described for the micromixer with obstacles. The only difference here is the value of L , which is 2.40x10^{-4} m.

As it can be observed, both the velocity and Reynolds number are lower when there are no obstacles present. In one cutline from the mixer with obstacles, the Reynolds number was double the one obtained in here, meaning there is a better mixing, with more turbulence, in the case of the structures containing the obstacles.

The average velocity obtained in this micromixer was 6.24x10^{-4} m/s, slightly lower than the mixer with the obstacles. The Péclet number was, as such, also lower, with the value of 8.723x10^{4}.

4.9. MICROFLUIDICS FOR SAMPLE PREPARATION

The aluminum mask obtained by laser exposure can be seen in figure 4.17a. One Su-8 mold was fabricated using the mask (figure 4.17b). In order to use smaller silicon substrates, a few of the structures were cut. These structures however were of no relevance to the work in this thesis. The heights of the mold were obtained by using the profilometer. Three-point heights were taken from the mixer and magnetic separator to be utilized in order to obtain an average. The heights obtained for the mixer and the magnetic separator are close to the expected height of 50 µm, with the obtained values having an error of 2.32% and 3.50%, respectively.

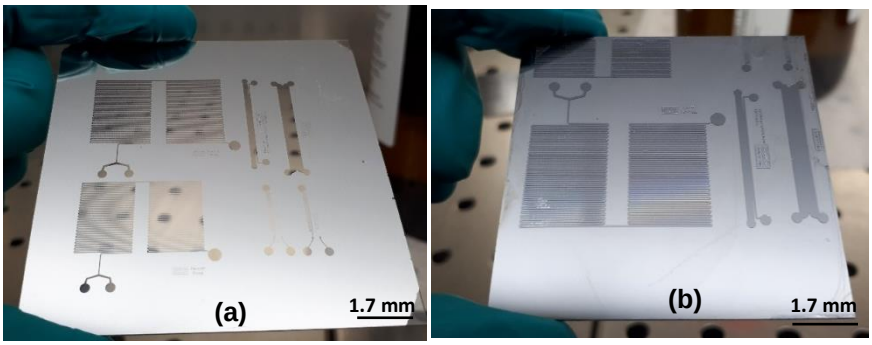

FIGURE 4-17 (a) Aluminum mask of the microfluidic structures. (b) SU-8 mold of the micromixer and magnetic separators.

Using these molds, PDMS structures were fabricated and bonded to glass substrates. Before doing the assay with biological samples, dyes were used to see if mixing occurred in the mixer and if the fluids flowed as supposed in the magnetic separator. Two syringe pumps were used: one injected the red and green dyes at flow rate of 25 µL/min in the inlets of the micromixer while the other injected blue dye in the inlet of the separator closer to the magnet at a flow rate of 25 µL/min. Both PDMS structures were joined by a tube. The setup of the experiment can be seen in figure 4.18a. Initially only the green dye was passing to the mixer due to pressure differences, but after manual tweaking, both the green and red dyes started to enter the mixer at the same time. The mixed color has still a red tint to it. To better see the mixing, dyes with more color intensity should be used. The fluids traveled through the mixer and passed to the magnetic separator with no issues, sticking to the left side of the magnetic structure as seen on figure 4.18b. After the pumping of the blue dye started, both fluids were still going out through the left outlet, instead of the expected (blue dye leaving through the right outlet and red dye leaving through left outlet). This started to happen at the same time that a leak of dyes occurred in the mixer, indicating too much fluid pressure or improper bonding. This leak slowed the flowrate inside the structures. This slowdown of the flowrate caused a small and intermittent passage of reddish fluid in the separator, with the blue dye occupying the whole of the separator.

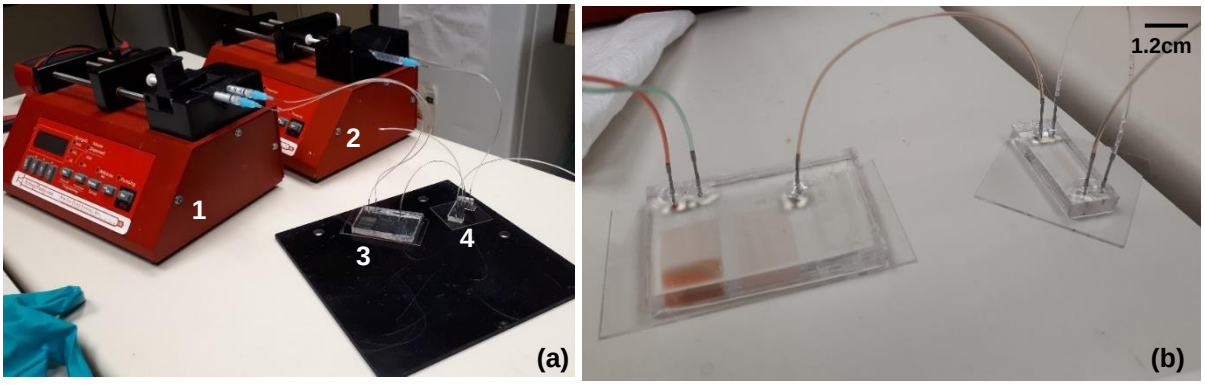

FIGURE 4-18 (a) Experimental set-up for the sample preparation using the microfluidic modules: (1) Syringe pump connected to the inlets of the micromixer and containing the syringes of urease sample and of Ab-magnetic particles solution in the biological assay, or the red and green dyes in the dyes assay, (2) Syringe pump connected to one inlet of the magnetic separator and containing the syringe of buffer in the biological assay, or the blue dye in the dyes assay, (3) Micromixer PDMS structure connected with a tube to the (4) Magnetic separator PDMS structure. (b) Photo the mixing of red and green dyes in the micromixer.

To better understand what was happening, an assay using only the magnetic separator and two dyes was performed. Both the dyes were injected with a flow rate of 25 µL/min. In figure 4.19a, a clear distinction between the dyes can be seen, as it is expected, with no mixing observed. However, at some point in the assay, the dyes started to leave through the same outlet. This probably happened due to the outlets having slighter different pressures. Changing the flow rates, making one slightly lower than the other (red dye injected with 15 µL/min and blue dye injected at 45 µL/min), in order to change the pressure and see if any changes in the outlet flow happened, the fluids started mainly leaving through the opposite outlet as before, though small quantities were still going through the other outlet. Tweaking with the flow rates can probably lead to a better fluid separation in the outlets, though the structure should probably be changed to guarantee perfect flow, for example, a more delineated division between both outlets.

The individual structure of the magnetic separator was also used to see if, when passing a magnetic particle solution through the channel, the magnet on the side opposite to the passage would attract the particles (figure 4.19b). Passing a diluted magnetic solution in the right inlet and a buffer in the left inlet, it was possible to see that the particles were attracted to the left side of the separator into the buffer solution. If the flow rate was slow (5-15 µL/min), the particles would stay attached to the wall, however, if the flowrate was increased, the particles would still be attracted to the magnet but would then keep moving alongside the wall and leave through the outlet. Both ways still lead to a separation of the particles from the original solution, so it's a matter of seeing the most appropriate way of separation. The advantage of using higher flowrates is that the user doesn't have to take the magnet out for the particles to flow, although this may cause a significant dilution of the particles with the buffer, making it more difficult to detect. That is the advantage of the particles staying attached to the wall. After the assay, the user can remove the magnet and pass a desired volume of buffer to get a more concentrated solution of particles.

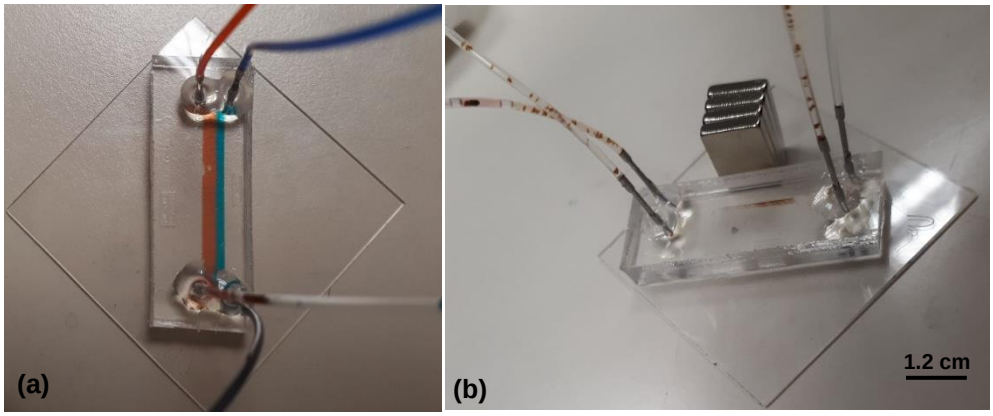

FIGURE 4-19 (a) Passage of red and blue dyes in the magnetic separator. Clear separation of dyes with no diffusion of fluids is observed. (b) Attraction of the Micromod 250nm magnetic particles to the magnet passing on the left side of the separator.

For the biological sample preparation, two syringe pumps were also used, one to inject the urease solution (60 mg/ml) and magnetic particles-antibodies solution previously prepared, in the inlets of the mixer with a flow rate of 25 µL/min. The second syringe pump was used to inject the PBS Tween 20 buffer in the right side of the magnetic separator at a flowrate of 15 µL/min (side close to the magnet). The solutions entered the mixer without issues. In the magnetic separator the option of the slower flowrate of buffer was adopted, meaning the particles were attracted to the magnet and stayed attached. After passing all the urease solution, pumping of the syringes in the mixer was stopped and the magnet removed. The magnetic particles flowed with the passage of buffer and were collected in an Eppendorf, though some of the particles were lost. An Eppendorf with the magnetic particles solution was compared to the Eppendorf containing the collected magnetic particles supposedly attached to the urease, with the latter being much more diluted.

The collected particles were then used to perform a sandwich ELISA in biochips surface (figure 4.20a). As control, a solution of Ab-magnetic particles attached to urease prepared in an Eppendorf was used (figure 4.20b).

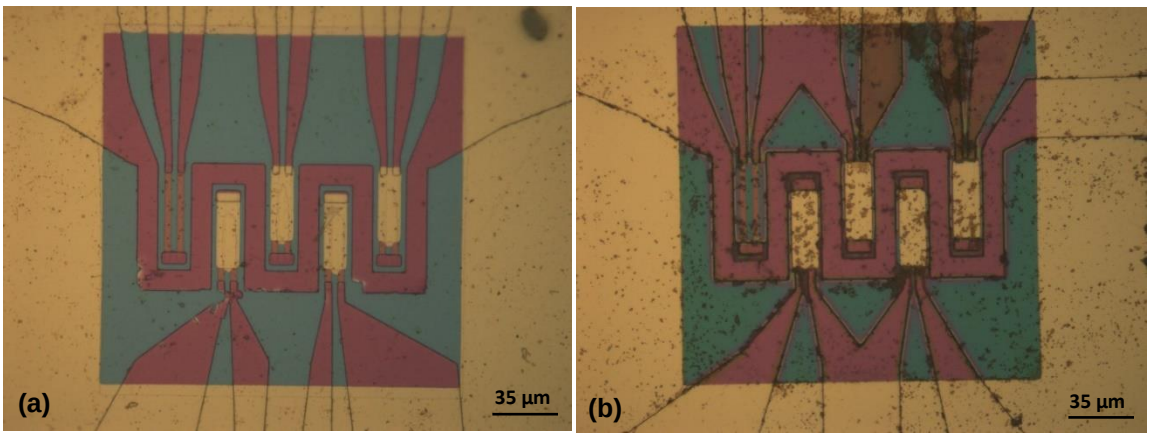

FIGURE 4-20 (a) Sandwich ELISA assay using the sample prepared on the microfluidic structures (200x magnification). Urease solution with 40 mg/mL was used. (b) Positive control with a direct Sandwich using 40 mg/mL of jack bean urease pre-recognized with Ab-magnetic particles without microfluidic sample preparation (200x magnification).

In the microfluidics assay, the concentration of magnetic particles in the surface is lesser than the ones in the conventional assay, which is explained because of the higher dilution of the former magnetic particles solution. The fact that magnetic particles are visible in figure 4.20a is an indicator that the antibodies were able to attach to the urease during mixing, and that the magnetic particles were successfully separated in the magnetic separator. This serves as proof of concept, although much optimization is still needed.

5. CONCLUSIONS AND FUTURE PROSPECTS

With the increase in population and migration to cities, a higher need for civil infrastructures that rely on sustainable principles is emerging. One of the most promising has its bases in the harnessing of biological processes in soils, more specifically, the process known as biocementation or microbially induced calcite precipitation. This process describes the phenomena of precipitation of calcium carbonate as a consequence of microbial metabolic activity. Although calcite precipitation may be achieved by many different processes, enzymatic hydrolysis of urea by urease produced by microbes is the most energy efficient. One of the challenges involving the biological approach to biocementation is centered around the performance monitoring of both biological and chemical system components, with these often requiring discrete samples that need tests performed on them, usually in a laboratory, giving no real-time information and being labor intensive. This leads to a need for a method of monitoring that is reliable and able to give *in situ* information about the state of the system. One possibility is the use of a LOC device that integrates one or several laboratory functions on a relatively small and portable apparatus.

The work performed on this thesis is aimed at optimizing a magnetoresistive platform for urease quantification that acts as a LOC. This was accomplished by testing which were the best detection methods, obtaining a calibration curve for urease, growing *B. pasteurii* followed by urease concentration and quantification using colorimetric methods, and finally, obtaining a rough PDMS device capable of preparing the sample without much manual work.

Both direct ELISA and sandwich ELISA were compared as detection methods for jack bean urease, no visual difference being obtained between the two, though the sandwich ELISA is considered to be the preferred method for analyzing samples containing other proteins other than urease. In the negative controls, were no urease was used, some particles were still observed to be attached to the surface, though the difference between the control and bioactive substrate was clearly notable. This might be due to the free cysteine residues present in the antibody that bind to the linker via amine bonds.

Using concentrations of urease between 0.5 mg/mL and 70 mg/mL, a calibration curve for quantification of urease using the direct ELISA method was obtained, with 0.5 mg/mL being the detection limit for the conditions employed, and 70 being the saturation limit of urease in solution. A saturation of sensors could be observed around the 60 mg/mL urease concentration. During the assays performed using the platform, some sensors were short circuited due to aluminum corrosion most likely caused by degradation of the passivation layer coupled with the electric current passing and immersion in an ionic solution.

A culture of *B. pasteurii* was grown, obtaining a growth curve using OD measurements at 600 nm. Using the Eq.4.1 [68] an average value of $2.52x10^8$ cells was achieved in the end of the growth. The proteins and cell debris resulting from sonication and centrifugation of the *B. pasteurii* cells and medium were subjected to total protein quantification by BCA kit, as well an urease activity assay in order to calculate the specific enzymatic activity. What was observed was that there was an increase in the specific enzymatic activity with the dilution factor as a result of the increase in the urease activity with dilution. According to Sumner and Howell [76] urease activity increases with increasing buffer dilution until a point is reached beyond which further dilution may cause the activity to decrease. This increase can be explicated by the inhabitation of urease caused by urea in alkaline solutions as the one used in this work, or by the inhibition of the complex ammonia-urea whose formation is favored in alkaline solutions with high urea concentrations [76], [77].

A SDS-PAGE gel electrophoresis, as well as a western blot, were also performed to separate and visualize the urease. A 12% polyacrylamide gel with duplicates of concentrate with a dilution of 1:100 and filtrate and pure urease from Jack bean at 40 mg/ml concentration was run. Three distinct bands with disparate weights appeared in the pure urease lane, when only one band should appear [78]. The extra two bands could be explained by a possible contamination by other proteins. In the western blot, after optimizing the materials and conditions, only one of the bands with the molecular weight of 100 kDa of jack bean urease appeared in the membrane. The fact that only these 100 kDa bands were the only ones to have appeared in the pure urease lane may explain that the others are indeed part of protein contaminants. The fact that no bands from the concentrate were revealed probably means that either the antibody doesn't bind strongly enough with this urease, that it was present in very small quantities that couldn't be detected using a western blot, although the latter is extremely unlikely, or that the dab used might not be in the best conditions.

Using the concentrate containing *B. pasteurii* urease for biochips surface functionalization, the need for switching the method from urease surface immobilization to a urease pre-recognized by Ab-magnetic particles before immobilization arouse due to a layer preventing attachment of the target molecule. However, these tests also resulted with no *B. pasteurii* urease being detected, although the layer was no longer present. These results could mean that the antibody isn't recognizing the urease or that the enzyme is present in an extremely low amount, which is in accordance to the results obtained by the immunodetection through western blot. A biosensor functionalized with *B. pasteurii* urease using the sandwich ELISA detection method was read in the platform, with no shift in the baseline being observed. These can be due to low urease amount, antibody not recognizing the enzyme, difficulty for the recognition complexes to diffuse in the sample and bind to urease due to a high concentration of other proteins, or that there are proteins interfering with urease. By doing dilution of the *B. pasteurii* urease in a jack bean urease solution, a significant decrease in the amount of particles present in the surface was observed, with gradual increase with dilution factor. This means there is occurring some sort of inhibition of both ureases that is caused by

some protein present in the concentrate solution. These results corroborate what was seen in the colorimetric assays, with urease enzymatic activity increasing with dilutions.

Comsol simulations for the mixer, with both and no obstacles, were performed considering laminar flow and transport of diluted species were first carried out. By analyzing the results, it is seen that around the obstacles there is a great increase in fluid velocity as it is to be expected, varying one order of magnitude, which in turn leads to an increase in the Reynolds number, enhancing mixing. In both structures the Reynols number was below 1, indicating creeping flow. The average velocity of the fluid is 7.25×10^{-4} m/s for the mixer with obstacles and 6.24×10^{-4}m/s for the one without obstacles. The Péclet number was calculated, the values of 9.33×10^{4} and 8.723×10^{4} being obtained for the micromixer with and without obstacles, respectively. The high Péclet number obtained is indicative of slower solute species diffusion, as opposed to the phenomenon of advection. As such, the interfaces between flow streams are dictated only by the flow rate in the inlets.

Using the sample preparation module fabricated in PDMS with both dyes and biological samples, some issues occurred regarding the passing of solutions through the mixer inlets and the magnetic separator outlets, with one of the inlets/outlets being preferred for the entering/leaving of the fluids. This happens due to difference in pressures. The testing of the individual structure of the magnetic separator lead to the conclusion that if the flow rate was slow (5-15 µL/min), the particles would stay attached to the wall close to the magnet after being attracted to it, and if the flowrate was increased. the particles, although still attracted to the magnet, would then keep moving alongside the wall and leave through the outlet. The final solution obtained in the biological assay containing the magnetic particles diluted in PBS buffer was used to perform a sandwich ELISA in a biochip. Magnetic particles were observed attached to the sensors surface, although in less quantity when compared to manual sample preparation due to, most likely, the dilution factor. This indicates that the sample preparation using the microfluidic structure was successful.

Even though not all the initial objectives were met, with the work performed through this thesis it was possible to calibrate the LOC device for urease quantification, to uncover some future issues regarding urease extracted from soil to be solved so that a reliable quantification can occur, and finally, to optimize the sample preparation with the use of microfluidics.

Concerning future work, it is of upmost importance the necessity of statistical significance regarding all the assays performed with the conclusions discussed throughout this document needing validation since they are mainly assumptions regarding the experimental results obtained and literature review. Therefore, further studies are required in order to confirm these findings and report them.

Additionally, both the sandwich detection method as well as the method using urease pre-recognized with antibodies and magnetic particles should be read in the platform for more quantitative information. The assays in the platform should use particle attraction for a more sensitive measure.

Furthermore, a western blot using fresh reagents should be performed to see if there is an appearance of *B. pasteurii* urease bands. In the case that they do not show, a more suitable antibody should be found. Still regarding the study of *B. pasteurii* urease, further dilution factors must be used in the colorimetric assays in order to find the saturation and starting point of the decrease of urease activity.

Finally, the sample preparation PDMS module should be optimized, mainly finding the best flow rates that lead to a better fluid separation in the outlets as well as improve the structures to guarantee perfect flow.

Overall, in the future, there is still much work and optimization to be done before the use of the LOC apparatus for urease field quantifications.

BIBLIOGRAPHY

[1] J. T. DeJong, B. M. Mortensen, B. C. Martinez, and D. C. Nelson, "Bio-mediated soil improvement," *Ecol. Eng.*, vol. 36, no. 2, pp. 197–210, 2010.

[2] M. Burbank *et al.*, "Biogeochemical processes and geotechnical applications: progress, opportunities and challenges," *Géotechnique*, vol. 63, no. 4, pp. 287–301, 2013.

[3] J. K. Mitchell and J. C. Santamarina, "Biological Considerations in Geotechnical Engineering," *J. Geotech. Geoenvironmental Eng.*, vol. 131, no. 10, pp. 1222–1233, 2005.

[4] S. Stocks-Fischer, J. K. Galinat, and S. S. Bang, "Microbiological precipitation of CaCO3," *Soil Biol. Biochem.*, vol. 31, no. 11, pp. 1563–1571, 1999.

[5] K. L. Bachmeier, A. E. Williams, J. R. Warmington, and S. S. Bang, "Urease activity in microbiologically-induced calcite precipitation," *J. Biotechnol.*, vol. 93, no. 2, pp. 171–181, 2002.

[6] M. Madigan, *Brock Biology of Organisms*, 12th ed. Pearson/Benjamin Cummings, 2009.

[7] N. Kaur, M. S. Reddy, and A. Mukherjee, "Biomineralization of calcium carbonate polymorphs by the bacterial strains isolated from calcareous sites," *J. Microbiol. Biotechnol.*, vol. 23, no. 5, pp. 707–714, 2013.

[8] L. R. Volpatti and A. K. Yetisen, "Commercialization of microfluidic devices," *Trends Biotechnol.*, vol. 32, no. 7, pp. 347–350, 2014.

[9] S. M. F. Cardoso, "Development of a Urease Quantification Biosensor to Monitor Biocementation Processes in Soils," Master's Thesis, Instituto Superior Técnico, 2015.

[10] J. P. P. Valentim, "Optimization of a Lab-On-Chip Device to Study the Biocementation of Soils," Master's Thesis, Instituto Superior Técnico, 2016.

[11] B. L. Banagan, B. M. Wertheim, M. J. S. Roth, and L. F. Caslake, "Microbial strengthening of loose sand," *Lett. Appl. Microbiol.*, vol. 51, no. 2, pp. 138–142, 2010.

[12] L. J. Stal, "Microphytobenthos as a biogeomorphological force in intertidal sediment stabilization," *Ecol. Eng.*, vol. 36, no. 2, pp. 236–245, 2010.

[13] J. V Giraldez and G. Sposito, "Infiltration in Swelling Soils," vol. 21, no. 1, pp. 33–44, 1985.

[14] S. M. Al-Thawadi, "Ureolytic bacteria and calcium carbonate formation as a mechanism of strength enhancement of sand," *J. Adv. Sci. Eng. Res.*, vol. 1, no. SEPTEMBER 2011, pp. 98–114, 2011.

[15] N. K. Dhami, M. S. Reddy, and M. S. Mukherjee, "Biomineralization of calcium carbonates and their engineered applications: A review," *Front. Microbiol.*, vol. 4, no. OCT, pp. 1–13, 2013.

[16] H. L. Mobley and R. P. Hausinger, "Microbial ureases: significance, regulation, and molecular characterization.," *Microbiol. Rev.*, vol. 53, no. 1, pp. 85–108, 1989.

[17] R. E. Riding and S. M. Awramik, *Microbial sediments*, vol. 139, no. 3–4. 2000.

[18] F. G. Ferris, V. Phoenix, Y. Fujita, and R. W. Smith, "Kinetics of calcite precipitation induced by ureolytic bacteria at 10 to 20??C in artificial groundwater," *Geochim. Cosmochim. Acta*, vol. 68, no. 8, pp. 1701–1722, 2004.

[19] C. Langdon *et al.*, "Effect of calcium carbonate saturation state on the rate of calcification of an experimental coral reef," *Global Biogeochem. Cycles*, vol. 14(2), no. 10.1594/PANGAEA.721195, pp. 639–654, 2000.

[20] D. Mujah, M. A. Shahin, and L. Cheng, "State-of-the-Art Review of Biocementation by Microbially Induced Calcite Precipitation (MICP) for Soil Stabilization," *Geomicrobiol. J.*, vol. 34, no. 6, pp. 524–537, 2017.

[21] M. B. Burbank, T. J. Weaver, T. L. Green, B. Williams, and R. L. Crawford, "Precipitation of calcite by indigenous microorganisms to strengthen liquefiable soils," *Geomicrobiol. J.*, vol. 28, no. 4, pp. 301–312, 2011.

[22] scott B. Mulrooney and R. P. Hausinger, "Sequence of the Klebsiella aerogenes Urease Genes and Evidence for Accessory Proteins Facilitating Nickel Incorporation," *J. Bacteriol.*, vol. 172, no. 10, pp. 5837–5843, 1990.

[23] L. van Paassen, *Biogrout: Ground Improvement by Microbially Induced Carbonate Precipitation*. pp. 161-178, 2009.

[24] M. G. Gomez *et al.*, "Field-scale bio-cementation tests to improve sands," *Proc. Inst. Civ. Eng. - Gr. Improv.*, vol. 168, no. 3, pp. 206–216, 2015.

[25] A. Salek-Maghsoudi *et al.*, "Recent advances in biosensor technology in assessment of early diabetes biomarkers," *Biosens. Bioelectron.*, vol. 99, pp. 122–135, 2018.

[26] C. Situ, M. H. Mooney, C. T. Elliott, and J. Buijs, "Advances in surface plasmon resonance biosensor technology towards high-throughput, food-safety analysis," *TrAC - Trends Anal. Chem.*, vol. 29, no. 11, pp. 1305–1315, 2010.

[27] J. Ali, J. Najeeb, M. Asim Ali, M. Farhan Aslam, and A. Raza, "Biosensors: Their Fundamentals, Designs, Types and Most Recent Impactful Applications: A Review," *J. Biosens. Bioelectron.*, vol. 8, no. 1, pp. 1–9, 2017.

[28] R. L. Edelstein *et al.*, "The BARC biosensor applied to the detection of biological warfare agents," *Biosens. Bioelectron.*, vol. 14, no. 10–11, pp. 805–813, 2000.

[29] M. I. H. Ansari, S. Hassan, A. Qurashi, and F. A. Khanday, "Microfluidic-integrated DNA nanobiosensors," *Biosens. Bioelectron.*, vol. 85, pp. 247–260, 2016.

[30] C. K. Dixit and A. Kaushik, *Microfluidics for biologists: Fundamentals and applications*. pp. 1-38, 2016.

[31] D. G. Rackus, M. H. Shamsi, and A. R. Wheeler, "Electrochemistry, biosensors and microfluidics: a convergence of fields," *Chem. Soc. Rev.*, vol. 44, no. 15, pp. 5320–5340, 2015.

[32] M. Alvarez, K. Zinoviev, M. Moreno, and L. M. Lechuga, "Cantilever biosensors," *Opt. Biosens.*, no. i, pp. 419–452, 2008.

[33] A. Ymeti *et al.*, "Fast, ultrasensitive virus detection using a young interferometer sensor," *Nano Lett.*, vol. 7, no. 2, pp. 394–397, 2007.

[34] D. L. Graham, H. A. Ferreira, and P. P. Freitas, "Magnetoresistive-based biosensors and biochips," *Trends Biotechnol.*, vol. 22, no. 9, pp. 455–462, 2004.

[35] L. Jogschies *et al.*, "Recent developments of magnetoresistive sensors for industrial applications," *Sensors*

(Switzerland), vol. 15, no. 11, pp. 28665–28689, 2015.

[36] C. Reig, M.-D. Cubells-Beltrán, and D. Ramírez, "Magnetic Field Sensors Based on Giant Magnetoresistance (GMR) Technology: Applications in Electrical Current Sensing," *Sensors*, vol. 9, no. 10, pp. 7919–7942, 2009.

[37] W. Thomson, "On the Electro-Dynamic Qualities of Metals:--Effects of Magnetization on the Electric Conductivity of Nickel and of Iron," *Proc. R. Soc. London*, vol. 8, pp. 546–550, 1856.

[38] B. Dieny *et al.*, "Magnetotransport properties of magnetically soft spin-valve structures (invited)," *J. Appl. Phys.*, vol. 69, no. 8, pp. 4774–4779, 1991.

[39] P. P. Freitas, R. Ferreira, S. Cardoso, and F. Cardoso, "Magnetoresistive sensors," *J. PhysicsCondensed Matter*, vol. 19, no. 16, p. 165221, 2007.

[40] U. Hartmann, *Magnetic Multilayers and Giant Magnetore si stance*. New York: Springer-Verlag Berlin Heildberg, 2000.

[41] G. Lin, D. Makarov, and O. G. Schmidt, "Magnetic sensing platform technologies for biomedical applications," *Lab Chip*, vol. 17, no. 11, pp. 1884–1912, 2017.

[42] S. J. Osterfeld *et al.*, "Multiplex protein assays based on real-time magnetic nanotag sensing.," *Proc. Natl. Acad. Sci. U. S. A.*, vol. 105, no. 52, pp. 20637–40, 2008.

[43] V. C. Martins *et al.*, "Challenges and trends in the development of a magnetoresistive biochip portable platform," *J. Magn. Magn. Mater.*, vol. 322, no. 9–12, pp. 1655–1663, 2010.

[44] S. Chakraborty, *Microfluidics and Microfabrication*. New York: Springer, 2010.

[45] S. Mitra and S. Chakraborty, *Microfluidics and Nanofluidics Handbook: Chemistry, physics, and life science principles*. 2012.

[46] D. E. Angelescu, *Highly Inthegrated Microfluidics Design*. pp. 139-166, 2011.

[47] "Reynolds number and regime flows." [Online]. Available: http://www.writeopinions.com/reynolds-number. [Accessed: 24-Oct-2017].

[48] H. Yu, Z. Z. Chong, S. B. Tor, E. Liu, and N. H. Loh, "Low temperature and deformation-free bonding of PMMA microfluidic devices with stable hydrophilicity via oxygen plasma treatment and PVA coating," *RSC Adv.*, vol. 5, no. 11, pp. 8377–8388, 2015.

[49] D. Bartolo, G. Degré, P. Nghe, and V. Studer, "Microfluidic stickers," *Lab Chip*, vol. 8, no. 2, pp. 274–279, 2008.

[50] N. A. Peppas and A. R. Khare, "Preparation, structure and diffusional behavior of hydrogels in controlled release," *Adv. Drug Deliv. Rev.*, vol. 11, no. 1–2, pp. 1–35, 1993.

[51] J. Heo and R. M. Crooks, "Microfluidic biosensor based on an array of hydrogel-entrapped enzymes," *Anal. Chem.*, vol. 77, no. 21, pp. 6843–6851, 2005.

[52] C. W. Tsao, "Polymer microfluidics: Simple, low-cost fabrication process bridging academic lab research to commercialized production," *Micromachines*, vol. 7, no. 12, 2016.

[53] S. H. Tan, N. T. Nguyen, Y. C. Chua, and T. G. Kang, "Oxygen plasma treatment for reducing hydrophobicity of a sealed polydimethylsiloxane microchannel," *Biomicrofluidics*, vol. 4, no. 3, pp. 1–8, 2010.

[54] C. M. B. Ho, S. H. Ng, K. H. H. Li, and Y.-J. Yoon, "3D printed microfluidics for biological applications," *Lab Chip*, vol. 15, no. 18, pp. 3627–3637, 2015.

[55] A. Bonyár, H. Sántha, B. Ring, M. Varga, J. G. Kovács, and G. Harsányi, "3D Rapid Prototyping Technology (RPT) as a powerful tool in microfluidic development," *Procedia Eng.*, vol. 5, pp. 291–294, 2010.

[56] "Point-of-care Diagnostic Testing," 2010 [Online]. Available: https://report.nih.gov/nihfactsheets/ViewFactSheet.aspx?csid=112. [Accessed: 18-Nov-2017].

[57] D. Mark, S. Haeberle, G. Roth, F. Von Stetten, and R. Zengerle, "Microfluidic lab-on-a-chip platforms: Requirements, characteristics and applications," *NATO Sci. Peace Secur. Ser. A Chem. Biol.*, no. 3, pp. 305–376, 2010.

[58] H. Jung, M.-S. Chun, and M.-S. Chang, "Sorting of human mesenchymal stem cells by applying optimally designed microfluidic chip filtration.," *Analyst*, vol. 140, no. 4, pp. 1265–74, 2015.

[59] P. G. Gross, E. P. Kartalov, A. Scherer, and L. P. Weiner, "Applications of microfluidics for neuronal studies," *J. Neurol. Sci.*, vol. 252, no. 2, pp. 135–143, 2007.

[60] G. Mauleon, C. P. Fall, and D. T. Eddington, "Precise spatial and temporal control of oxygen within in vitro brain slices via microfluidic gas channels," *PLoS One*, vol. 7, no. 8, 2012.

[61] C. Caviglia *et al.*, "Impedimetric toxicity assay in microfluidics using free and liposome-encapsulated anticancer drugs," *Anal. Chem.*, vol. 87, no. 4, pp. 2204–2212, 2015.

[62] D. Huh, B. D. Matthews, A. Mammoto, M. Montoya-Zavala, H. Y. Hsin, and D. E. Ingber, "Reconstituting Organ-Level Lung Functions on a Chip," *Science (80-.).*, vol. 328, no. 5986, pp. 1662–1668, 2010.

[63] F. A. Cardoso, "Design, optimization and integration of magnetoresistive biochips," Doctoral Dissertation, Instituto Superior Técnico, 2011.

[64] T. M. Dias, "Magnetoresistive chip-based platform for the evaluation of cfDNA integrity as a potential biomarker in cancer diagnosis," Master's Thesis, Instituto Superior Técnico, 2011.

[65] M. Honda, Y. Baba, T. Sekiguchi, I. Shimoyama, and N. Hirao, "Electrochemical immobilization of biomolecules on gold surface modified with monolayered l-cysteine," *Thin Solid Films*, vol. 556, pp. 307–310, 2014.

[66] S. Ferretti, S. Paynter, D. A. Russell, K. E. Sapsford, and D. J. Richardson, "Self-assembled monolayers: a versatile tool for the formulation of bio-surfaces," *TrAC Trends Anal. Chem.*, vol. 19, no. 9, pp. 530–540, 2000.

[67] R. R. Pedreira, "Bio – Cimentação de Solos Arenosos para Melhoramento das suas Características Hidro - Mecânicas,"Master's Thesis, Instituto Superior Técnico, 2014.

[68] S. K. Ramachandran, V. Ramakrishnan, and S. S. Bang, "Remediation of concrete using micro-organisms," *ACI Materials Journal*, vol. 98, no. 1. pp. 3–9, 2001.

[69] M. J. Madou, *Microfabrication and nanotechnology Volume II - Manufacturing Techniques for Microfabrication and Nanotechnology*, Third. Boca Raton: CTaylor & Francis Group, 2011.

[70] V. C. Martins *et al.*, "Femtomolar limit of detection with a magnetoresistive biochip," *Biosens. Bioelectron.*, vol. 24, no. 8, pp. 2690–2695, 2009.

[71] V. C. B. Martins, "A Magnetoresistive Biochip Platform: detection of DNA hybridization and antibody/cell recognition,"Doctoral Thesis, Instituto Superior Técnico, 2008.

[72] A. A. S. Bhagat and I. Papautsky, "Enhancing particle dispersion in a passive planar micromixer using rectangular obstacles," *J. Micromechanics Microengineering*, vol. 18, no. 8, p. 85005, 2008.

[73] J. J. Lai, K. E. Nelson, M. A. Nash, A. S. Hoffman, P. Yager, and P. S. Stayton, “Dynamic bioprocessing and microfluidic transport control with smart magnetic nanoparticles in laminar-flow devices,” *Lab Chip*, vol. 9, no. 14, p. 1997, 2009.

[74] “How big is the average protein?” [Online]. Available: http://book.bionumbers.org/how-big-is-the-average-protein/. [Accessed: 27-Oct-2017].

[75] “Conversion: weight-moles (for proteins).” [Online]. Available: http://molbiol.edu.ru/eng/scripts/01_04.html. [Accessed: 24-Oct-2017].

[76] F. Howell and B. Sumner, “Buffer Effects upon Urease Activity,” *J. Biol. Chem.*, pp. 619–626, 1934.

[77] C. L. Deasy, “The Mechanism of Urease Inhibition by Urea,” *J. Am. Chem. Soc.*, vol. 69, no. 2, pp. 294–295, 1947.

[78] B. Krajewska, “Ureases I. Functional, catalytic and kinetic properties: A review,” *J. Mol. Catal. B Enzym.*, vol. 59, no. 1–3, pp. 9–21, 2009.

[79] “National Diagnostics: Overview of Western Blotting.” [Online]. Available: https://www.nationaldiagnostics.com/electrophoresis/article/overview-western-blotting. [Accessed: 15-Oct-2017].

APPENDIX A: PROTEIN BLAST, PROTEIN LADDER AND CALIBRATION CURVES

A.1 PROTEIN BLAST

urease [Sporosarcina pasteurii]
Sequence ID: CAA55175.1
▶ See 1 more title(s)

Range 1: 3 to 569 GenPept Graphics ▼ Next Match ▲ Previous Match

Score	Expect	Method	Identities	Positives	Gaps
692 bits(1787)	0.0	Compositional matrix adjust.	333/568(59%)	427/568(75%)	2/568(0%)

```
Query  274  IHRKEYANKYGPTTGDKIRLGDTNLLAEIEKDYALYGDECVFGGGKVIRDGMGQSCGHPP  333
            I+R++YA  YGPT GD++RL DT+L  E+EKDY   GDE  FGGGKV+R+GMG++  +
Sbjct  3    INRQQYAESYGPTVGDRVRLADTDL-GEVEKDYYYLGDEVNFGGGKVLREGMGENGTYTR  61

Query  334  AIS-LDTVITNAVIIDYTGIIKADIGIKDGLIASIGKAGNPDIMNGVFSNMIIGANTEVI  392
             + LD ++TNA+I+DYTGI KADIG+KDG I  IGK GNPDIM+GV  NMI+G  TEVI
Sbjct  62   TENVLDLLLTNALILDYTGIYKADIGVKDGYIVGIGKGGNPDIMDGVTPNMIVGTATEVI  121

Query  393  AGEGLIVTAGAIDCHVHYICPQLVYEAISSGITTLVGGGTGPAAGTRATTCTPSPTQMRL  452
            A EG IVTAG ID HVH+I P  V  A+++GITTL GGGTGPA G++ATT TP P  +
Sbjct  122  AAEGKIVTAGGIDTHVHFINPDQVDVALANGITTLFGGGTGPAEGSKATTVTPGPWNIEK  181

Query  453  MLQSTDYLPLNFGFTGKGSSSKPDELHEIIKAGAMGLKLHEDWGSTPAAIDNCLTIAEHH  512
            ML+ST+ LP+N G  GKG  S    + E I AGA GLK+HEDWG+TPA+ID  LT+A+
Sbjct  182  MLKSTEGLPINVGILGKGHGSSIAPIMEQIDAGAAGLKIHEDWGATPASIDRSLTVADEA  241

Query  513  DIQINIHTDTLNEAGFVEHSIAAFKGRTIHTYHSEGAGGGHAPDIIKVCGIKNVLPSSTN  572
            D+Q+ IH+DTLNEAGF+E ++ A  GR IH++H EGAGGGHAPDI+ + G  NVLPSSTN
Sbjct  242  DVQVAIHSDTLNEAGFLEDTVRAINGRVIHSFHVEGAGGGHAPDIMAMAGHPNVLPSSTN  301

Query  573  PTRPLTSNTIDEHLDMLMVCHHLDREIPEDLAFAHSRIRKKTIAAEDVLNDIGAISIISS  632
            PTRP T NTIDEHLDMLMVCHHL + IPED+AFA SRIR +TIAAED+L+D+G IS++S+
Sbjct  302  PTRPFTVNTIDEHLDMLMVCHHLKQNIPEDVAFADSRIRPETIAAEDILHDLGIISMMST  361

Query  633  DSQAMGRVGEVISRTWQTADPMKAQTGPLKCDSSDNDNFRIRRYIAKYTINPAIANGFSQ  692
            D+ AMGR GE++ RTWQTAD MK Q GPL  + + +DNFR++RY++KYTINPAIA G +
Sbjct  362  DALAMGRAGEMVLRTWQTADKMKKQRGPLAEEKNGSDNFRLKRYVSKYTINPAIAQGMAH  421

Query  693  YVGSVEVGKLADLVMWKPSFFGTKPEMVIKGGMVAWADIGDPNASIPTPEPVKMRPMYGT  752
             VGS+E GK ADLV+W+P FFG K + VIKGG++A+A IGDP+ASIPTP+PV  R MYGT
Sbjct  422  EVGSIEEGKFADLVLWEPKFFGVKADRVIKGGIIAYAQIGDPSASIPTPQPVMGRRMYGT  481

Query  753  LGKAGGALSIAFVSKAALDQRVNVLYGLNKRVEAVSNVRKLTKLDMKLNDALPEITVDPE  812
            +G      +I F+SK+++ Q V    GL +R+  V N R + K DMK ND   +I ++PE
Sbjct  482  VGDLIHDTNITFMSKSSIQQGVPAKLGLKRRIGTVKNCRNIGKKDMKWNDVTTDIDINPE  541

Query  813  SYTVKADGKLLCVSEATTVPLSRNYFLF  840
            +Y VK DG++L       +P+++ YFLF
Sbjct  542  TYEVKVDGEVLTCEPVKELPMAQRYFLF  569
```

FIGURE A.1 Protein BLAST (NCBI) between the *C. ensiformis* urease and *S. pasteurii* urease amino acids sequence. The query ID reports to urease from *C. ensiformis* and the Subject ID reports to urease from *S. pasteurii*.

A.2 PROTEIN LADDER

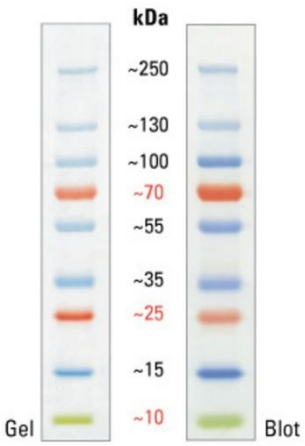

FIGURE A.2 Page Ruler™ Plus Prestained Protein Ladder (ThermoFischer Scientific) used for the Western Blot. The bands weight vary from 10 to 250 kDa.

A.3 CALIBRATION CURVES

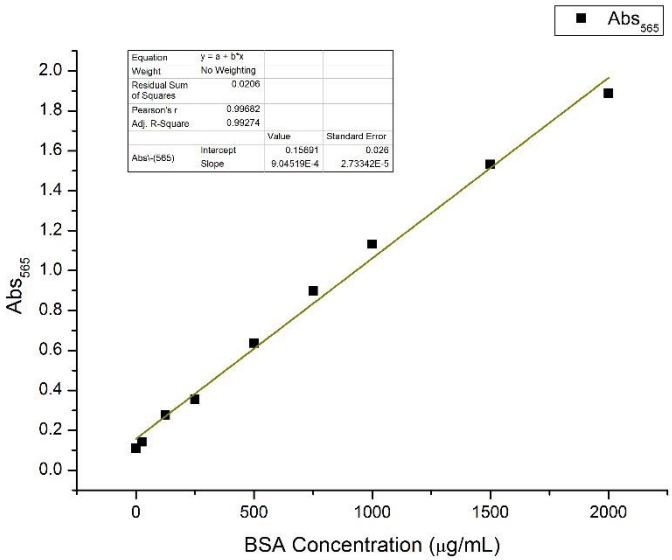

FIGURE A.3 Calibration curve for total protein quantification obtained measuring the absorbances at 565 nm of BSA standards with known concentrations. The parameters relative to the linear fit made to the data is also represented in the figure.

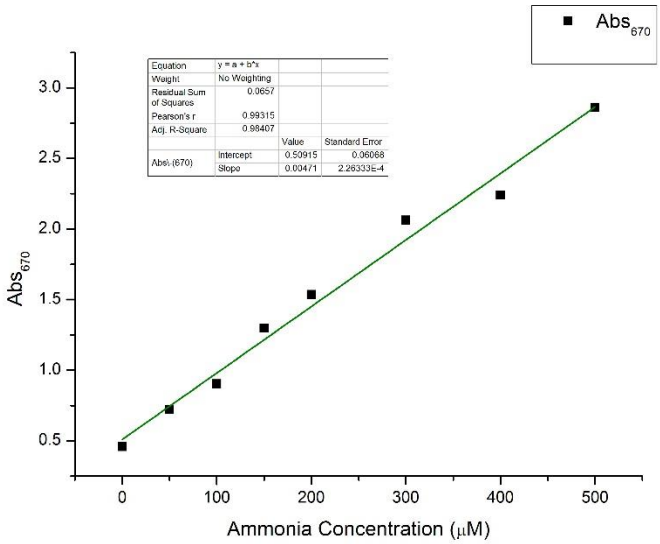

FIGURE A.4 Calibration curve for urease activity quantification obtained measuring the absorbances at 670 nm of ammonium chloride standards with known concentrations. The parameters relative to the linear fit made to the data is also represented in the figure.

APPENDIX B: RUN SHEETS FOR SPIN VALVE BIOCHIP AND FOR HARD MASK FOR PATTERNING MICROFLUIDIC CHANNELS

B.1 RUN SHEET FOR SPIN VALVE BIOCHIP 6 INCH

RUN: WAFER #14 Susana Freitas

Process Start : **Process Finish :**

SV# =Ta 15/ NiFe 28/ CoFe 28/ Cu 27/ CoFe 33/ MnIr 75/Ta 50.

MR= 8% Hf= 12 Oe

STEP 1	**1st Exposure –** Spin valve Definition	Date:

1) Coating PR: Vapor Prime 30 min (Recipe - 0)

Step description	Conditions
Wafer dehydration	Vacuum, 10 Torr, 2 min. N2 inlet, 760 Torr, 3 min. Heating to 130ºC
Priming	Vacuum, 1 Torr, 3 min. HDMS, 6 Torr, 5 min.
Purge prime exhaust	Vacuum, 4 Torr, 1 min. N2 inlet, 500 Torr, 2 min. Vacuum, 4 Torr, 2 min.
Return to atmosphere	N2 inlet, 3 min.

2) Coat 1.5 μm PR (Recipe 6/2)

Coating Parameters	
First Step	Dispense photoresist on the sample and spinning at 800 rpm for 5 sec.
Second step	Spin at 2500 rpm for 30 sec. to obtain ~1.45μm thickness.
Third step	Soft bake at 85ºC for 60 seconds.

3) Machine: DWL

Mask: uchipnov L1 (em /h2) Map: uchipnov

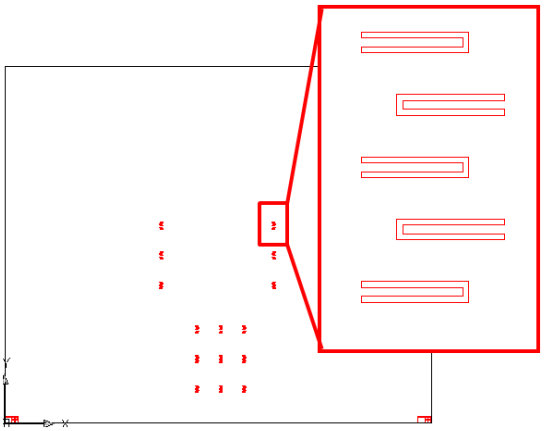

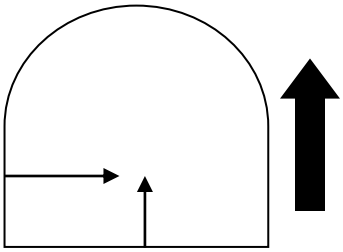

X=8000

Y=5000

Alignement mark position: X= 168 , Y= 55.7

Energy : 75

Power : 100mW

Focus : -20

4) Develop : Recipe 6/2 Developer: TMA238WA

Development parameters:
Bake at 110°C for 60s
Cool for 30s
Developer for 60s

5) Optical Inspection:

Sample	**Comments**

STEP 2 **Ion Milling –** Spin valve etching	Date:

Machine: **N3600**

Thickness= 270 A (etch rate: ~1.05 A/s → time: 400s 55A of overetch

Standard Etching Recipe (junction_etch) :

Junction_etch

190 W / 735 V / 105 mA / 350 V / 11 sccm

Assist Gun: 65W/ +500V/-200V 10sccm Ar; 30 rpm 70º subst.pan (set = 60ºpan)

Wafer	samples	Etching Turn	Time	Effect
1	1 - 6			Contrast between metal and oxide

Assist Gun	Power (W)	V+ (V)	I+ (mA)	V- (V)	I- (mA)	Ar Flux (sccm)	Pan (deg)	Rotation (rpm)
Read Values	193	724	104.5	344.8	2.6	11.2	60	30

Optical Inspection:

Sample	Comments

STEP 3 **Resist strip** Date:

Hot μ-strip + ultrasonic

Rinse with IPA + DI water + dry N_2

Started: Stopped:

Total Time in hot μ-strip : Ultrasonic Time :

Optical inspection:

Sample	Comments

STEP 4 **2nd Exposure –** Contact Date:

1) Coating PR: Vapor Prime 30 min (Recipe - 0)

Step description	Conditions
Wafer dehydration	Vacuum, 10 Torr, 2 min. N2 inlet, 760 Torr, 3 min. Heating to 130ºC
Priming	Vacuum, 1 Torr, 3 min. HDMS, 6 Torr, 5 min.
Purge prime exhaust	Vacuum, 4 Torr, 1 min. N2 inlet, 500 Torr, 2 min. Vacuum, 4 Torr, 2 min.
Return to atmosphere	N2 inlet, 3 min.

2) Coat 1.5 μm PR (Recipe 6/2)

Coating Parameters	
First Step	Dispense photoresist on the sample and spinning at 800 rpm for 5 sec.
Second step	Spin at 2500 rpm for 30 sec. to obtain ~1.45μm thickness.
Third step	Soft bake at 85ºC for 60 seconds.

3) Pre-development Developer: TMA238WA

Pre-development parameters:
No bake
Developer for 20s

4) Machine: DWL

Mask: uchipnov L2 Map: uchipnov

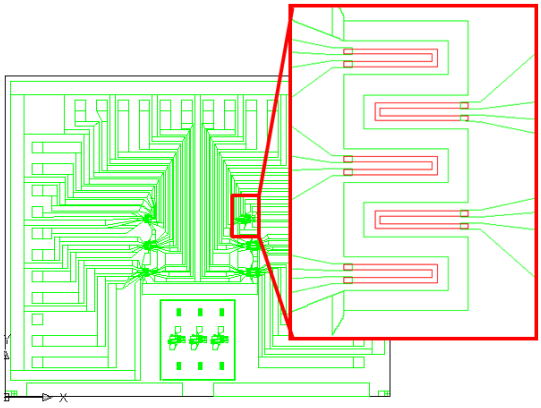

Alignement mark position: X= 168 , Y= 55.7

Energy : 77.5

Power : 90 mW

Focus : +35

5) Develop : Recipe 6/2 Developer: TMA238WA

Development parameters:
Bake at 110°C for 60s
Cool for 30s
Developer for 60s

6) Optical Inspection:

Sample	**Comments**

STEP 5 **Contacts deposition**	Date:

Machine: **Nordiko 7000**

Seq.Metalization – mod.2 – f.9 (1' soft sputter etch) P=60W/40W, p=3mTorr, 50 sccm Ar

mod.4 – f.1 (3000A Al, 1'20'') P=2 kW, 3mTorr, 50 sccm Ar

mod 3 – f.19 (150A TiW, 27'') P=0.5 kW, 3mTorr, 50sccm Ar + 10 sccm N_2

Readings – Module 2					
Run#	Power1	Power2	Gas flux	Pressure	
	60 W	39 W	50.1 sccm	3 mTorr	60 s

Readings – Module 4					
Run#	Power	Voltage	Current	Gas flux	Pressure
	2kW	394	5.12 A	50.0 sccm	3 mTorr (80s)

Readings – Module 3					
Run#	Power	Voltage	Current	Gas flux	Pressure
	0.5kW	4.26	1.18 A	49.6 sccm	3 mTorr

STEP 6 **Aluminum Lift-Off** Date:

Hot μ-strip + ultrasonic

Rinse with IPA + DI water + dry N_2

Started: Stopped:

Total Time in hot μ-strip : Ultrasonic Time :

Optical inspection:

Sample	**Comments**

STEP 7	**Passivation layer -3000Å SiN**	Date:

Machine: Electrotech
(3000Å)
Holder:300ºC
Showerhead: 350ºC

	Deposition Time	**SiN thickness (A)**	**NH_3 gas flux (sccm)**	**SiH_4 gas flux (sccm)**	**N_2 gas flux (sccm)**	**Pressure (mT)**	**Power Source RF (W)**
Set Values		3000	500	300	3500	850	500

Optical inspection:

Sample	**Comments**

STEP 8	**3rd Exposure –** passivation layer	Date:

1) Coating PR: Vapor Prime 30 min (Recipe - 0)

Step description	Conditions
Wafer dehydration	Vacuum, 10 Torr, 2 min. N2 inlet, 760 Torr, 3 min. Heating to 130ºC
Priming	Vacuum, 1 Torr, 3 min. HDMS, 6 Torr, 5 min.
Purge prime exhaust	Vacuum, 4 Torr, 1 min. N2 inlet, 500 Torr, 2 min. Vacuum, 4 Torr, 2 min.
Return to atmosphere	N2 inlet, 3 min.

2) Coat 1.5 μm PR (Recipe 6/2)

Coating Parameters	
First Step	Dispense photoresist on the sample and spinning at 800 rpm for 5 sec.
Second step	Spin at 2500 rpm for 30 sec. to obtain ~1.45µm thickness.
Third step	Soft bake at 85ºC for 60 seconds.

3) **Machine:** DWL

Mask: uchipnov_L3ninv Map: uchipnov

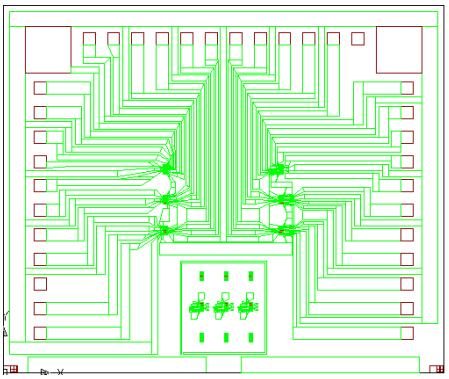

Alignement mark position: X= 168 , Y= 55.7

Energy : 67.5

Power : 100mW

Focus : -20

4) Develop : Recipe 6/2 Developer: TMA238WA

Development parameters:
Bake at 110°C for 60s
Cool for 30s
Developer for 60s

5) Optical Inspection:

Sample	Comments

STEP 9	**Reactive ion etching –** pads opening	Date:

Equipment:LAM Rainbow 4520

Process recipe: 6

Expected thickness: **Thickness to etch:** 3000A

Etch rate: ~ 5.47 Å/s

Second step: Time – 4 x 150s
Calc. etch time: 548s

Etching conditions: Low power no O2

	Pressure (Torr)	Etch time (s)	Power (RF)	Ar Flux (sccm)	CF_4 Flux (sccm)
Expected	140 mTorr	-300 s *-over-etch*: 300s	100 W	200	100
Observed		- s -cooling: s *-over-etch*: s			

Optical Inspection:

Sample	Comments

STEP 10	**Resist strip**	Date:

Hot μ-strip + ultrasonic

Rinse with IPA + DI water + dry N_2

Started: Stopped:

Total Time in hot μ-strip : Ultrasonic Time : 1h

Optical inspection:

Sample	Comments

STEP 11 **4th Exposure –** Au pad for chemistry Date:

1) Coating PR: Vapor Prime 30 min (Recipe - 0)

Step description	Conditions
Wafer dehydration	Vacuum, 10 Torr, 2 min. N2 inlet, 760 Torr, 3 min. Heating to 130ºC
Priming	Vacuum, 1 Torr, 3 min. HDMS, 6 Torr, 5 min.
Purge prime exhaust	Vacuum, 4 Torr, 1 min. N2 inlet, 500 Torr, 2 min. Vacuum, 4 Torr, 2 min.
Return to atmosphere	N2 inlet, 3 min.

2) Coat 1.5 μm PR (Recipe 6/2)

Coating Parameters	
First Step	Dispense photoresist on the sample and spinning at 800 rpm for 5 sec.
Second step	Spin at 2500 rpm for 30 sec. to obtain ~1.45μm thickness.
Third step	Soft bake at 85ºC for 60 seconds.

3) Pre-development Developer: TMA238WA

Pre-development parameters:
No bake
Developer for 20s

4) Machine: DWL

Mask: uchipnov L4 and testuchipnovL4 Map: uchipnov

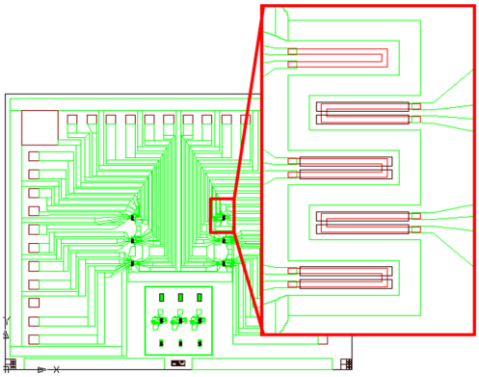

Alignment mark position: X= 168 , Y= 55.7

Energy : 90

Power : 100mW

Focus : -20

5) Develop : Recipe 6/2 Developer: TMA238WA

Development parameters:
Bake at 110°C for 60s
Cool for 30s
Developer for 60s

5) Optical Inspection:

STEP 12a	**Cut wafer before loading in Alcatel**	Date:

Machine: **Disco Dad**

When the Au film is deposited by N3000: no need to cut wafer here, as 6inch wafer can fit.

When Au film is deposited by Alcatel: need to cut into 1/4 wafer to fit into the sample holders-

STEP 12	**Au pads deposition**	Date:

Machine: **Alcatel**

50 A Cr/ 400 A Au

Material	Power	Gas flux (Ar)	Pressure	Time	Base pressure
Cr	20 W	20 sccm	293 mTorr	1 m	7.7E-7
Au	20 W	20 sccm	293 mTorr	7 m	

STEP 13	**Au lift-off**	Date:

Hot μ-strip + ultrasonic

Total Time in hot μ-strip : 4h Ultrasonic Time : 2h

Optical inspection:

Sample	**Comments**

STEP 14	**Coating with PR to protect dies**	Date:

Machine: SVG tracks

Coat 1.5 μm PR (Recipe 6/2)

Coating Parameters	
First Step	Dispense photoresist on the sample and spinning at 800 rpm for 5 sec.
Second step	Spin at 2500 rpm for 30 sec. to obtain ~1.45μm thickness.
Third step	Soft bake at 85ºC for 60 seconds.

STEP 15 **Dicing**	Date:

Machine: **DISCO DAD 321**

Die size: X = 7200 +200 (separation) ; X = 6000 +200 (separation)

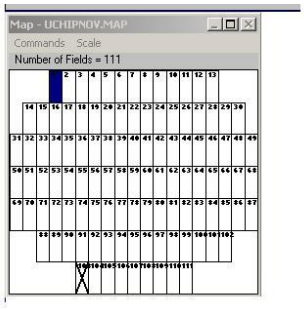

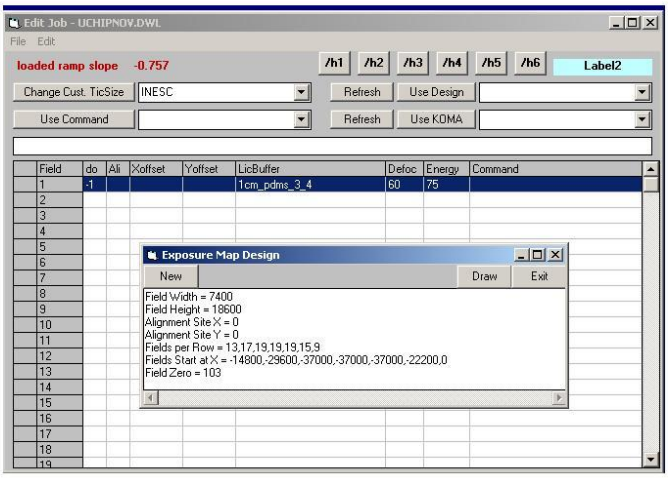

Biochips
Die area: 7400 x 18600 um

Mapa: uchipnov

~ 10 min/die

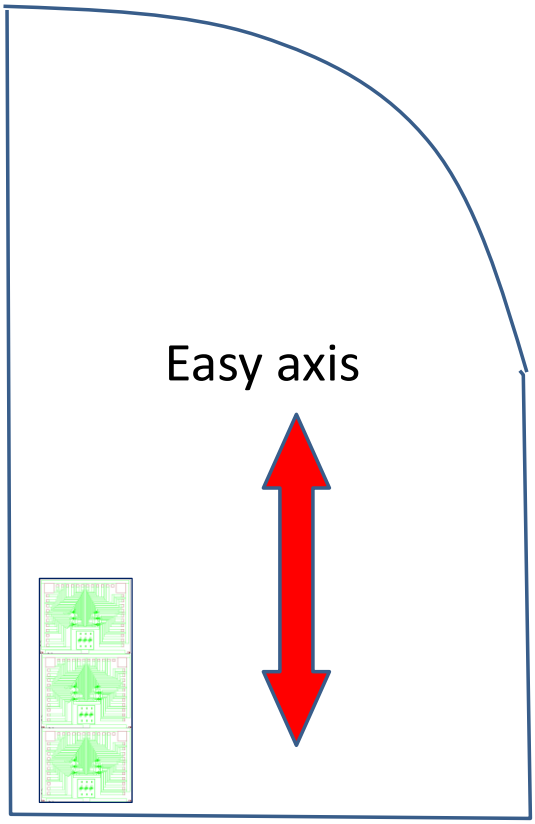

AutoCAD file: Biochip_oldDesign

Masks:

uchipnov L1
uchipnov L2 (com pré-revelação)
uchipnov_L3ninv (non-inverted, for LAM

Alignment marks:
X= 168 , Y= 55.76

B.2 RUN SHEET OF HARD MASK FOR PATTERNING MICROFLUIDIC CHANNELS

Responsible:

Glass Hard Mask for patterning microfluidic channels

Process Start: **Process Finish:_**

Step 1. Substrate Cleaning and Preparation	**Date:** **Responsible:**

1.1. Substrate: Boroaluminosilicate (CORNING 1737 AMLCD Glass substrates) of 0.7 mm thickness (2 x 2 in)

1.2. Procedure:

- Acetone to remove the glue followed by IPA to remove acetone residues;
- Washing with DI water;
- Drying carefully with compressed air.

1.3. Observations:

Step 2. Al deposition – 1500 Å thickness film	**Date:** **Responsible: Eng. Fernando**

2.1. Substrate: Cleaned boroaluminosilicate substrate

2.2. Equipment: Nordiko 7000 (clean-room)

2.3. Conditions:

Mode	Power(W)	Air flux (sccm)	Pressure (mTorr)
MOD4 F8 Al 1500 Å	2000	50.1	3.2

2.4. Observations:

Step 3. Photolithography	**Date: 06/09/2016** **Responsible: Eng. Virginia**

3.1. Substrate: Boroaluminosilicate with Al layer

3.2. Equipment and Conditions:

3.2.1. Coating (SVG track) – 1.5µm of positive PR (Recipe 6/2 at coating track): spinning for 5s @ 0.8krpm +30s @ 2.5krpm to obtain ≈1.45µm, followed by soft-bake at 85ºC for 1 min;

3.2.2. Exposure (DWL 2.0):

Map: AMSION

Mask: MicroSEP non-inverted (@/h4)

Size: 58 x 58 mm^2

Mask	E	F	Time	X_0,Y_0 (µm)
MicroSEP	60	40		X_0 = 3 000 Y_0 = 3 000

MASK:

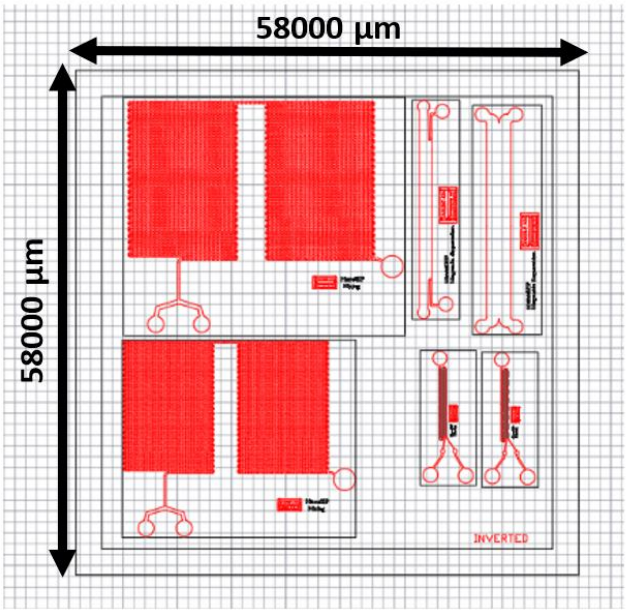

3.2.3. Developing (SVG track) – baking at 110ºC for 1 min, followed by developing during 1 min (Recipe 6/2 at development track);

3.2.4. Microscope verification of Al mask exposure

3.2.5. Observations:

Step 4. Aluminum Wet Etching	**Date:** **Responsible:**

4.1. Substrate: Boroaluminosilicate with Al layer + PR

4.2. Equipment: Wet bench (at clean-room)

4.3. Conditions of Al etch:

Solvent	T (ºC)	Time
TechniEtch Al 80 MOS Aluminum etchant	Room temperature	~ 3 min

4.4. Substrate washing with DI water and drying with compressed air.

4.5. Observations:

Step 5. PR strip	**Date:** **Responsible:**

5.1. Substrate: Boroaluminosilicate with Al layer + PR (after etching)

5.2. Equipment: Wet bench (outside clean-room)

5.3. Conditions:

Solvent	T (ºC)	Time
Microstrip 3001	65	20 min

5.4. Substrate washing with IPA, followed by rinsing DI water and drying with compressed air

5.5. Observations:

PDMS for microchannels

Process Start: **Process Finish**

Step 1. Substrate cleaning and preparation	**Date:** **Responsible: Débora Albuquerque**

1.1. Substrate: Silicon Die substrate

1.2. Conditions:

- Acetone to remove PR followed by IPA to remove acetone residues;
- Washing with DI water;
- Drying carefully with compressed air
- Surface cleaning with oxygen plasma for **20 min** in the gray area.

1.3. Observations:

Step 2. Resist Coating	**Date:** **Responsible: Débora Albuquerque**

2.1. Substrate: Cleaned silicon Die substrate

2.2. Equipment:

- StuartR digital hotplate from ERT
- Spinner Model WS-65OMZ-23NPP/LITE from Laurell Technologies Corporation;
- Contact lithography system

2.3. Coating procedure to achieve H = 50 µm:

2.3.1. Pre-bake (Dehydration step): Silicon Die substrate is baked with the use of the hot plate at 100 ºC, 10 min followed by cooling down under laminar flow.

2.3.2. Coating: PR SU-8 50 is manually distributed over the silicon wafer (starting in the middle, until ¾ of the wafer will be covered by the photoresist) and rested for 30s before running of the spinner. Spinning is performed in two-step process under following conditions:

Spinning speed	Acceleration ramp	Spinning time
500 rpm	100 rpm/s	10 s
2000 rpm	300 rpm/s	37 s

2.3.3. Soft bake: Baking is carried out at the hot plate in a two-step process:

- 65º C for 3 min;
- followed by 95º C for 8 min;
- relaxation time – 10 min under laminar flow.

2.3.4. Exposure: Contact lithography system for 20 s.

2.3.5. Post exposure bake: Baking is carried out at the hot plate in a two-step process:

- 65º C for 1 min;
- followed by 95º C for 7 min;
- relaxation time – 10 min under laminar flow.

2.3.6. Developing: Process is performed with the use of PGMA solvent for ~7 min. Sample is rinsed with the IPA and dried carefully with the air gun.

2.4. Observations:

Step 3. PDMS Preparation	**Date:** **Responsible: Débora Albuquerque**

3.1 Substrate: Silicon Die substrate with PR
3.2 Equipment: Scientech SA-80 Rev-c scale
3.3 Mixture conditions: Weighed PDMS and curing agent with the 10:1 ratio and mix vigorously for around 2 min (or until the mixture will become white). In the next step degas mixture for 1h (using the exicator) or until bubbles disappear.
3.4 Observations:

Step 4. PDMS Patterning	**Date:** **Responsible: Débora Albuquerque**

4.1 Substrate: Silicon Die substrate with PR
4.2 Mixture conditions: Procedure occurs inside a laminar flow chamber.

4.2.1 Polymer Casting: Place the mold in the petri dish, and pour PDMS on that. From the top of the surface remove the bubbles with the spatula (if they occur).

4.2.2 Polymer Curing: Cure the mixture inside an oven for 1h at 70 °C.

4.2.3 Master Removal: Before removing PDMS from the mold wait until the PDMS has time to cool down to the room temperature. Cut the PDMS in two steps - firstly maintaining 1-2 mm from the silicon (silicon is brittle) and peel it off, secondly cut to the size a little bit smaller than 2 x 2 inch – it facilitates proper bonding.

4.3 Observations:

Step 5. PDMS Bonding	**Date:** **Responsible: Débora Albuquerque**

5.1 Substrate: Silicon Die substrate with PR and glass
5.2 Bonding conditions: Procedure occurs inside the gray area and wet bench. PDMS needs to be immersed in water for 30 min in the bath (70°C). Glass is submerged in IPA (30 min in the bath at 70°C) followed by immersing it in DI water (30 min in the bath at 70°C). After cleaning/hydrophilic procedure, glass and PDMS (with the features facing up) are placed in the oxygen plasma for 1 min. In the final step, glass is immediately placed over the PDMS.